Universidad Autónoma de Madrid

Facultad de Ciencias

Departamento de Biología Molecular

Stability, placement and interactions of the divisome components in nucleoid-deprived *Escherichia coli* cells

TESIS DOCTORAL

Memoria presentada para optar al grado de Doctor en Ciencias

Manuel Pazos Don Pedro

TUTOR ACADÉMICO:

José Berenguer Carlos

DIRECTORES:

Miguel Vicente Muñoz

Paolo Natale

Consejo Superior de Investigaciones Científicas

Centro Nacional de Biotecnología

Madrid, 2013

Cover: Fluorescence microscopy image of CSR603 cells overproducing FtsZ*-VM

Este trabajo se ha realizado en el Centro Nacional de Biotecnología (CNB-CSIC) bajo la dirección del Doctor Paolo Natale y del Profesor de Investigación Miguel Vicente Muñoz, y en la Universidad de Texas (Houston, EEUU) durante una estancia de 6 meses en el laboratorio del Profesor William Margolin. Ha sido financiado por el programa de Formación de Personal Investigador del Ministerio de Educación y Ciencia.

Agradecimientos:

- A Miguel, por darme la oportunidad y los medios para poder realizar esta tesis doctoral y haberme animado, ayudado y enseñado a ser mejor científico en estos años.

- A Paolo, por todo el tiempo y el esfuerzo que ha dedicado a este proyecto ("trabajando codo con codo"), por tener siempre tiempo para explicarme y enseñarme algo nuevo cada día, por su incansable espíritu crítico, por sus consejos, y por guiarme y ayudarme a mejorar esta tesis.

- To William Margolin for all the good advices and help since I was in his lab, and to all the people in his lab (Daniel, Heather, Jennifer, Jesús, Jenny, Kim and Tushar) for making me feel like at home and having a lot of fun there.

- A todo el laboratorio del 217:

- a Pilar y Mercedes, por su paciencia y sabiduría, no sólo científica, por ser el buffer que todo lo tampona y hacer que todos los días sean mejores.

- a Cris, por toda la química que me ha ayudado a recordar y ser mi compi durante casi toda esta tesis.

- a todos los demás que están o estuvieron (Moira, Anabel, Susanne, Marcin, Alicia, Marta, Javi, Magaly) por todo el tiempo que hemos pasado juntos en estos años, toda vuestra ayuda, las cosas que me habeis enseñado y todos los buenos momentos que hemos pasado.

- A mis amigos de toda la vida porque ¿qué sería de la vida sin ellos?

- Finalmente a mi familia, especialmente a mis padres y a mi hermano, por todo lo que no abarca esta tesis, porque sin ellos hubiera sido imposible empezarla, continuarla y acabarla.

Contents

CONTENTS

Figure Index

Table Index

Abbreviations

Abbreviations

Amp	Ampicillin
Cm	Chloramphenicol
Da	Dalton
DAPI	4', 6'-diamidino-2-phenylindole
DNA	Deoxyribonucleic acid
His_6	Hexa-histidine tag
Kan	Kanamycin
LB	Luria Bertani
OD	Optical density at 600 nm
PCR	Polymerase chain reaction
PDB	Protein Data Bank
RNA	Ribonucleic acid
SDS	Sodium dodecyl sulfate
SDS-PAGE	SDS-polyacrilamide gel electrophoresis
Sn	Spectinomycin
Ts	Thermosensitive
UV	Ultraviolet light

Summary

Escherichia coli cell division is carried out by the formation of a septal ring-like complex placed at midcell, the divisome. Its correct placement at midcell is essential for the obtention of two identical viable daughter cells. Nucleoid Occlusion (NO) and MinCDE systems act on the placement of the proto-ring and specifically on the Z-ring. The proto-ring is the first subcomplex formed during the midcell assembly of the divisome, and it is made up of three essential proteins: FtsZ, FtsA and ZipA. Its assembly starts with the formation of an FtsZ-ring like structure (Z-ring), which is stabilized and tethered to the cytoplasmic membrane via ZipA and FtsA. During proto-ring assembly several modulatory proteins regulate the Z-ring formation, enhancing and stabilizing its formation (e.g. ZapA, ZapB, ZapC or ZapD) or inhibiting it (e.g. ClpX, MinC, SlmA or SulA).

The work presented in this thesis is focused on the study of the proto-ring formation and placement using nucleoid free cells, also known as maxicells. In the section 1 of *Results*, the experimental procedure for the production of maxicells was optimized starting with the conditions given by Sancar *et al., (1979).* Next to the chromosome degradation, in section 2 a small inventory of the proto-ring and proto-ring associated proteins was described, remarking a significant decrease in the FtsZ levels due to the action of the protease complex ClpXP. The absence of a functional nucleoid occlusion (NO) system led to study the role of the septum site positioning system MinCDE, which maintains its protein levels and the oscillatory movement in maxicells. This role over the FtsZ placement was tested in growing cells and in maxicells using three FtsZ variants: $FtsZ^{+}$ and two artificially anchored to the inner membrane by the carboxyl-terminal amphipathic membrane targeting sequence of MinD (MinDmts), which allows FtsZ binds to the membrane without the assistance of FtsA and ZipA. In section 3 the effect of ZipA and FtsA over the FtsZ stability was studied and described. A new role for ZipA was found, showing its ability to avoid the FtsZ degradation by the ClpXP protease complex. The globular domain (FZB) was identified as the only region of ZipA necessary for the interaction and protection of FtsZ. These results were not shown either by FtsA or FtsA*, which were also unable to interfere with the FtsZ protection carried out by ZipA. Section 4 describes the interaction between different cell division proteins, by Bimolecular Fluorescent Complementation (BiFC). Up to 35 different pair of proteins combinations were assayed in growing cells, involving proto-ring components (FtsZ, FtsA/FtsA* and ZipA) and FtsZ-effector proteins (ZapA, ZapB, MinC, SulA and SlmA), and identifying six examples of protein-protein interaction, i.e. ZipA-FtsZ, ZipA-ZapA, ZapB-FtsZ, ZapB-ZapA, ZapB-ZipA and ZapB-ZapB. Whereas in maxicells, which do not grow actively and the FtsZ levels are significantly decreased, the ZipA-ZapA or the ZipA-ZapB interaction did not take place; in growing cells under FtsZ depletion only ZipA-ZapB interaction was observed. Therefore we

suggest that FtsZ bridges the interaction between ZipA and ZapA, and the ZipA-ZapB interaction does not depend on the FtsZ protein levels but most likely on an active growth of the cell.

Introducción

1. El proceso de división celular en *Escherichia coli*

En bacterias la división celular se lleva a cabo mediante la formación de un complejo septal en forma de anillo, el divisoma, situado en el centro de la célula para invaginar la membrana citoplásmica junto con la membrana externa y la pared celular. Es un proceso controlado en el tiempo y en el espacio que asegura la generación de dos células hijas idénticas (Vicente *et al.*, 2006).

Diferentes cepas mutantes incapaces de dividir han sido usadas para identificar genes cuyos productos son necesarios para la division celular. Muchos de los genes identificados se nombraron *fts* (del inglés *filamentous temperature sensitive*) porque fueron aislados de cepas incapaces de dividirse pero capaces de crecer a 42ºC generando largos filamentos (Hirota *et al.*, 1968, Ryter *et al.*, 1968, Castellazzi *et al.*, 1972, Howard-Flanders & Theriot, 1966). Al menos diez genes son esenciales para la división celular, dentro de las cuales seis (*ftsW*, *ftsI*, *ftsL*, *ftsQ*, *ftsA* y *ftsZ*) están agrupados en un complejo génico denominado *dcw* (del inglés, *division and cell wall*) compuesto por genes implicados en división celular y síntesis de precursores del peptidoglicano (Vicente & Errington, 1996). Este complejo génico está altamente conservado, en concreto en bacterias en forma de bastón (Tamames *et al.*, 2001).

El ensamblaje de las proteínas de división en el centro de la célula en *E. coli* comienza en el citoplasma con la formación del anillo citosólico (formado por FtsZ, FtsA, ZipA y FtsK), el posterior reclutamiento de los subcomplejos denominados conector periplásmico (FtsL, FtsB y FtsQ) y fábrica de peptidoglicano (FtsW, FtsI), y finalmente de la proteína FtsN (Figura 1). Previamente a la formación del anillo citosólico, FtsZ, FtsA y ZipA se ensamblan y forman el denominado proto-anillo, estructura esencial para la correcta localización del plano de división y para el posterior reclutamiento de las proteínas restantes (Vicente *et al.*, 2006). Una vez que el proto-anillo está formado, la proteína ADN translocasa FtsK es reclutada. FtsK es una proteína de membrana que consta de un dominio transmembrana amino terminal (N-terminal) esencial para su localización en el septo de división (Draper *et al.*, 1998, Wang & Lutkenhaus, 1998, Yu *et al.*, 1998a) y un dominio citoplásmico carboxilo terminal (C-terminal) implicado en el acoplamiento de la división celular a la finalización de la segregación cromosómica, previniendo la escisión del cromosoma durante la constricción del septo de división (Liu *et al.*, 1998, Yu *et al.*, 1998b). En una etapa más tardía son reclutados el resto de componentes del divisoma. El subcomplejo denominado conector periplásmico, formado por FtsQ, FtsB y FtsL, une el anillo citosólico con la fábrica de peptidoglicano (compuesto por FtsW y FtsI). FtsN se ensambla una vez que todas las anteriores están localizadas en el anillo septal (Addinall *et al.*, 1997), siendo necesaria en la estabilización del proto-anillo y de FtsQ (Busiek *et al.*, 2012, Rico *et al.*, 2010), y en el

reclutamiento de AmiC y del sistema Tot-Pal, ambos componentes no esenciales para la división e implicados en la rotura del peptidoglicano (Heidrich *et al.*, 2001) e invaginación de la membrana externa (Gerding *et al.*, 2007) respectivamente, para asegurar la separación de las dos células hijas.

2. Ensamblaje del proto-anillo

El ensamblaje del proto-anillo comienza con la formación de una estructura anular de FtsZ (anillo de FtsZ), el cual servirá como soporte para el reclutamiento del resto de proteínas de división celular (Rueda *et al.*, 2003). En *E. coli* el anillo de FtsZ se ha observado como una estructura helicoidal dinámica que se mueve dentro del citosol y que acaba formando el anillo (Thanedar & Margolin, 2004, Fu *et al.*, 2010). Además, en *Caulobacter crescentus* se ha visto mediante tomografía crioelectrónica que el anillo de FtsZ está formado por pequeños protofilamentos solapados de FtsZ (Li *et al.*, 2007). El anillo de FtsZ se estabiliza y ancla a la membrana citoplásmica mediante ZipA y FtsA (Addinall *et al.*, 1996, Addinall & Lutkenhaus, 1996, Hale & de Boer, 1999). Ambas proteínas se reclutan y unen al anillo de FtsZ de forma independiente, aunque al menos una de ellas debe estar presente para la formación de dicho anillo (Pichoff & Lutkenhaus, 2002, Hale & de Boer, 1999).

La proporción entre los componentes del proto-anillo es esencial para la división celular (Rueda *et al.*, 2003), habiendo aproximadamente 5000 moléculas de FtsZ, 50-200 de FtsA y 1500 de ZipA por célula (Pla *et al.*, 1991, Wang & Gayda, 1992, Hale & de Boer, 1997). Cualquier disminución o sobreproducción de éstos causa el bloqueo de la división celular, debido a la alteración en el anillo de FtsZ como indica la aparición de estructuras helicoidales en lugar de anillos (Ma *et al.*, 1996, Pichoff & Lutkenhaus, 2005). El aumento de los niveles de FtsZ rompe el bloqueo, indicando que la proporción entre los componentes del proto-anillo es esencial para el correcto ensamblaje y mantenimiento del anillo de FtsZ (Hale & de Boer, 1997, Dai & Lutkenhaus, 1992).

2.1 FtsZ

Es una proteína GTPasa citoplásmica de 40.3 kDa que presenta homología estructural con la proteína tubulina eucariótica (Löwe & Amos, 1998, Nogales *et al.*, 1998), está conservada casi universalmente en bacterias y ha sido extensamente estudiada (Adams & Errington, 2009, Mingorance *et al.*, 2010). Ensayos *in vitro* muestran que FtsZ polimeriza formando protofilamentos de forma dependiente de la presencia de Mg^{2+}, de cationes monovalentes y de GTP (Lu *et al.*, 1998, Sossong *et al.*, 1999, Tadros *et al.*, 2006, Mendieta *et al.*, 2009, Romberg,

2003). Se dispone de la estructura cristalina de FtsZ de diversos organismos como *Methanococcus jannaschii* (Löwe & Amos, 1998), *Pseudomonas aeruginosa* (Cordell *et al.*, 2003), *Mycobacterium tuberculosis* (Leung *et al.*, 2004), *Thermotoga maritima* (Oliva *et al.*, 2004), *Bacillus subtilis* (Oliva *et al.*, 2007, Haydon *et al.*, 2008) y *Aquifex aeolicus* (Oliva *et al.*, 2007). FtsZ está compuesta por dos dominios globulares, el extremo N-terminal implicado en la interacción con el siguiente monómero (Oliva *et al.*, 2004) y el extremo C-terminal necesario para la interacción con otras proteínas de división como FtsA y ZipA (Figura 2) (Wang *et al.*, 1997, Ma & Margolin, 1999, Liu *et al.*, 1999, Mosyak *et al.*, 2000, Haney *et al.*, 2001, Szwedziak *et al.*, 2012). El sitio de interacción a GTP está formado entre la interfaz de dos monómeros que interactúan de forma "cabeza-cola", y por lo tanto la actividad GTPasa depende de la dimerización de FtsZ (Mingorance *et al.*, 2001, Scheffers *et al.*, 2002). Los polímeros de FtsZ continuamente incorporan y eliminan monómeros con una velocidad de reemplazo del orden de diez segundos, dependiendo de la unión de GTP y de la actividad GTPasa respectivamente (Mingorance *et al.*, 2001, Chen & Erickson, 2005, Stricker *et al.*, 2002). Mediante asociaciones laterales entre dichos protofilamentos se forman estructuras de mayor orden, dependiendo de las condiciones del ensayo *in vitro* (p. ej. pH y presencia de Ca^{2+}) o de la presencia de otras proteínas de división (estabilizadores del anillo de FtsZ) como ZipA, ZapA, ZapB, ZapC o ZapD. El desensamblaje del anillo de FtsZ también está regulado dentro de la célula por las proteínas ClpX, MinC, SlmA o SulA, las cuales regulan en el tiempo y espacio la formación del anillo de FtsZ (inhibidores del anillo de FtsZ).

2.2 ZipA

ZipA (del inglés *FtsZ interacting protein A*) es una proteína de la membrana citoplásmica de 36.5 kDa, que sólo está presente en γ-proteobacterias. Está formada por un pequeño extremo periplásmico N-terminal, un segmento transmembrana y una gran parte citosólica C-terminal que puede ser subdividida en tres dominios: el dominio cargado y repetido Map-Tau (+/-), la región rica en prolinas y glutaminas (P/Q rich) y el dominio globular situado en el extremo C-terminal (FZB, del inglés *FtsZ Binding*) (Hale & de Boer, 1997, RayChaudhuri, 1999) (Figura 3). Los datos obtenidos de la estructura cristalina de la proteína muestran que el dominio FZB interacciona con FtsZ por una cavidad hidrofóbica expuesta en la superficie (Moy *et al.*, 2000, Mosyak *et al.*, 2000). La interacción ZipA-FtsZ se ha referido únicamente a este dominio ya que el dominio P/Q rich, probablemente plegado como un largo brazo desestructurado, simplemente mantiene anclada a la membrana citoplásmica la molécula de FtsZ unida. Al dominio Map-Tau no se le asignó un papel en la unión a FtsZ ya que permanece cerca de la superficie de la membrana,

lejos del dominio de unión a FtsZ (RayChaudhuri, 1999, Moy *et al.*, 2000, Mosyak *et al.*, 2000, Erickson, 2001).

ZipA es necesaria para la estabilización del anillo de FtsZ, anclándolo a la membrana citoplásmica (Pichoff & Lutkenhaus, 2002). El dominio FZB es necesario y suficiente para la interacción con FtsZ, ya que él solo es capaz de ser reclutado al septo de división (Hale *et al.*, 2000). Recientes estudios indican que ZipA dimeriza independientemente de la presencia de FtsZ (Skoog & Daley, 2012), sugiriendo la presencia de ZipA en el septo de división en forma monomérica y dimérica. ZipA también es necesaria para el reclutamiento de FtsK (Pichoff & Lutkenhaus, 2002, Hale & de Boer, 2002), FtsQ, FtsL y FtsN (Hale & de Boer, 2002).

In vitro ZipA, y específicamente el dominio FZB, promueve la formación de estructuras de FtsZ de mayor orden mediante la interacción con el extremo carboxilo de FtsZ (RayChaudhuri, 1999, Hale *et al.*, 2000). Además se ha descrito mediante microscopía de fuerza atómica (AFM) que, dependiendo de la composición lipídica, ZipA es capaz de modular la forma y el estado de agregación de los protofilamentos de FtsZ (Mateos-Gil *et al.*, 2012) sugiriendo que ZipA hace de enlace flexible entre los protofilamentos de FtsZ y la membrana citoplásmica.

2.3 FtsA

FtsA es una proteína citoplasmática de 45.3 kDa, clasificada como ATPasa por presentar homología estructural con la actina eucariota, la chaperona Hsp70 y la hexoquinasa (Bork *et al.*, 1992). FtsA une ATP, pero no hay evidencias de actividad ATPasa en *E. coli*, al contrario que en *B. subtilis* y *P. aeruginosa* (Feucht *et al.*, 2001, Paradis-Bleau *et al.*, 2005). La estructura cristalina de la proteína de *T. maritima* (van den Ent & Löwe, 2000) muestra similitudes con respecto a la de los miembros de la familia de la actina, con cuatro dominios: 1A, 2A, 2B y 1C, el cual reemplaza al dominio ausene 1B. El sitio de unión a ATP está formado por los dominios 1A y 2A. Mietras que FtsA de *Streptococcus pneumoniae* es capaz de polimerizar en presencia de ATP (Lara *et al.*, 2005, Krupka *et al.*, 2012), FtsA de *T. maritima* forma protofilamentos similares a los de la actina mediante la interacción de los dominios 2A y 1C de un monómero y los dominios 2B y 1A del otro (Szwedziak *et al.*, 2012). El dominio 1C de FtsA de *E. coli* es esencial para el reclutamiento de proteínas tardías del divisoma, como FtsI y FtsN (Corbin *et al.*, 2004, Rico *et al.*, 2004, Busiek *et al.*, 2012), mientras que el dominio 2B está implicado en la interacción con FtsZ (Szwedziak *et al.*, 2012) (Figura 4). Además tiene una hélice anfipática en el extremo C-terminal que interacciona con la membrana citoplásmica (Pla *et al.*, 1990, Yim *et al.*, 2000, Pichoff & Lutkenhaus, 2005).

El papel de FtsA en el anclaje y estabilización del anillo de FtsZ se hace más patente cuando una mutación puntual en el dominio 2B denominada FtsA*, triptófano en lugar de arginina en la posición 286, es capaz de compensar la ausencia de ZipA para la división celular (Geissler *et al.*, 2003). Además esta mutación elimina la inhibición de la división producida por un exceso de ZipA o FtsZ (Geissler *et al.*, 2003), y complementa parcialmente la ausencia de FtsK (Geissler & Margolin, 2005). Se ha descrito que los mutantes de FtsA deficientes en la interacción consigo mismos, incluyendo a FtsA*, son capaces de eludir la necesidad de ZipA para el reclutamiento de proteínas tardías de división celular pero mantienen su capacidad de interaccionar con FtsZ, y fomentan el ensamblaje del anillo de FtsZ (Pichoff *et al.*, 2012). Además, la presencia de FtsA* sustituyendo a FtsA genera una disminución en la longitud de las células y estabiliza el anillo de FtsZ de manera más fuerte, confiriéndole resistencia a MinC, el inhibidor de la polimerización de FtsZ del sistema MinCDE (Geissler *et al.*, 2007).

3. Proteínas efectoras del anillo de FtsZ

La concentración de FtsZ es constante durante el ciclo celular (Rueda *et al.*, 2003), siendo esencial el control estricto de su dinámica de ensamblaje para la estabilidad de FtsZ y la regulación de la división. Diferentes proteínas actúan en este punto en *E. coli*, promoviendo el ensamblaje o desensamblaje del anillo de FtsZ.

3.1 Proteínas estabilizadoras del anillo de FtsZ

Las proteínas estabilizadoras del anillo de FtsZ son proteínas no esenciales para la viabilidad de la célula que interaccionan con FtsZ y estabilizan el anillo de FtsZ. Por esta razón se las denomina Zap (del inglés, *FtsZ-associated proteins*). Al contrario que FtsA y ZipA, los mutantes individuales de las proteínas Zap son capaces de crecer y dividirse como células normales, al contrario que los mutantes dobles o triples, que muestran fenotipos sinérgicos tales como inhibición de la división celular o letalidad sintética (Ebersbach *et al.*, 2008, Galli & Gerdes, 2010, Gueiros-Filho & Losick, 2002).

ZapA es una proteína citoplásmica de 12.6 kDa que se recluta al anillo de división mediante interacción directa con FtsZ, promoviendo el ensamblaje y estabilidad del anillo de FtsZ (Gueiros-Filho & Losick, 2002). La estructura cristalina (de *P. aeruginosa*) muestra un tetrámero antiparalelo formado por dos dímeros asociados por la interacción de las hélices superenrolladas de los extremos C-terminal (Low *et al.*, 2004) (Figura 5). La cantidad de ZapA en *E. coli* es aproximadamente de 6000 moléculas por célula (Mohammadi *et al.*, 2009) y existe en un equilibrio entre forma dimérica y tetramérica en función de la concentración de proteína, aunque

la forma dimérica se ha postulado como la forma predominante dentro de la célula (Small *et al.*, 2007, Low *et al.*, 2004). *In vitro* ZapA se une a FtsZ con una estequiometría 1:1 promoviendo su polimerización y la estabilidad de los polímeros formados, mediante la inhibición de la actividad GTPasa de FtsZ (Gueiros-Filho & Losick, 2002, Small *et al.*, 2007). Se ha propuesto que dicha inhibición podría ser debida a que ZapA promovueve un cambio conformacional en la molécula de GTP unida a FtsZ que impide su hidrolización, estabilizando los polímeros. Sin embargo, un segundo modelo sugiere que el dímero o tetrámero de ZapA podría entrelazar los protofilamentos de FtsZ, promoviendo las interacciones laterales entre ellos.

ZapB es una proteína citoplásmica de 9.6 kDa que se recluta al anillo de FtsZ mediante su interacción con ZapA (Galli & Gerdes, 2010) y localizándose en la cara interna de éste. En ausencia de ZapB las células siguen siendo viables aunque presentan un fenotipo elongado con anillos o espirales de FtsZ localizados en sitios erróneos, mientras que la sobreproducción de ZapB provoca divisiones aberrantes de la célula (Ebersbach *et al.*, 2008). La estructura cristalina muestra un dímero de ZapB formado por dos hélices superenrolladas monoméricas (Ebersbach *et al.*, 2008) (Figura 5). *In vitro* los dímeros de ZapB interaccionan formando grandes manojos. Mientras que la región N-terminal de ZapB es esencial para la interacción con ZapA, ni la región N-terminal ni la C-terminal son necesarias para la dimerización de ZapB (Galli & Gerdes, 2012). El número relativamente alto de moléculas de ZapB en la célula (aprox. 13000) hace posible que pequeños polímeros de ZapB interconecten polímeros de FtsZ previamente unidos a moléculas de ZapA, promoviendo su organización en un anillo. Sin embargo experimentos *in vitro* muestran que a concentraciones altas ZapB provoca una diisminución en la capacidad de ZapA para estabilizar y formar manojos de FtsZ (Galli & Gerdes, 2012). No está bien establecido el mecanismo de acción de ZapB, ya que ZapB también es capaz de estimular el ensamblaje del anillo de FtsZ en ausencia de ZapA, como se muestra al sobreproducir ZapB en una cepa Δ*zapA*Δ*zapB* (Galli & Gerdes, 2010).

ZapC es una proteína citoplásmica de 20.6 kDa que se ha identificado como regulador del anillo de FtsZ con funciones solapadas con ZapA y ZapB (Durand-Heredia *et al.*, 2011, Hale *et al.*, 2011). FtsZ recluta a ZapC al centro de la célula durante la formación del proto-anillo, independientemente de la presencia de ZipA, FtsA, ZapA y ZapB (Hale *et al.*, 2011). Las células que carecen o sobreproducen ZapC muestran un aumento en su longitud y defectos en la morfología y localización del anillo de FtsZ (Durand-Heredia *et al.*, 2011, Hale *et al.*, 2011). *In vitro* ZapC está presente mayoritariamente como monómero, aunque se ha descrito una débil interacción entre monómeros y una posible oligomerización mediada por FtsZ mediante experimentos de sedimentación entre FtsZ y ZapC (Hale *et al.*, 2011). Además ZapC es capaz de

fomentar las interacciones laterales entre protofilamentos de FtsZ y estabilizarlos mediante una reducción de la actividad GTPasa de FtsZ (Hale *et al.*, 2011).

ZapD es una proteína citoplásmica de 28.3 kDa que se localiza en el centro de la célula de manera dependiente de FtsZ, por interacción directa con el extremo C-terminal de FtsZ, pero independiente de FtsA, ZipA, ZapA y ZapC (Durand-Heredia *et al.*, 2012). ZapD está presente en la célula en una cantidad de entre 500 y 800 moléculas. Mientras que su sobreproducción interfiere con el ensamblaje del anillo de FtsZ, y por lo tanto con la división de la célula, su ausencia no produce ningún efecto fenotípico. ZapD y ZapA ejercen funciones solapantes ya que la ausencia de ZapD sólo provoca un defecto en la division de la célula cuando ZapA también está ausente. La interacción directa con FtsZ también se ha demostrado mediante microscopía electrónica, viéndose la formación de manojos de FtsZ en presencia de ZapD, en los cuales la actividad GTPasa de FtsZ se ve disminuída aproximadamente un 60% (Durand-Heredia *et al.*, 2012).

4.2. Proteínas inhibidoras del anillo de FtsZ

Otro conjunto de proteínas reguladoras desestabilizan el anillo de FtsZ inhibiendo su formación. Pertenecen a distintos mecanismos celulares implicados en la estrecha regulación de los niveles de FtsZ y de su proceso de ensamblaje.

ClpX es una proteína de 46.4 kDa, perteneciente a la clase Clp/Hsp100 de proteínas AAA+ (ATPasas Asociadas con varias Actividades celulares) (Hanson & Whiteheart, 2005). ClpX es una proteína desplegadora dependiente de ATP que reconoce sus proteínas sustrato a través de al menos cinco tipos distintos de señales de reconocimiento (Flynn *et al.*, 2003, Sauer *et al.*, 2004) (Figura 6), y usa la energía obtenida de la hidrólisis de ATP para desplegar y suministrar dichas proteínas a ClpP (Glynn *et al.*, 2009), la proteasa que las degrada. Se ha demostrado que el complejo ClpXP es responsable de la degradación de FtsZ, ya que FtsZ presenta una señal de reconocimiento de ClpX en sus últimos dieciocho aminoácidos del extremo C-terminal (Camberg *et al.*, 2009). De esta manera ClpXP modula la polimerización dinámica de FtsZ (Camberg *et al.*, 2009) y la división celular (Camberg *et al.*, 2011) a través de la degradación de FtsZ.

MinC es una proteína citoplásmica de 28.4 kDa, componente del sistema Min de posicionamiento del septo de división. Es el componente efector del sistema que interacciona con FtsZ e inhibe el ensamblaje del anillo de FtsZ. Tiene dos dominios funcionales (Figura 6) (Hu & Lutkenhaus, 2000) que interaccionan con FtsZ, siendo ambos necesarios para el correcto funcionamiento del sistema Min (Zhou & Lutkenhaus, 2005). El dominio N-terminal de MinC

bloquea el ensamblaje del anillo de FtsZ cuando se sobreproduce en experimentos *in vivo* (Hu & Lutkenhaus, 2000). Este dominio interacciona con la interfaz del dímero de FtsZ y acorta los polímeros de FtsZ sin inhibir su actividad GTPasa (Dajkovic *et al.*, 2008a). El dominio C-terminal MinC, junto con MinD, se une al extremo C-terminal de FtsZ por la misma región que FtsA y ZipA, y probablemente desplace a ambas proteínas del anillo de FtsZ, generando el desensamblaje de éste (Shen & Lutkenhaus, 2009).

SlmA (del inglés *Synthetic lethal with a defective Min system*) es una proteína citoplásmica de 22.8 kDa que se asocia al nucleoide y bloquea la formación del anillo de FtsZ en la región celular ocupada por el nucleoide. Su función antagonista sobre el anillo de FtsZ se ve incrementada tras su unión a ADN (Cho *et al.*, 2011, Tonthat *et al.*, 2011). Se ha obtenido su estructura cristalina y se ha descrito el sitio de unión a ADN (Figura 6) (Tonthat *et al.*, 2011), al igual que las secuencias de ADN a las que se une en el cromosoma de *E. coli* (SBSs, del inglés *SlmA binding sequences*). Dichas SBSs contienen un sitio palindrómico con la secuencia consenso 5'- GTGAGTACTCAC -3' y se distribuyen por todo el cromosoma excepto en la region Ter (Cho *et al.*, 2011), la cual es la region del cromosoma (aproximadamente en el sitio opuesto al oriC) donde termina la replicación. *In vitro* el complejo SlmA-ADN no afecta a la actividad GTPasa de FtsZ, y por lo tanto a la formación de protofilamentos (Cho *et al.*, 2011). La estructura cristalina de SlmA-FtsZ muestra un dímero de SlmA entre dos moléculas de FtsZ, sugiriendo que SlmA separa los protofilamentos de FtsZ, afectando al ensamblaje de estructuras de mayor orden de FtsZ (Tonthat *et al.*, 2011). Sin embargo el mecanismo de inhibición de la formación del anillo de FtsZ por SlmA no está claro, aunque parece que la dimerización u oligomerización de SlmA es un factor clave (Cho *et al.*, 2011).

SulA es una proteína citoplásmica de 18.8 kDa que inhibe la formación del anillo de FtsZ durante la respuesta SOS (Huisman & D'Ari, 1981, Huisman *et al.*, 1984). Está presente en la célula en forma de dímeros que inhiben el ensamblaje del anillo de FtsZ y promueven el desensamblaje de aquellos ya existentes mediante la interacción directa con la superficie del monómero de FtsZ (Figura 6) (Cordell *et al.*, 2003). SulA inhibe la actividad GTPasa y la polimerización FtsZ (Cordell *et al.*, 2003, Mukherjee *et al.*, 1998, Trusca *et al.*, 1998, Dajkovic *et al.*, 2008b, Chen *et al.*, 2012) mediante el secuestro de los monómeros de FtsZ del reservorio intracelular (Dajkovic *et al.*, 2008b, Chen *et al.*, 2012). Como los monómeros de FtsZ necesitan de la unión a GTP para formar polímeros y la hidrólisis de dicho GTP provoca el desensamblaje de los monómeros dentro del polímero, se ha sugerido que el secuestro de los monómeros de FtsZ por SulA promueve el desensamblaje del polímero por la propia actividad GTPasa de FtsZ.

4. Maquinaria de posicionamiento del septo

El correcto posicionamiento del septo de división es esencial para aegurar la formación de dos células hijas morfológica y geneticamente idénticas. En *E. coli* hay dos mecanismos encargados de este propósito: oclusión por nucleoide (NO) y Min (Rothfield *et al.*, 2005), los cuales ejecutan su función sobre el primer paso en la formación del divisoma, el ensamblaje del proto-anillo y en concreto sobre la formación del anillo de FtsZ.

4.1 Oclusión por nucleoide (NO)

Este mecanismo está compuesto por el nucleoide bacteriano y por su proteína asociada SlmA, inhibidora de la división. NO evita la formación del anillo de FtsZ sobre los nucleoides, coordinando la división celular con la segregación cromosómica (Figura 7) (Sun & Margolin, 2004, Woldringh *et al.*, 1991, Bernhardt & de Boer, 2005). SlmA es una proteína antagonista de FtsZ que se une a secuencias específicas de ADN. Una vez unida al ADN, su habilidad de interferir con la polimerización de FtsZ se ve aumentada.

4.2 Sistema Min

El sistema Min (de minicélulas) evita la formación del anillo de FtsZ cerca de los polos y está compuesto por las proteínas MinC, MinD y MinE, las cuales están codificadas en el operon *minB*. Los mutantes *minB* fueron identificados por ser defectuosos en división celular, ocurriendo la septación cerca de los polos en vez de en el centro de la célula. La septación en los polos genera una pequeña célula esférica sin cromosoma llamada minicélula y una célula más larga de lo normal (Davie *et al.*, 1984, de Boer *et al.*, 1988, de Boer *et al.*, 1989, Lee & Price, 1993). La sobreexpresión del operón *minB* genera un fenotipo filamentado similar al observado en los mutantes *fts* (Ward & Lutkenhaus, 1985, Bi & Lutkenhaus, 1993, Raskin & de Boer, 1999a, Raskin & de Boer, 1999b).

MinC es un inhibidor de la división celular que interacciona con FtsZ y evita la formación de polímeros, y por lo tanto del anillo de FtsZ (de Boer *et al.*, 1990, de Boer *et al.*, 1992).

MinD es una proteína ATPasa periférica de membrana que, después de unir ATP, interacciona cooperativamente con la membrana citoplásmica mediante su hélice anfipática situada en el extremo C-terminal (MinDmts, del inglés *membrane targetting sequence*) (Hu *et al.*, 2002b, Lackner *et al.*, 2003, Suefuji *et al.*, 2002, Szeto *et al.*, 2002), formando estructuras helicoidales. Es necesario que MinD forme dímeros para que se una a la membrana citoplásmica (Lackner *et al.*, 2003, Hu & Lutkenhaus, 2003, Wu *et al.*, 2011, Szeto *et al.*, 2002, Szeto *et al.*,

2003). La interacción de MinD con la membrana citoplásmica provoca un aumento de su afinidad por MinC, reclutándose dicha proteína a la membrana citoplásmica y formándose el complejo MinCD. Dicho complejo se localiza a lo largo de toda la membrana citoplásmica, evitando el ensamblaje del proto-anillo (de Boer *et al.*, 1989).

El tercer componente, MinE, confiere especificidad topológica al sistema, ya que dirige la localización de los complejos MinCD a los polos de la célula. MinE es un dímero compuesto por dos monómeros de 88 aminoácidos, con una α-hélice en el extremo N-terminal por la cual interacciona con MinD (Ma *et al.*, 2003, Park *et al.*, 2011). El dominio C-terminal es necesario para la formación del dímero (Park *et al.*, 2011). MinE tiene una alta afinidad por el complejo MinCD anclado a la membrana e interacciona con la interfaz del dímero de MinD por el mismo sitio por el que lo hace MinC (Wu *et al.*, 2011).

La unión de MinE al complejo MinCD desplaza a MinC, estimulando la actividad ATPasa de MinD y provocando la redistribución del complejo hacia una región del citoplasma en la que la concentración de MinE sea suficientemente baja (Raskin & de Boer, 1997, Rowland *et al.*, 2000). La acción combinada de MinCDE genera el movimiento oscilatorio de un polo a otro de la célula (Figura 8) (Raskin & de Boer, 1999a, Raskin & de Boer, 1999b, Hu & Lutkenhaus, 2001, Szeto *et al.*, 2002, Szeto *et al.*, 2003). Esta oscilación provoca que haya mayor concentración del complejo MinCD en los polos celulares que en el centro, donde se permite la formación del anillo de FtsZ (Meinhardt & de Boer, 2001).

5. Enfoque desde la biología sintética

La reconstrucción *in vitro* de la maquinaria de división bacteriana está entre los principales objetivos a la hora de definir las funciones de los componentes individuales del anillo de división. La reconstitución de algunos procesos individuales de la división como la formación del anillo de FtsZ (Osawa *et al.*, 2008) o las interacciones entre las proteínas MinD y MinE han sido llevadas a cabo con éxito en ambientes acelulares (Loose *et al.*, 2008).

En esta tesis se presenta el uso de las maxicélulas de *E. coli* como contenedores celulares que, manteniendo intacta su morfología y estructura además de las maquinarias de transcripción y traducción, permiten estudiar las interacciones proteicas sin la necesidad de purificar sus componentes.

5.1 Maxicélulas

Las maxicélulas son células de *E. coli* cuyos nucleoides han sido degradados sin afectar a su capacidad de sintetizar ARN y proteínas. Inicialmente se utilizaron como sistema *in vitro* de transcripción y traducción de genes de interés codificados en plásmidos en un ambiente libre de cromosoma (Sancar *et al.*, 1979). La degradación del nucleoide se consigue mediante el daño del ADN cromosómico de células que no pueden repararlo. Dicho daño puede producirse mediante exposición a radiación ultravioleta (UV) o mediante pequeños péptidos de unión a ADN, p. ej. microcina B17 (Mayo *et al.*, 1988). La radiación UV provoca la formación de dímeros de pirimidina, que distorsionan la hélice del ADN de tal forma que su replicación es bloqueada. Debido al pequeño tamaño y alto número de copias de los plásmidos introducidos, es estadísticamente más probable que el daño se produzca en el ADN cromosómico que en el plasmídico.

Las cepas salvajes de *E. coli* reparan estos daños mediante la indución de la respuesta SOS. Para evitar dicha respuesta de reparación del ADN y provocar la degradación del ADN cromosómico (Skarstad & Boye, 1993) se deben utilizar cepas *recA* incapaces de inducir dicho mecanismo. En ausencia de una respuesta SOS functional y de un mecanismo de reparación de ADN la célula provoca la degradación del nucleoide la cual conlleva a la muerte de la célula (Kuzminov, 1999).

La respuesta SOS es la primera respuesta a daño del ADN, y está regulada por las proteínas LexA y RecA (Michel, 2005). LexA es un represor transcripcional y RecA es la proteasa específica de LexA que funciona como regulador de la cascada SOS. LexA se une a un motivo específico (caja-SOS) "aguas arriba" de los genes *lexA, uvrAB, sulA, umuCD, dinP, polB, recA, uvrD, ruvAB, recN y dinA*, cuyos productos génicos actúan en la regulación de la respuesta SOS, reparación por escisión de nucleótido, parada de la división celular y reparación de mutagénesis propensa a error (Emmerson & West, 1977, Siegel, 1983, Shurvinton & Lloyd, 1982, Lloyd *et al.*, 1983, Little *et al.*, 1981, Sedliakova *et al.*, 1980, Fogliano & Schendel, 1981, Huisman & D'Ari, 1981, Bagg *et al.*, 1981, Wagner *et al.*, 1999, Iwasaki *et al.*, 1990, Napolitano *et al.*, 2000). Bajo condiciones normales de crecimiento LexA reprime la respuesta SOS. El daño del ADN conlleva la formación de roturas de cadena sencilla (ssDNA) que disparan la unión a RecA y a SSB (proteína de unión a ADN de cadena sencilla). La formación del complejo ssDNA-RecA-SSB activa la actividad proteolítica de RecA, la cual degrada LexA y por lo tanto activa la transcripción de los genes de la respuesta SOS (Little & Mount, 1982). Una vez que se ha completado la reparación del daño del ADN y se ha eliminado la presencia de ssDNA, se desensambla el complejo ssDNA-RecA-SSB y disminuye la actividad proteolítica de RecA. Esto

genera la acumulación de LexA que s unirá a los motivos caja-SOS reprimiendo la transcripción de los genes de la respuesta SOS. En una cepa *recA* la ausencia de RecA mantiene la respuesta SOS reprimida por LexA y los daños acumulados en el ADN no pueden ser reparados, lo cual provoca que finalmente la exonucleasa V (RecBCD) degrade dicho ADN y la célula pierda su viabilidad (Skarstad & Boye, 1993, Kannan & Dharmalingam, 1990).

Introduction

1. Cell division process in *Escherichia coli*

In bacteria, cell division is carried out by the formation of a septal ring-like complex, the divisome, which is placed at midcell to invaginate the cytoplasmic membrane together with the outer membrane and the cell wall. It is a spatially and temporally controlled process that ensures the generation of two almost identical daughters cells (Vicente *et al.*, 2006).

Several non-dividing mutant strains have been used to identify genes whose products are required for cell division. Many of the identified genes were named as filamentous temperature sensitive (*fts*) because they were isolated as strains unable to divide, but able to grow at 42ºC resulting in the production of long filaments (Hirota *et al.*, 1968, Ryter *et al.*, 1968, Castellazzi *et al.*, 1972, Howard-Flanders & Theriot, 1966). There are at least ten genes identified as essential for cell division, where six of them (*ftsW*, *ftsI*, *ftsL*, *ftsQ*, *ftsA* and *ftsZ*) are located in a gene cluster called division and cell wall (*dcw*) composed of genes involved in cell division or in peptidoglycan precursor synthesis (Vicente & Errington, 1996). This cluster is highly conserved, specifically in rod-shaped bacteria (Tamames *et al.*, 2001).

Midcell assembly of the division proteins in *E. coli* has been described as starting from the cytoplasmic components FtsZ, FtsA, ZipA and FtsK forming the cytoplasmic ring; then recruiting the periplasmic connector (FtsL, FtsB and FtsQ) and the peptidoglycan factory (FtsW and FtsI) subcomplexes, and the FtsN protein (Figure 1). Prior to the formation of the cytoplasmic ring, FtsZ, FtsA and ZipA assemble into a structure defined as the proto-ring, essential for the correct localization of the division plane and for the assembly of the reamining division proteins (Vicente *et al.*, 2006). Once the proto-ring is assembled, the DNA translocase FtsK is recruited, a membrane protein consisting of an amino-terminal (N-terminal) membrane domain essential for localization at the cell division septum (Draper *et al.*, 1998, Wang & Lutkenhaus, 1998, Yu *et al.*, 1998a) and a large cytoplasmic carboxyl-terminal (C-terminal) domain involved in the coupling of cell division to the completion of chromosome segregation, preventing chromosome scission upon septum closure (Liu *et al.*, 1998, Yu *et al.*, 1998b). Next to the cytoplasmic ring formation, the rest of the divisome components are recruited at a late assembly stage. The periplasmic connector subcomplex formed by FtsQ, FtsB and FtsL links up the cytoplasmic ring with the peptidoglycan machinery composed by FtsW and FtsI. FtsN assembles when all the previous divisome components are localized at the septal ring (Addinall *et al.*, 1997), being necessary for stabilization of the proto-ring and the FtsQ ring (Busiek *et al.*, 2012, Rico *et al.*, 2010) and for the recruitment of the amidase AmiC and the Tol-Pal system, two-non essential division components involved in the peptidoglycan splitting (Heidrich *et al.*, 2001) and the outer membrane

invagination (Gerding *et al.*, 2007), respectively, to ensure the separation between the daughter cells.

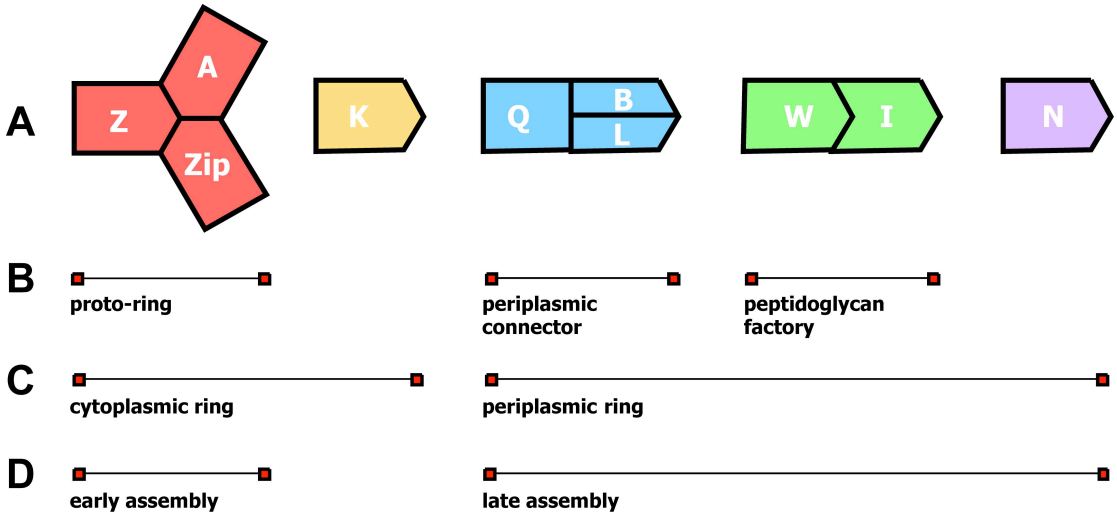

Figure 1. Essential components of the cell division ring and their assembly in *Escherichia coli*.

Ten essential proteins form the cell division ring, assembling in subcomplexes in a concerted way (A). In a first step or early assembly, FtsZ, ZipA and FtsA localize at midcell forming the proto-ring (B and D). FtsK binds to the proto-ring to complete the cytoplasmic ring (C). At a late assembly stage the periplasmic connector (FtsQ, FtsB and FtsL) and the peptidoglycan factory (FtsW and FtsI) are recruited to the midcell and form the periplasmic ring (C and D). FtsN is recruited to the divisome at a final step when all the proteins have been already recruited. Fts protein names have been abbreviated by excluding Fts. Zip = ZipA.

2. Proto-ring assembly

The proto-ring assembly starts with the formation of an FtsZ ring-like structure (Z-ring) that functions as a scaffold during divisome assembly (Rueda *et al.*, 2003). In *E. coli* the Z-ring has been shown as a dynamic helical structure that moves within the cytosol and eventually forms the ring (Thanedar & Margolin, 2004, Fu *et al.*, 2010). Moreover, cryoelectron tomography of *Caulobacter crescentus* cells showed that the Z-ring consists of short overlapped protofilaments of FtsZ (Li *et al.*, 2007). It is further described that the Z-ring is stabilized and tethered to the cytoplasmic membrane via ZipA and FtsA (Addinall *et al.*, 1996, Addinall & Lutkenhaus, 1996, Hale & de Boer, 1999). Both of them are recruited and bound to the Z-ring in an independent manner, but at least one of them must be present for the Z-ring formation (Pichoff & Lutkenhaus, 2002, Hale & de Boer, 1999).

Proto-ring components ratio is determinant for cell division (Rueda *et al.*, 2003). There are approximately 5000 molecules of FtsZ, 50-200 of FtsA and 1500 of ZipA per *E. coli* cell (Pla *et*

al., 1991, Wang & Gayda, 1992, Hale & de Boer, 1997). Any depletion or overproduction of them causes cell division blockage, resulting from disturbance in the Z-ring function, as indicated by the spiral-like structures observed (Ma *et al.*, 1996, Pichoff & Lutkenhaus, 2005). An FtsZ protein level increase can relieved the blockage, indicating that a proper ratio between proto-ring components is required for the correct assembly and maintenance of the Z-ring (Hale & de Boer, 1997, Dai & Lutkenhaus, 1992).

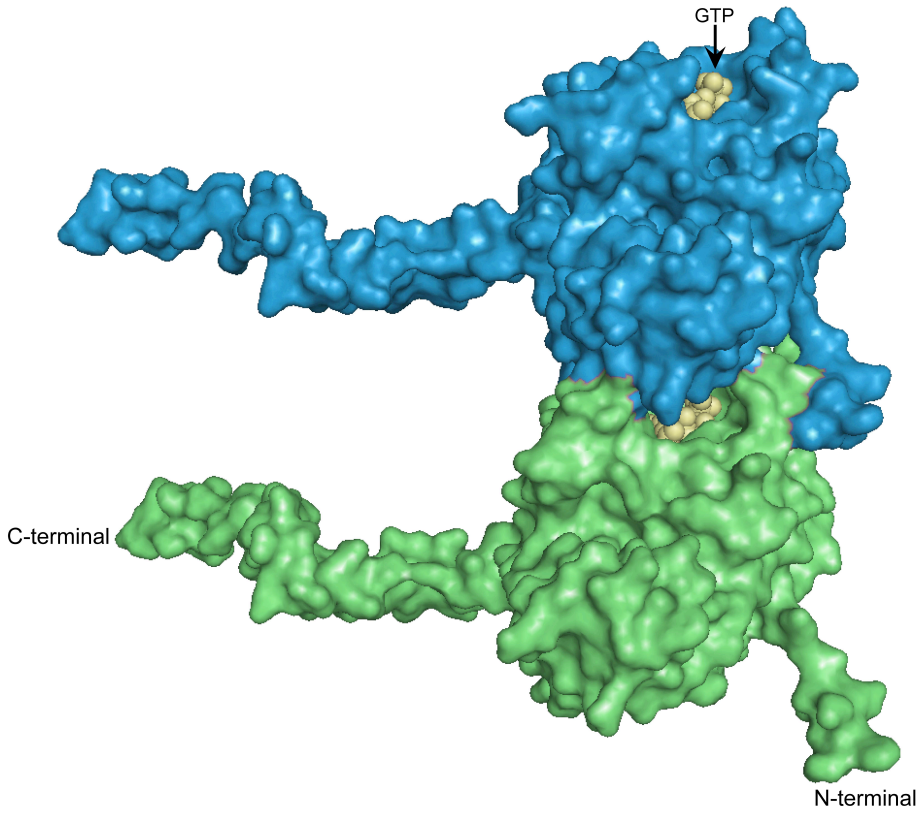

Figure 2. *E. coli* FtsZ dimer structure modelled from the crystal structure of *Methanococcus jannaschii*.

Two FtsZ monomers are represented (colored in green and blue) in a head-to-tail dimer, showing the GTP binding site formed in the interface between them and the GTP molecule (yellow). The structure shown is adapted from Gómez-Puertas P. (personal communication) in which the C-terminal end is modelled on the published crystal structure (Löwe & Amos, 1998).

2.1. FtsZ

It is a 40.3 kDa cytoplasmic GTPase that has structural homology to the eukaryotic tubulin (Löwe & Amos, 1998, Nogales *et al.*, 1998), that is almost universally conserved in bacteria and extensively studied (Adams & Errington, 2009, Mingorance *et al.*, 2010). *In vitro* experiments show that FtsZ polymerizes into protofilaments in a Mg^{2+}, monovalent cation and GTP-dependent manner (Lu *et al.*, 1998, Sossong *et al.*, 1999, Tadros *et al.*, 2006, Mendieta *et al.*, 2009, Romberg, 2003). Structural data is available from different organisms as *Methanococcus*

jannaschii (Löwe & Amos, 1998), *Pseudomonas aeruginosa* (Cordell *et al.*, 2003), *Mycobacterium tuberculosis* (Leung *et al.*, 2004), *Thermotoga maritima* (Oliva *et al.*, 2004), *Bacillus subtilis* (Oliva *et al.*, 2007, Haydon *et al.*, 2008) and *Aquifex aeolicus* (Oliva *et al.*, 2007). FtsZ contains two globular domains, with an N-terminal end involved in the interaction with the next monomer (Oliva *et al.*, 2004), and a C-terminal end necessary for the interaction with other cell division proteins as FtsA and ZipA (Figure 2) (Wang *et al.*, 1997, Ma & Margolin, 1999, Liu *et al.*, 1999, Mosyak *et al.*, 2000, Haney *et al.*, 2001, Szwedziak *et al.*, 2012). The GTP binding site is formed by the interface between two monomers that interact head-to-tail, and therefore the GTPase activity depends on FtsZ dimerization (Mingorance *et al.*, 2001, Scheffers *et al.*, 2002). FtsZ polymers are continuously incorporating and removing FtsZ molecules with a rapid turnover (approx. 10 seconds), depending on the GTP binding and on the GTPase activity respectively (Mingorance *et al.*, 2001, Chen & Erickson, 2005, Stricker *et al.*, 2002). Lateral associations between protofilaments can achieve higher-order FtsZ structures, which depend on the *in vitro* assay conditions (i.e. pH and presence of Ca^{2+}) or on the presence of other cell division proteins *in vivo* (Z-ring stabilizing proteins) as ZipA, ZapA, ZapB, ZapC or ZapD that stabilize. Dissasembly of the Z-ring is regulated by the proteins ClpX, MinC, SlmA or SulA, which are involved in the spatial and temporal regulation of the Z-ring formation (Z-ring inhibiting proteins).

2.2. ZipA

ZipA (FtsZ interacting protein A) is a 36.5 kDa bitopic inner membrane protein, only found in γ-proteobacteria. It is formed by a short periplasmic N-terminal region, a single transmembrane segment and a large cytosolic C-terminal part that can be further subdivided into three domains: the Map-Tau repeat and charged domain (+/-), the proline-glutamine enriched region (P/Q rich) and the globular domain at its C-terminal end (FZB) (Hale & de Boer, 1997, RayChaudhuri, 1999) (Figure 3). Protein crystallization data showed that the FZB (from FtsZ Binding) domain directly interacts with the C-terminal end of FtsZ via a surface exposed hydrophobic cavity (Moy *et al.*, 2000, Mosyak *et al.*, 2000). The ZipA-FtsZ interaction was reported to be limited to this region as the P/Q rich domain most likely folds as a long extended unstructured arm and thought to link the bound FtsZ molecule to the cytoplasmic membrane. No function in FtsZ binding was assigned to the charged Map-Tau domain since it would be topologically located near the membrane surface, far away from the FtsZ binding domain (RayChaudhuri, 1999, Moy *et al.*, 2000, Mosyak *et al.*, 2000, Erickson, 2001).

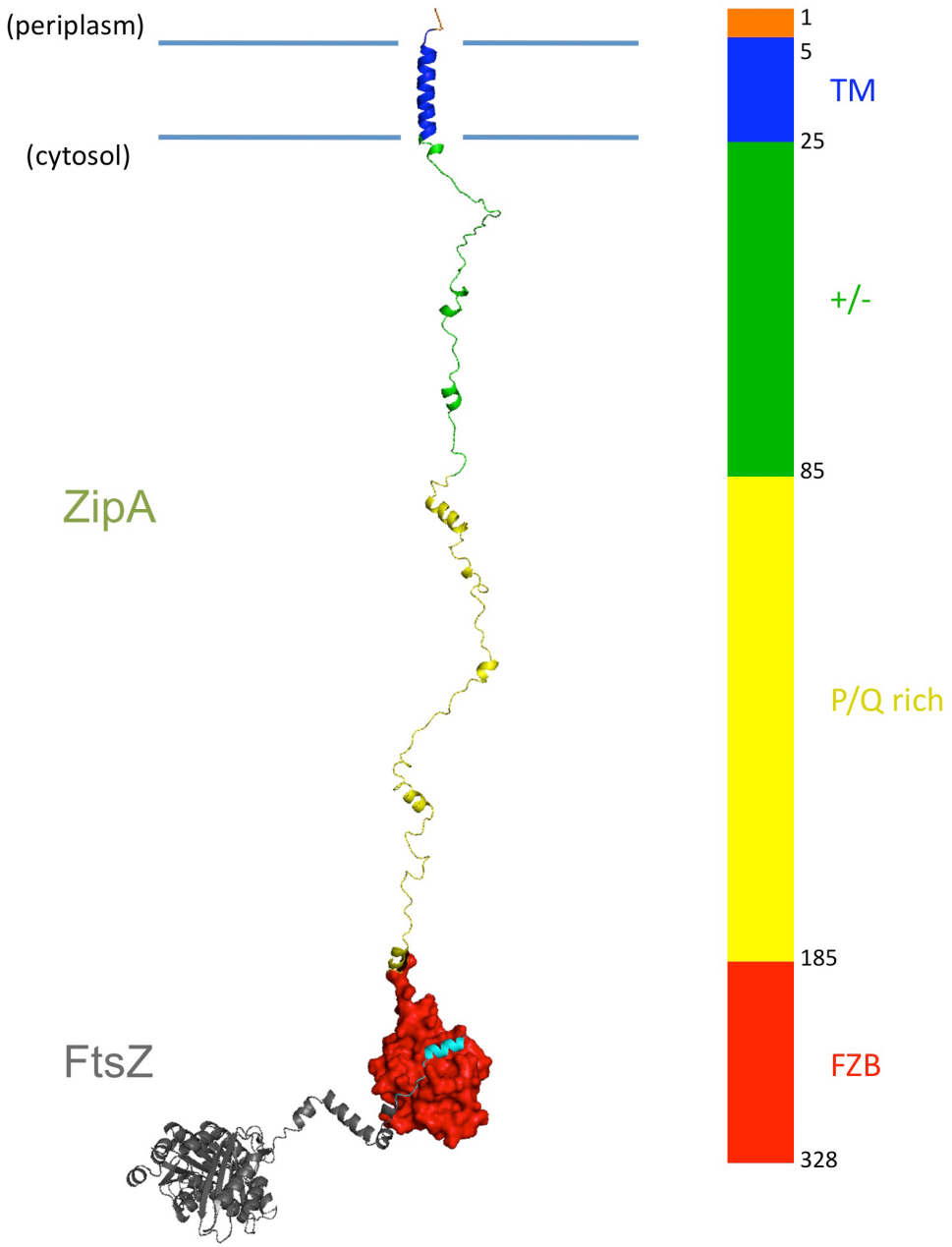

Figure 3. Structure of ZipA and its interaction with FtsZ in *E. coli*.

ZipA is a inner membrane protein with a short N-terminal periplasmic domain, a single transmembrane segment (TM) and a large cytoplasmic domain that can be subdivided in three different regions: the Map-Tau repeat and charged domain (+/-), the proline-glycine enriched region (P/Q rich) and the globular domain (FZB, from FtsZ Binding domain). Crystal structure of the interaction between the FZB domain of ZipA and the C-terminal end of FtsZ (cyan coloured). Rest of FtsZ coloured in gray) (PDB entry 1F47, adapted from Mosyak *et al.*, 2000 and Gómez-Puertas P., 2006, personal communication).

ZipA is needed for Z-ring stabilization, tethering it to the inner membrane (Pichoff & Lutkenhaus, 2002). Its FZB domain is described to be necessary and sufficient for the interaction with FtsZ, as FtsZ can recruit it to the division septum (Hale *et al.*, 2000). It has been described that ZipA dimerize in an FtsZ-independent manner (Skoog & Daley, 2012), suggesting that monomers and ZipA dimers are present at the division septum. ZipA is also required for the late assembly recruitment of FtsK (Pichoff & Lutkenhaus, 2002, Hale & de Boer, 2002), FtsQ, FtsL and FtsN (Hale & de Boer, 2002).

In vitro, ZipA and specifically the FZB domain, promotes the formation of higher-order FtsZ structures as bundles or sheets, by the interaction with the C-terminal end of FtsZ (RayChaudhuri, 1999, Hale *et al.*, 2000). Moreover, it has been recently described by atomic force microscopy that depending of the lipid composition, ZipA is able to modulate the shape and the aggregation state of the FtsZ protofilaments (Mateos-Gil *et al.*, 2012) suggesting that ZipA may be a flexible linker between the FtsZ protofilaments and the inner membrane.

2.3. FtsA

FtsA is a 45.3 kDa cytoplasmic protein, classified as an ATPase due to its structural homology with the eukaryotic actin, the Hsp70 chaperone and hexokinase (Bork *et al.*, 1992). FtsA binds ATP, but there is no evidence of any ATPase activity in *E. coli,* instead of in *B. subtilis* and *P. aeruginosa* (Feucht *et al.*, 2001, Paradis-Bleau *et al.*, 2005). FtsA crystal structure from *T. maritima* (van den Ent & Löwe, 2000) showed similar structure to the actin family members with four domains, 1A, 2A, 2B and 1C, which replace the absent domain 1B. The ATP-binding pocket is formed by the 1A and 2A domains. Whereas *Streptococcus pneumoniae* FtsA is able to polymerize in an ATP-dependent manner (Lara *et al.*, 2005, Krupka *et al.*, 2012), *T. maritima* FtsA forms actin-like protofilaments involving domains 2A and 1C on one monomer and 2B and 1A on the other (Szwedziak *et al.*, 2012). Domain 1C of *E. coli* FtsA is essential for the recruitment of late assembly cell division proteins, as FtsI and FtsN (Corbin *et al.*, 2004, Rico *et al.*, 2004, Busiek *et al.*, 2012), and domain 2B is involved in the interaction with FtsZ (Szwedziak *et al.*, 2012) (Figure 4). It also has a C-terminal amphipatic helix that is involved in the interaction with the inner membrane (Pla *et al.*, 1990, Yim *et al.*, 2000, Pichoff & Lutkenhaus, 2005).

The role of FtsA in tethering and stabilizing the Z-ring becomes evident when studying a point mutation in the 2B domain (arginine 286 to tryptophan) named FtsA* that is able to bypass the ZipA requirement for cell division (Geissler *et al.*, 2003). This point-mutation suppresses the cell division blockage produced by a ZipA or FtsZ excess (Geissler *et al.*, 2003), and partially complements the absence of FtsK (Geissler & Margolin, 2005). It has been described that FtsA mutants impaired for self-interaction, including FtsA*, are able to bypass the ZipA requirement for the recruitment of late assembly cell division proteins, maintaining their FtsZ binding capacity and supporting the Z-ring assembly (Pichoff *et al.*, 2012). Moreover, the FtsA* presence instead FtsA results in a decrease in cell length, stabilizing the Z-ring in a stronger way than FtsA and conferring resistance to MinC, the FtsZ-polymerization inhibitor of the MinCDE system (Geissler *et al.*, 2007).

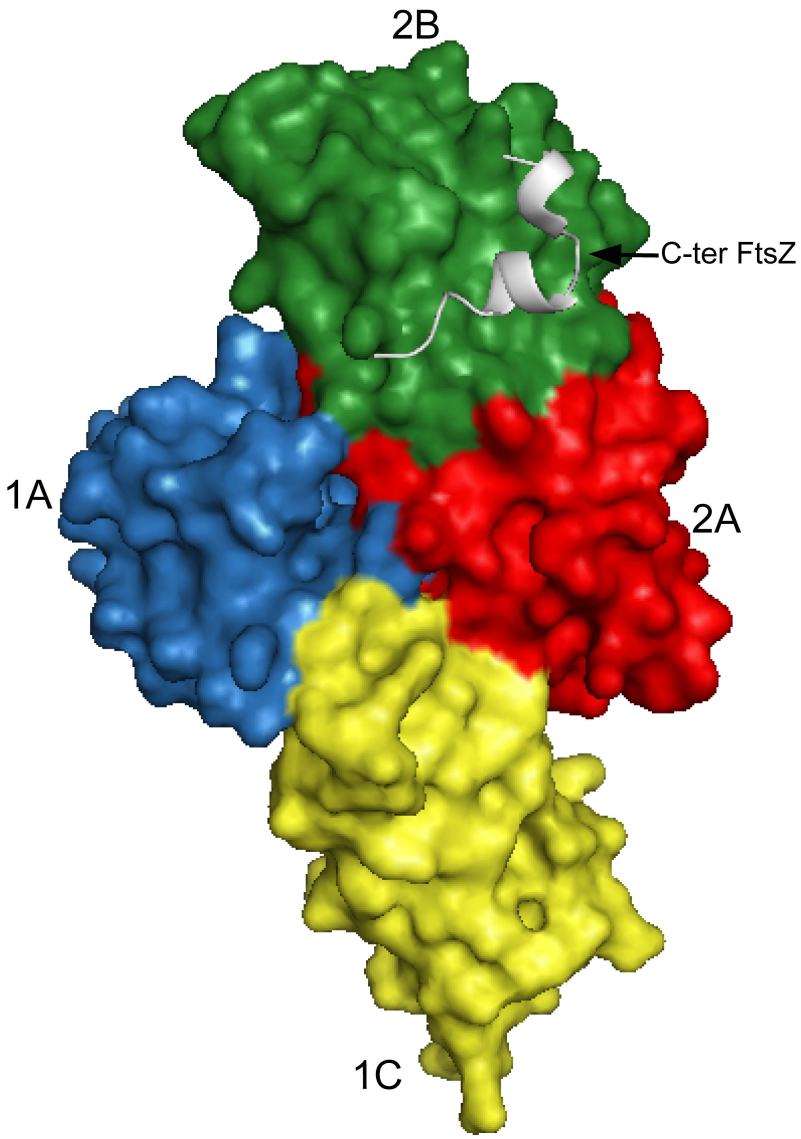

Figure 4. *Thermotoga maritima* FtsA crystal structure showing its interaction with FtsZ.

FtsA domains have been colour-coded according to the actin subdomain architecture (van den Ent & Löwe, 2000). The last sixteen C-terminal amino acid residues of FtsZ (white coloured) interact with the FtsA 2B domain (PDB entry 4A2A, adapted from Szwedziak *et al.*, 2012). ATP binding region is not visible in this image.

3. Z-ring effector proteins

The FtsZ concentration remains essentially constant throughout the cell cycle (Rueda *et al.*, 2003) and therefore a precise balance in FtsZ assembly dynamics is critical for FtsZ stability and cell division regulation. In *E. coli* different proteins have been proposed to be involved in regulating the assembly or disassembly of the Z-ring.

3.1. Z-ring stabilizing proteins

Z-ring stabilizing proteins are non-essential proteins for cell viability that interact with FtsZ and stabilize the Z-ring. For this reason they are named FtsZ-associated proteins (Zap). In contrast to FtsA and ZipA, single mutants can grow and divide as normal cells, but double or triple mutants show synergic phenotypes as inhibition of cell division or synthetic lethality (Ebersbach *et al.*, 2008, Galli & Gerdes, 2010, Gueiros-Filho & Losick, 2002).

ZapA is a 12.6 kDa cytoplasmic protein that is recruited to the division ring by direct interaction with FtsZ, enhancing the assembly and stability of the Z-ring (Gueiros-Filho & Losick, 2002). *P. aeruginosa* ZapA crystal structure shows an anti-parallel tetramer formed by two dimers associated through a C-terminal coiled coil interaction (Low *et al.*, 2004) (Figure 5). *E. coli* contains approx. 6000 ZapA molecules per cell (Mohammadi *et al.*, 2009) and exists in a dimer-tetramer equilibrium correlated with the protein concentration, although dimer is postulated to be the predominant species within the cell (Small *et al.*, 2007, Low *et al.*, 2004). *In vitro*, ZapA binds FtsZ with a 1:1 stoichiometry promoting the polymerization of FtsZ and the stability of the formed polymers by inhibition of the FtsZ GTPase activity (Gueiros-Filho & Losick, 2002, Small *et al.*, 2007). This inhibition is suggested to be due to a conformational change in the GTP molecule bound to FtsZ, which is not hydrolysed. A second model suggests that the dimer or tetramer of ZapA crosslinks different FtsZ protofilaments, promoting the lateral interactions of FtsZ.

ZapB is a 9.6 kDa cytoplasmic protein that is early recruited to the Z-ring by ZapA (Galli & Gerdes, 2010), and proposed to localize at the inner face of the Z-ring. Cells lacking ZapB are viable but show an elongated phenotype with ectopic Z-rings and spirals, while ZapB overproduction promotes aberrant cell division (Ebersbach *et al.*, 2008). The ZapB crystal structure shows a protein dimer formed by two anti-parallel coiled-coil monomers (Ebersbach *et al.*, 2008) (Figure 5). *In vitro* ZapB dimers assemble into large bundles. The N-terminal region of ZapB is essential for the interaction with ZapA, whereas neither the N- nor the C-terminal ends are essential for ZapB dimerization (Galli & Gerdes, 2012). The relatively high number of ZapB molecules in the cell (~13000) was suggested to allow to small polymers of ZapB interconnect short FtsZ protofilaments decorated with ZapA, promoting their organization into a ring. However, *in vitro* experiments show that at higher concentrations ZapB promotes a decrease on the FtsZ stabilization and bundling promoted by ZapA (Galli & Gerdes, 2012). The detailed mechanism of action of ZapB is not understood, as ZapB is also able to stimulate ZapA-independent Z-ring assembly, as shown by ZapB overexproduction in a *ΔzapAΔzapB* strain (Galli & Gerdes, 2010).

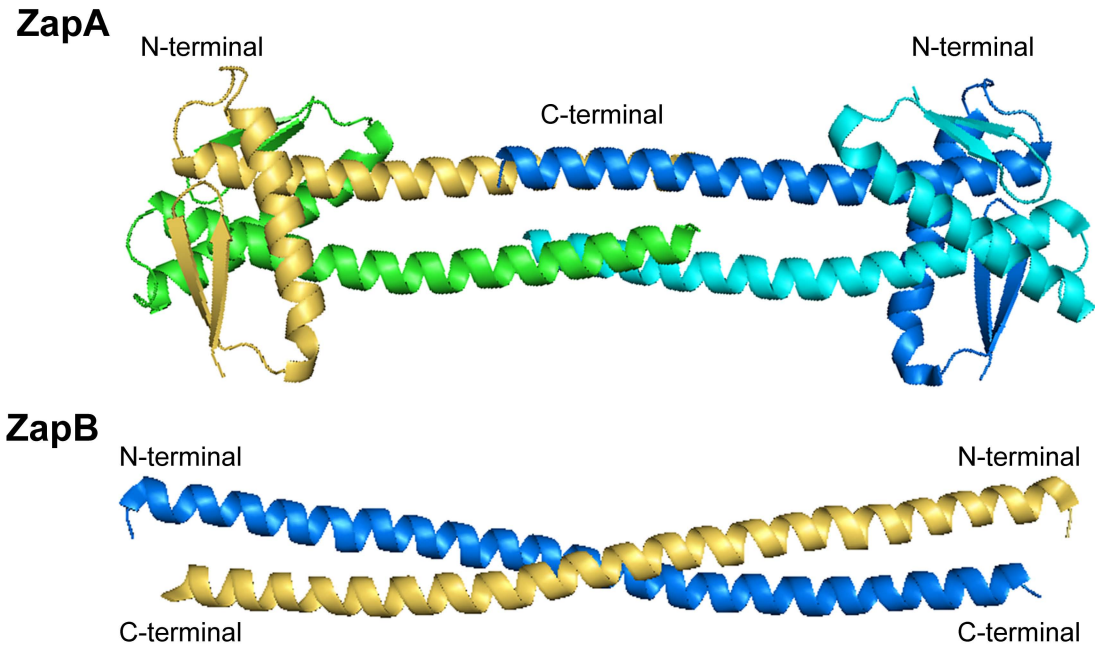

Figure 5. ZapA (*Pseudomonas aeruginosa*) and ZapB (*E. coli*) crystal structures.

ZapA dimerizes by the interaction of the N-terminal region of each monomer, and tetramers are formed by the association between the C-terminal domains of the dimers (PDB entry 1W2E, adapted from Low *et al.*, 2004). ZapB coiled-coil monomers interact in an anti-parallel manner to form dimers (PDB entry 2JEE, adapted from Ebersbach *et al.*, 2008).

ZapC is a 20.6 kDa cytoplamic protein identified as a Z-ring stabilizer, with a function that overlaps with ZapA and ZapB (Durand-Heredia *et al.*, 2011, Hale *et al.*, 2011). The protein is recruited to midcell by FtsZ during the proto-ring formation, independent on the presence of ZipA, FtsA, ZapA and ZapB (Hale *et al.*, 2011). Cells lacking or overproducing ZapC show an increase in cell length and defects in Z-ring morphology and localization (Durand-Heredia *et al.*, 2011, Hale *et al.*, 2011). *In vitro* ZapC is mostly present as a monomer, although weak interaction with itself has been shown, and a probable FtsZ-mediated oligomerization could be suggested from FtsZ:ZapC pelleting assays (Hale *et al.*, 2011). ZapC enhances the lateral association between FtsZ protofilaments and stabilizes them by reducing the FtsZ GTPase activity (Hale *et al.*, 2011).

ZapD is a 28.3 kDa cytoplasmic protein that localizes to midcell in an FtsZ-dependent manner, by direct interaction with the FtsZ C-terminal end, but independent of FtsA, ZipA, ZapA and ZapC (Durand-Heredia *et al.*, 2012). Its cellular concentration is approximately 500 to 800 molecules per cell. While overproduction of ZapD interferes with the assembly of the Z-ring, and therefore with cell division, cells lacking *zapD* present a wild type phenotype. ZapD and ZapA

exert overlapping functions as the deletion of ZapD only shows an effect on division when ZapA is missing. The direct interaction between ZapD and FtsZ was also visualized by electron microscopy, showing ZapD-mediated FtsZ bundling, in which the GTPase activity is decreased approximately 60% (Durand-Heredia *et al.*, 2012).

3.2. Z-ring inhibiting proteins

A specific set of regulatory proteins destabilizes the Z-ring, inhibiting its formation. They belong to different cell mechanisms involved in the tight regulation of the FtsZ protein level and its assembly process.

ClpX is a 46.4 kDa protein, member of the Clp/Hsp100 class of AAA+ proteins (ATPases Associated with various cellular Activities) (Hanson & Whiteheart, 2005). It is an ATP-dependent unfoldase that recognizes specific protein substrates through at least five different types of recognition signals (Flynn *et al.*, 2003, Sauer *et al.*, 2004) (Figure 6) and translocate the substrate protein to ClpP (Glynn *et al.*, 2009), the protease that degrades it. The ClpXP protease complex has been reported to be responsible for the FtsZ degradation, as FtsZ contains a ClpX-recognition signal within its last eighteen amino acid residues (Camberg *et al.*, 2009). ClpXP modulates the dynamic polymerization of FtsZ (Camberg *et al.*, 2009) and regulates the cell division through FtsZ degradation (Camberg *et al.*, 2011).

MinC is a 24.8 kDa cytoplasmic protein, which is part of the septum placement system MinCDE. It is the effector component that interacts with FtsZ and inhibits the Z-ring assembly. It has two functional domains (Figure 6) (Hu & Lutkenhaus, 2000, Cordell *et al.*, 2001), both of which interact with FtsZ and are required for the proper funtion of the Min system (Zhou & Lutkenhaus, 2005). The N-terminal domain of MinC blocks Z-ring assembly when is overexpressed *in vivo* (Hu & Lutkenhaus, 2000). It interacts at the FtsZ dimer interface and shortens the FtsZ polymers without inhibiting the GTPase activity of FtsZ (Dajkovic *et al.*, 2008a). The C-terminal domain of MinC, together with MinD, binds to the C-terminal end of FtsZ inhibiting cell division (Shen & Lutkenhaus, 2009). This interaction with FtsZ may displace than FtsA and ZipA from the Z-ring promoting its disruption (Shen & Lutkenhaus, 2009).

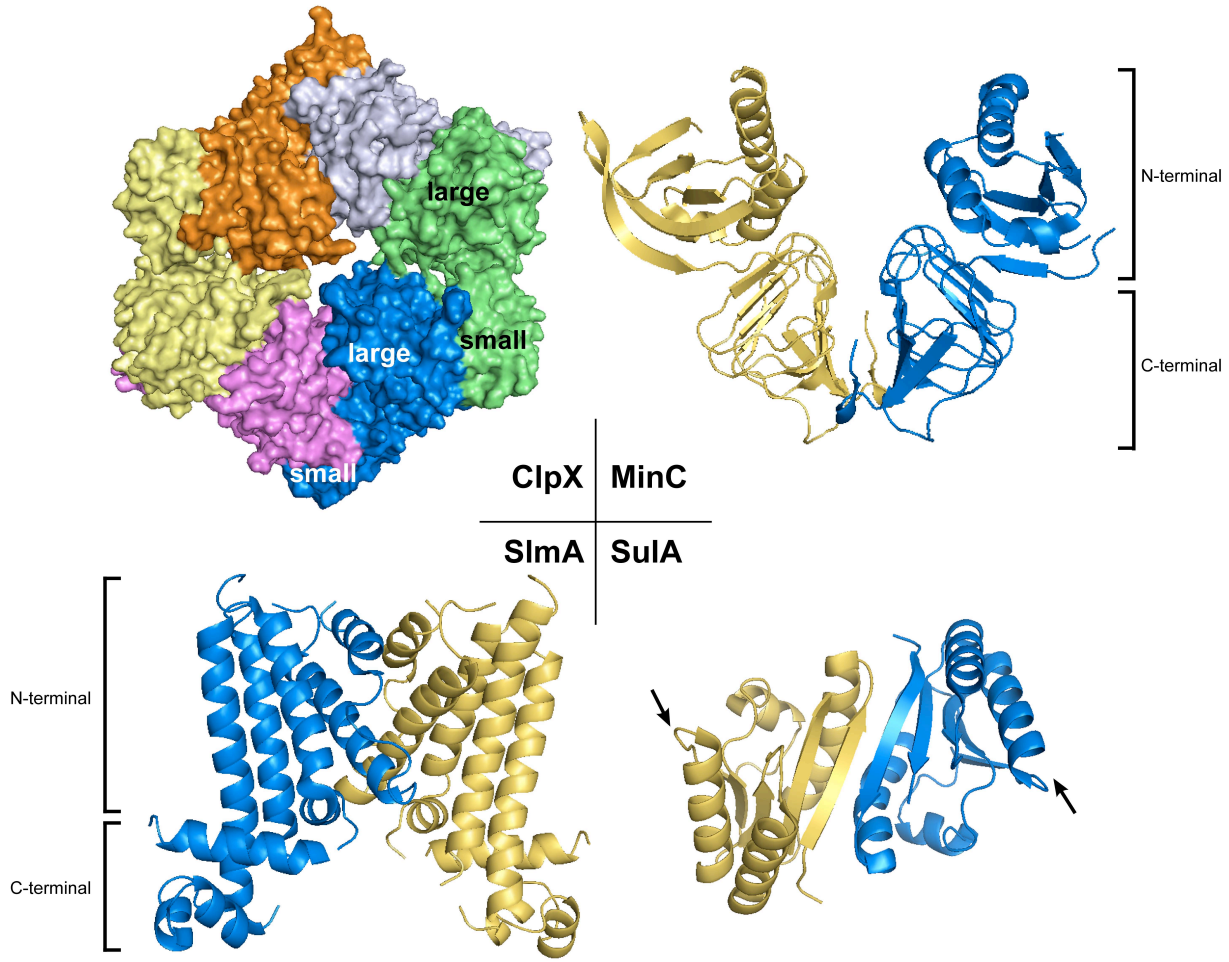

Figure 6. Crystal structures of ClpX (*E. coli*), MinC (*T. maritima*), SlmA (*E. coli*) and SulA (*P. aeruginosa*).

ClpX monomers, containing a large and a small domain, oligomerize forming hexamers that associate to the ClpP protease (view from ClpP distal view) (PDB entry 3HWS, adapted from Glynn *et al.*, 2009). MinC parallel dimer by the association of the C-terminal domains of each monomer (PDB entry 1HF2, adapted from Cordell *et al.*, 2001). SlmA parallel monomer with the C-terminal domains involved in the DNA binding and the N-terminal domains as dimer interface (PDB entry 3NXC, adapted from Tonthat *et al.*, 2011). SulA antiparallel dimer structure interacts with two FtsZ molecules by the helices indicated with arrows (PDB entry 1OFU2, adapted from Cordell *et al.*, 2003)

SlmA (from synthetic lethal with a defective Min system) is a 22.8 kDa cytoplasmic nucleoid-associated protein that blocks the Z-ring formation in the cell regions occupied by the nucleoid. The Z-ring antagonistic function of SlmA is significantly enhanced upon DNA binding (Cho *et al.*, 2011, Tonthat *et al.*, 2011). It has been described the crystal structure, the DNA-binding site (Figure 6) (Tonthat *et al.*, 2011), as well the SlmA-DNA binding sequences on the *E. coli* chromosome (SBSs). SBSs contain a palindromic site with the consensus, 5'-GTGAGTACTCAC-3', and are found over the entire chromosome except the Ter region (Cho *et al.*, 2011, Tonthat *et al.*, 2011), which is the chromosomal DNA region (approximately opposite

oriC) where the replication terminates. *In vitro* the SlmA-DNA complexes do not affect to the FtsZ GTPase activity and the formation of FtsZ protofilaments (Cho *et al.*, 2011). The SlmA-FtsZ crystal structure shows two FtsZ molecules sandwiching an SlmA dimer, suggesting that SlmA separates the FtsZ protofilaments and affects the higher order assembly of FtsZ filaments as bundles and sheets (Tonthat *et al.*, 2011). The mechanism behind the inhibition of Z-ring formation is not clear, but suggests the dimerization or oligomerization of SlmA as key factor (Cho *et al.*, 2011).

SulA is an 18.8 kDa cytoplasmic protein that inhibits Z-ring formation during the SOS response (Huisman & D'Ari, 1981, Huisman *et al.*, 1984). SulA forms dimers that inhibit the assembly of the Z-ring and promote the disassembly of existing Z-rings by direct interaction with the surface of the FtsZ monomer (Figure 6) (Cordell *et al.*, 2003). It inhibits the GTPase activity and the polymerization of FtsZ (Cordell *et al.*, 2003, Mukherjee *et al.*, 1998, Trusca *et al.*, 1998, Dajkovic *et al.*, 2008b, Chen *et al.*, 2012) by sequestering the FtsZ monomers from the intracellular pool (Dajkovic *et al.*, 2008b, Chen *et al.*, 2012). As FtsZ monomers need to bind GTP to form polymers and GTP hydrolysis promotes the disassembly of monomers from polymers, the FtsZ monomers sequestration by SulA is suggested to promote the disassembly of the polymer by the FtsZ own GTPase activity.

4. Septum placement machinery

The correct placement of the cell division septum is essential to ensure morphologically and genetically identical daughter cells. In *E. coli* there are two mechanisms responsible for this purpose: Nucleoid Occlusion (NO) and MinCDE (Rothfield *et al.*, 2005) that carry out their function over the first step of the divisome formation, the proto-ring assembly and specifically over the Z-ring formation.

4.1. Nucleoid occlusion

The bacterial nucleoid and its associated division inhibitor protein SlmA form the NO system. This system avoids the Z-ring formation over the bacterial nucleoid, coordinating cell division with chromosome segregation (Figure 7) (Sun & Margolin, 2004, Woldringh *et al.*, 1991, Bernhardt & de Boer, 2005). SlmA is an FtsZ antagonist that binds to specific sequences of the DNA. Once SlmA is bound to DNA its ability to interfere with FtsZ polymerization is enhanced (Cho *et al.*, 2011, Tonthat *et al.*, 2011).

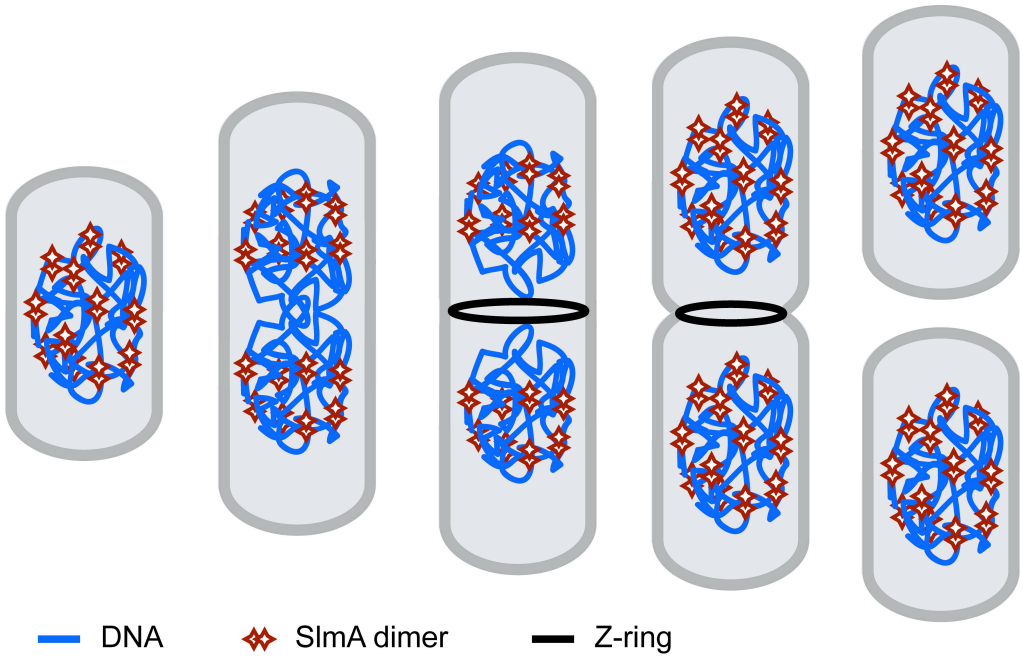

Figure 7. Nucleoid occlusion model in *E. coli*.

The bacterial nucleoid and its effector protein SlmA, bound to specific DNA sequences (SBSs), prevent Z-ring assembly over the nucleoid. During nucleoids segregation SlmA remains bound to the nucleoids leaving the midcell available for Z-ring assembly establishing the cell division site (adapted from Cho *et al.*, 2011).

4.2. Min system

The Min system (from minicells) prevents the Z-ring formation at the cell poles and is formed by MinC, MinD and MinE, three proteins that are encoded by the *minB* operon. The *minB* mutants were identified as cell division defectives, in which septation occurs near the cell poles instead of at midcell. Polar septation generates a small spherical cell lacking chromosomal DNA, named minicell, and a longer than normal cell (Davie *et al.*, 1984, de Boer *et al.*, 1988, de Boer *et al.*, 1989, Lee & Price, 1993). The overexpression of the *minB* operon provokes a phenotype similar to the filaments observed for *fts* mutants (Ward & Lutkenhaus, 1985, Bi & Lutkenhaus, 1993, Raskin & de Boer, 1999a, Raskin & de Boer, 1999b).

MinC is a weak cell division inhibitor that interacts with FtsZ and prevents the formation of FtsZ polymers and of the Z-ring (de Boer *et al.*, 1990, de Boer *et al.*, 1992).

MinD is a peripheral membrane ATPase that, upon binding ATP, interacts cooperatively with the cytoplasmic membrane via its C-terminal amphipathic helix (MinD membrane targeting sequence, MinDmts) (Hu *et al.*, 2002b, Lackner *et al.*, 2003, Suefuji *et al.*, 2002, Szeto *et al.*, 2002) forming coiled-structures. MinD dimerization is required for membrane binding (Lackner *et al.*, 2003, Hu & Lutkenhaus, 2003, Wu *et al.*, 2011, Szeto *et al.*, 2003, Szeto *et al.*, 2002).

Membrane bound MinD increases its affinity to bind MinC, promoting the recruitment of MinC to the inner membrane and the formation of the MinCD complex. The MinCD complex localizes all over the inner membrane avoiding the Z-ring assembly (de Boer *et al.*, 1989).

The third component, MinE confers topological specificity to localize the MinCD complexes at the cell poles. It is a dimer composed of two 88 residues monomers, with a C-terminal domain responsible for its dimerization (Park *et al.*, 2011) and a N-terminal α-helix domain binding with high affinity to membrane bound MinCD complex, and displacing MinC from the MinD dimer interface (Wu *et al.*, 2011).

When MinE binds to the MinCD complex displaces MinC, stimulates the ATPase activity of MinD and provokes the redistribution of the complex to a cytoplasmic region in which the MinE concentration is lower (Raskin & de Boer, 1997, Rowland *et al.*, 2000). The combined action of MinCDE results in promoting an oscillatory pole-to-pole movement (Figure 8) (Raskin & de Boer, 1999a, Raskin & de Boer, 1999b, Hu & Lutkenhaus, 2001, Szeto *et al.*, 2002, Szeto *et al.*, 2003). This oscilation results in a higher concentration of MinCD complex at cell poles than at midcell where it enables FtsZ to form the Z-ring (Meinhardt & de Boer, 2001).

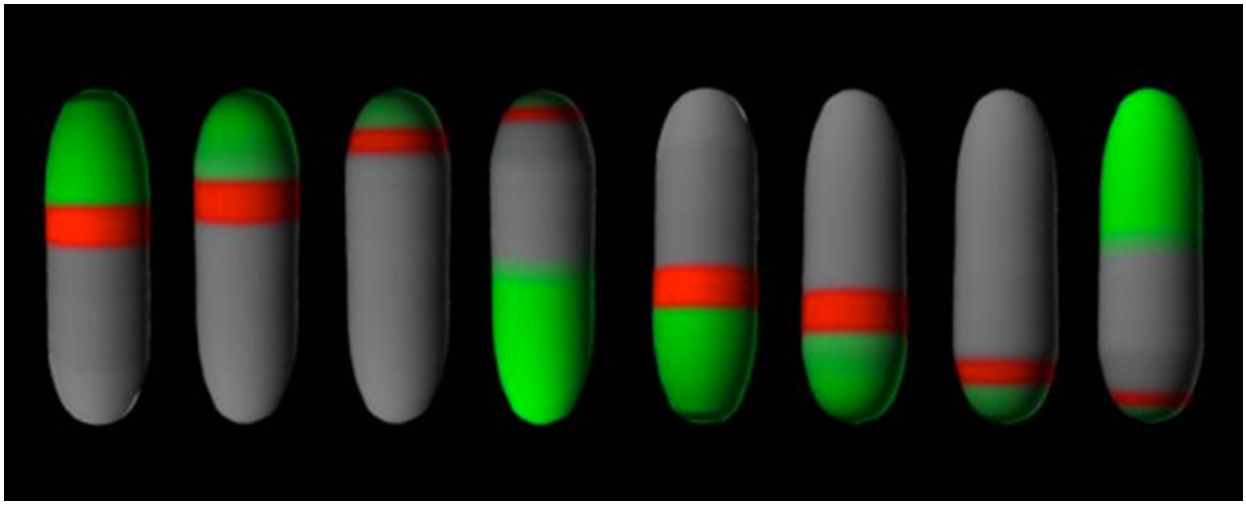

Figure 8. Oscillatory movement of the Min system in *E. coli.*

MinD bound to ATP is attached to the inner membrane of the cell, where recruits MinC forming the MinCD complex (green). MinE (red) interacts with MinD, displaces MinC from the MinCD complex, and stimulates the ATPase activity of MinD, releasing it also from the membrane. The MinCD complex formation is redistributed to the other cell pole, where the MinE concentration is lower. The MinCD oscillation from pole to pole avoids the formation of the Z-ring close to the cell poles, forcing it to the midcell (adapted from Meinhardt & de Boer, 2001).

5. Synthetic biology approach

The reconstruction of the bacterial cell division machinery *in vitro* is among the major goals in defining the role of its individual division ring components. The reconstitution of individual cell division processes as the FtsZ-ring formation (Osawa *et al.*, 2008) or the rapid membrane interactions of the proteins MinD and MinE were successfully performed in a cell free environment (Loose *et al.*, 2008).

This thesis presents the use of *E. coli* maxicells as a cellular container that, remaining intact the transcription and translation machinery, allows to study the protein-protein interactions without the need of purification.

5.1. Maxicells

Maxicells are *E. coli* cells, in which the nucleoids have been degraded without impairing their ability for RNA and protein synthesis. This system was previously used as an *in vitro* transcription-translation system for plasmid-encoded genes of interest in a chromosome-less background (Sancar *et al.*, 1979). Nucleoid degradation in maxicells is achieved by the accumulation of DNA damage in strains that are unable to repair it. DNA damage can be produced by exposure to ultraviolet light (UV) irradiation or by small DNA binding peptides as e. g. microcin B17 (Mayo *et al.*, 1988). UV irradiation provokes the pyrimidine dimers formation, that distort the DNA helix in such a way that replication past this site is blocked. Due to the smaller size and high number of copies of plasmid is more probable to damage the chromosomal DNA than the plasmids born.

E. coli cells repair these DNA damages by the induction of the SOS response. In order to avoid this DNA damage repair response and provoke the chromosomal DNA degradation (Skarstad & Boye, 1993), *recA* strains unable to induce this mechanism must be used for maxicells preparation. In the absence of a functional SOS response and DNA repair mechanism the cell switches to active DNA degradation which leads to cell death (Kuzminov, 1999).

The SOS response is the first DNA damage response, being regulated by the proteins LexA and RecA (Michel, 2005). LexA is a transcriptional repressor and RecA the LexA specific protease that functions as the master regulator of the SOS cascade. LexA binds to a specific LexA binding motif (SOS-box) upstream of *lexA*, *uvrAB*, *sulA*, *umuCD*, *dinP*, *polB*, *recA*, *uvrD*, *ruvAB*, *recN* and *dinA* genes whose gene products act in the SOS response regulation, nucleotide excision repair (NER), cell division stop and error-prone mutagenesis (EPM) repair (Emmerson & West, 1977, Siegel, 1983, Shurvinton & Lloyd, 1982, Lloyd *et al.*, 1983, Little *et al.*, 1981, Sedliakova

et al., 1980, Fogliano & Schendel, 1981, Huisman & D'Ari, 1981, Bagg *et al.*, 1981, Wagner *et al.*, 1999, Iwasaki *et al.*, 1990, Napolitano *et al.*, 2000). Under normal growth conditions LexA represses the SOS response. DNA damage leads to the formation of single stranded DNA (ssDNA) that triggers binding to RecA and the single stranded DNA binding protein SSB. Formation of the ssDNA-RecA-SSB complex activates RecA proteolytic activity resulting in the cleavage of LexA and transcription of the SOS response genes (Little & Mount, 1982). Once DNA damage repair is completed, and the presence of ssDNA is eliminated, the RecA-SSB-ssDNA protein complex disassembles and RecA reduces its proteolytic activity. Now, LexA accumulates, binds to the SOS-box motif and represses the transcription of the SOS genes. In a *recA* mutant strain the absence of RecA maintains the SOS genes repressed by LexA and the accumulation of DNA damage cannot be repaired, provoking eventually that Exonuclease V (RecBCD) degradates the damaged DNA and cells loose their viability (Skarstad & Boye, 1993, Kannan & Dharmalingam, 1990).

Objectives

Our aim is to investigate the early stages of the *Escherichia coli* divisome, the proto-ring formation. For this purpose we use maxicells as a novel approach to reconstruct the cell division machinery.

We will study the functionality of the Min system in the absence of nucleoid and evaluate the Min-directed Z-ring placement using different FtsZ variants.

We will study the role of the proto-ring components FtsA and ZipA on the stability of FtsZ by overproducing them in maxicells.

Finally, we will evaluate and visualize *in vivo* possible protein-protein interactions between the components of the proto-ring and the FtsZ-effector proteins by the combined use of bimolecular fluorescent complementation and maxicells.

Materials & Methods

1. Materials

1.1. *Escherichia coli* strains

The bacterial strains used in this study are described in Table 1.

Table 1. Strains used in this work

Strain	Genotype	Reference
BHB2688	*λimm434cItsb2 red3 Eam4 Sam7/λ, recA*	(Scalenghe *et al.*, 1981)
BW25113	*Δ(araD-araB)567, ΔlacZ4787(::rrnB-3), λ⁻, rph-1, Δ(rhaD-rhaB)568, hsdR514*	(Baba *et al.*, 2006)
CC118	*Δ(ara-leu)7697, ΔlacX74, ΔphoA20, galE, galK, thi, rpsE, rpoB, argE(am), recA1*	(Lee & Beckwith, 1986)
CGSC4280	*argG6, lac41, leuB6, his61, metB1, gal6, malA1, mt12, recA1, rpsL104, supE44, tonA2, tsx1, xyl7, λr, λ-*	(Genilloud *et al.*, 1984)
COLE1	*ArgE3, his4, leu6, proA2, thr1, thyA, ara14, chi1, galK2, lacY1, met, mtl1, rpsL(str31), recA (tif), sup37, tsx33, xyl5, ColE1R64+*	(Castellazzi *et al.*, 1972)
CSR603	*ara-14, argE3, galK2, gyrA98 (nalA98), leuB6, lacY1, mtl-1, proA2, phr-1, recA1, rpsL31, supE44, thi-1, tsx-33, thr-1, uvrA6, xyl-5, λ-, F-*	(Sancar *et al.*, 1979)
DH5α	*endA1, gyrA, hsdR17, relA, recA1, supE44, thi1, Δ(lacaya-argF)U169, ϕ80(lacZΔM15), F-*	(Hanahan, 1983)
DIH101	*galK2, hasS20(rB-,mB-), leu, proA2, recA13, StrR, F-, ara-14, lacY1, mtl-1, supE44, xyl-5, λ-, F′(KanR)*	(Ish-Horowicz & Burke, 1981)
JA221	*lacY1, leu6, ϕ80r, supE44, thr1, thi1, tonA2, λ-, F-, hsd, recA, trpES, F′(lacIq, lacZ+, lacY+, lacA, proA+, proB+)*	(Beggs, 1978)
JBS983	*Δ (dacA::kan), Δ (dacC), his, recA, supF*	(Broome-Smith *et al.*, 1985)
JBS1001	*Δ (dacC), his, recA, supF*	(Broome-Smith & Spratt, 1982)
JW0427	*BW25113 clpP::kan*	(Baba *et al.*, 2006)
JW0428	*BW25113 clpX::kan*	(Baba *et al.*, 2006)
MC4100	*araD205(argF-lac), araD139, deoC1, flbB5301, ptsF25, rpsL150, relA, rbsR, F-*	(Casadaban, 1976)
N100	*galK, lac+, recA*	(McKenney *et al.*, 1981)
NM530	*rk-, mk+, recA13, supF*	(Frischauf *et al.*, 1983)
PB143 /pDB346	*dadR trpE trpA tna ftsZ*^{0} *recA*::Tn*10* *aadA*$^{+}$*repA*$^{+}$*c*I857(ts) $P_{\lambda R}$::*ftsZ*$^{+}$	(Raskin & de Boer, 1997)

RYC1000	*araD205(argF-lac), araD139, deoC1, flbB5301, ptsF25, rpsL150, relA, rbsR, F-, mot, recA56, thi, ΔU169 (lacIPOZYA)*	(Genilloud *et al.*, 1984)
VIP978	*ara-14, argE3, galK2, gyrA98 (nalA98), leuB6, lacY1, mtl-1, proA2, phr-1, recA1, rpsL31, supE44, thi-1, tsx-33, thr-1, uvrA6, xyl-5, λ-, F-, clpP::Kan*	This work
VIP979	*ara-14, argE3, galK2, gyrA98 (nalA98), leuB6, lacY1, mtl-1, proA2, phr-1, recA1, rpsL31, supE44, thi-1, tsx-33, thr-1, uvrA6, xyl-5, λ-, F-, clpX::Kan*	This work
WM1074	F$^-$ *λ-, ilvG-, rfb-50, rph-1,* Δ*lacU169*	(Geissler *et al.*, 2007)
WM1657	WM1074 *ftsA**, Δ*zipA*::*kan*	(Geissler *et al.*, 2003)
XL1	*endA1, gyrA96, hsdR17, Δ(lac, pro, recA1, relA1, supE44, thi, F′(traD36, proAB, lacIqZM15, Tn10)*	(Bullock *et al.*, 1987)

1.2. Plasmids

The plasmids used in this study, their backbone vector and relevant properties are shown in Table 2.

Table 2. Plasmids used in this work

Plasmid	Backbone vector	Relevant properties	Reference
pBAD24	N/A	P_{BAD}, Amp^R	(Guzman *et al.*, 1995)
pBAD33	N/A	P_{BAD}, Cam^R	(Guzman *et al.*, 1995)
pBR322	N/A	Cloning vector	(Bolivar *et al.*, 1977)
pDR113	pMLB1115	P_{Lac}::*minE::gfpmut2*	(Raskin & de Boer, 1997)
pDR119	pMLB1113	P_{Lac}::*gfpmut2::minD*	(Raskin & de Boer, 1999b)
pDSW210	pTrc99A	AmpR, Promoter down mutations in −35 and −10 of pTrc99A	(Weiss *et al.*, 1999)
pET11-b	N/A	P_{T7}, Amp^R	Novagen
pET15-b	N/A	P_{T7}, Amp^R	Novagen
pET15-Zip	pET15-b	*his$_6$::zipA*	(RayChaudhuri, 1999)
pET28-a	N/A	P_{T7}, Kan^R	Novagen

pET-FtsZ-mts	pET11-b	*ftsZ*(Δ1099-1152 bp)::*venus*::*minD*(Δ1-762 bp)	(Osawa *et al.*, 2008)
pJPV50	pUC19	$P_{R\lambda}$::*ftsZ*	(Plá *et al.*, 1993)
pKFV37	pBAD18	*ftsZ*	Laboratory stock
pKG110	pLC112	CamR, P_{nah}	(Sourjik & Berg, 2004)
pMFV12	pET28-a	*his$_6$::ftsA*	(Yim *et al.*, 2000)
pPNV40	pTrc99A	*ftsA*	This work
pPZV23	pTrc99A	*his$_6$::zipA*	This work
pPZV24	pTrc99A	*his$_6$::zipA* (Δ340-814 bp)	This work
pPZV29	pTrc99A	*his$_6$::zipA*(Δ553-987 bp)	This work
pPZV30	pTrc99A	*his$_6$::zipA* (Δ817-987 bp)	This work
pPZV32	pTrc99A	*his$_6$::zipA* (Δ256-987 bp)	This work
pPZV33	pTrc99A	*ftsA**	This work
pPZV36	pTrc99A	*his$_6$::zipA* (Δ340-987 bp)	This work
pPZV38	pTrc99A	*zipA* (Δ1-552 bp)	This work
pPZV42	pTrc99A	*ftsZ*(Δ1099-1152 bp)::*venus*::*minD*(Δ1-762 bp)	This work
pPZV43	pBAD24	*his$_6$::zipA*	This work
pPZV46	pET28-a	*his$_6$::minE*	This work
pPZV49	pKG110	*ftsA**	This work
pPZV50	pKG110	*ftsA*	This work
pPZV51	pKG110	*zapA*	This work
pPZV52	pKG110	*zipA*	This work
pPZV53	pKG110	*minC*	This work
pPZV54	pKG110	*ftsZ*	This work
pPZV55	pKG110	*zapB*	This work
pPZV56	pKG110	*sulA*	This work
pPZV57	pKG110	*slmA*	This work
pPZV58	pKG110	*yfpN* ($YFP_{1\text{-}154\ aa}$-TAISR-) [1]	This work
pPZV59	pKG110	*yfpC* ($YFP_{155\text{-}238\ aa}$-HNMVKQK-) [2]	This work
pPZV60	pKG110	*yfpN* (-RSIAT-$YFP_{1\text{-}154\ aa}$)	This work
pPZV61	pKG110	*yfpC* (-KQKVMNH-$YFP_{155\text{-}238\ aa}$)	This work
pPZV68	pPZV59	*yfpC::ftsA**	This work

pPZV69	pPZV59	*yfpC::ftsA*	This work
pPZV70	pPZV59	*yfpC::minC*	This work
pPZV71	pPZV59	*yfpC::ftsZ*	This work
pPZV72	pPZV59	*yfpC::sulA*	This work
pPZV73	pPZV59	*yfpC::slmA*	This work
pPZV74	pPZV61	*zapA::yfpC*	This work
pPZV75	pPZV61	*zipA::yfpC*	This work
pPZV76	pPZV61	*zapB::yfpC*	This work
pPZV83	pPZV58	*yfpN::ftsA**	This work
pPZV84	pPZV58	*yfpN::ftsA*	This work
pPZV85	pPZV58	*yfpN::minC*	This work
pPZV86	pPZV58	*yfpN::ftsZ*	This work
pPZV87	pPZV58	*yfpN::sulA*	This work
pPZV88	pPZV58	*yfpN::slmA*	This work
pPZV92	pPZV60	*zapA::yfpN*	This work
pPZV93	pPZV60	*zipA::yfpN*	This work
pPZV94	pPZV60	*zapB::yfpN*	This work
pPZV98	pDSW210	*zapA::yfpC*	This work
pPZV99	pDSW210	*zipA::yfpC*	This work
pPZV100	pDSW210	*zapB::yfpC*	This work
pPZV101	pDSW210	*yfpC::minC*	This work
pPZV102	pDSW210	*yfpC::ftsZ*	This work
pPZV103	pDSW210	*yfpC::sulA*	This work
pPZV104	pDSW210	*yfpC::slmA*	This work
pPZV113	pDSW210	*zipA::yfpN*	This work
pPZV114	pDSW210	*zapA::yfpN*	This work
pPZV115	pDSW210	*yfpN::slmA*	This work
pPZV118	pDSW210	*yfpC::ftsA**	This work
pPZV119	pDSW210	*yfpC::ftsA*	This work
pPZV128	pBAD33	his_6*::zipA*	This work
pPZV129	pTrc99A	*ftsZ*::*venus*::*minD*(Δ1-762 bp)	This work
pPZV130	pMA-RQ	*ftsZ*::*venus*::*minD*(Δ1-762 bp)	This work

pPZV131	pBAD33	*ftsA*	This work
pPZV132	pBAD33	*ftsA**	This work
pPZV133	pTrc99A	*ftsZ*	This work
pPZV134	pTrc99A	*venus::minD*(Δ1-762bp)	This work
pPZV135	pTrc99A	*ftsZ(*Δ1-1098 bp)*::venus::minD*(Δ1-762 bp)	This work
pTrc99A	N/A	P_{Trc}, Amp^R	(Amann *et al.*, 1983)
pZAQ	pBR322	*ftsQ-ftsA-ftsZ*	(Ward & Lutkenhaus, 1985)

N/A: not applicable; [1] *yfpN* = *eyfp* 1-462 bp = YFP 1-154 aa ; [2] *yfpC* = *eyfp* 463-717 bp = YFP 155-238 aa

bp starting from ATG start codon

1.3. Antisera

The polyclonal antisera used in this work are described in Table 3.

Table 3. Antisera used in this work

Target protein	Antibody	Dilution (IF)	Dilution (WB)	Source or reference
FtsA	MVM1	1:150	1:5000	Laboratory stock
FtsZ	MVJ9	1:350	1:20000	(Pla *et al.*, 1991)
FtsZ	MVC2	1:400	1:5000	Laboratory stock
GFP	Anti-GFP	N/A	1:3000	Roche
GFP	Anti-GFP	N/A	1:1000	Prof. W. Margolin (University of Texas, Health Science Center, Houston, Texas, USA)
MinC	Anti-MinC	N/A	1:1000	Prof. L. Rothfield (University of Connecticut Health Center, Farmington, CT, USA)
MinD	Anti-MinD	N/A	1:1000	Prof. L. Rothfield (University of Connecticut Health Center, Farmington, CT, USA)
MinE	MVP1	N/A	1:2000	This work
SlmA	Anti-SlmA	N/A	1:2000	Prof. P. de Boer (Case Western Reserve University School of Medicine, Cleveland, Ohio, USA)
ZipA	MVC1	1:400	1:5000	Laboratory stock

N/A: not applicable

1.4. Primers

Oligonucleotide primers used in this work are listed in Table 4.

Table 4. Primers used in this work

Primer	Sequence (5′→3′)	Orientation	Target
1452	ATATA*ACTAGT*GGCGTTGGCGTCTTTGACTTCGCG	Rv [a]	*zipA*
1453	ATATA*CATATGGGATCC*ATGTCTGCACAACCCGTC	Fw [b]	*zapA*
1454	TTTTT*ACTAGT*GACCTCTTCCATGCGACCCAG	Rv	*zapB*
1455	AAAAA*ACTAGT*ATGTTTGAACCAATGGAACTTACC	Fw	*ftsZ*
1456	AAAAA*ACTAGT*ATGATCAAGGCGACGGAC	Fw	*ftsA*
1457	AAAAA*ACTAGT*ATGTCAAACACGCCAATCGAGC	Fw	*minC*
1458	AAAAA*ACTAGT*ATGTACACTTCAGGCTATGC	Fw	*sulA*
1459	AAAAA*ACTAGT*ATGGCAGAAAAACAAACTGCG	Fw	*slmA*
1466	TTTTT*CATATGGGATCC*ATGATGCAGGATTTGCGTCTG	Fw	*zipA*
1467	TTTTT*ACTAGT*TTCAAAGTTTTGGTTAGTTTTTTCGG	Rv	*zapA*
1468	ATATA*CATATGGGATCC*ATGACAATGTCATTAGAAGTGTTTGAG	Fw	*zapB*
1469	ATATA*GAGCTCAAGCTT*TTAATCAGCTTGCTTACGCAGGAA	Rv	*ftsZ*
1470	ATATA*GAGCTCAAGCTT*TTAAAACTCTTTTCGCAGCCAAC	Rv	*ftsA*
1471	ATATA*GAGCTCAAGCTT*TCAATTTAACGGTTGAACGGTCAAAGCG	Rv	*minC*
1472	ATATA*GAGCTCAAGCTT*TTAATGATACAAATTAGAGTG	Rv	*sulA*
1473	ATATA*GAGCTCAAGCTT*TTACTGCAACTGTGCCGCAATTAGCGGCC	Rv	*slmA*
1478	ACA*ATGCATGGATCC*ATGAGTAAAGGAGAAGAAC	Fw	*yfpN* [c]
1479	AGAAATTGCTGTTGCCATGATGTATACATTGTGTGAG	Rv	*yfpN* (1)
1480	CACA*ACTAGT*TCTAGAAATTGCTGTTGCCATG	Rv	*yfpN* (2)
1481	TTTT*ATGCATGGATCC*ATGGACAAACAAAAGAATGGA	Fw	*yfpC* [d]
1482	TTGACCATGTTGTGTTTGTATAGTTCATCCATGCCATG	Rv	*yfpC* (1)
1483	CACA*ACTAGT*TTTCTGCTTGACCATGTTGTGTTTG	Rv	*yfpC* (2)
1484	TCTATCGCCACGATGAGTAAAGGAGAAGAACTTTTCACTGG	Fw	*yfpN* (1)
1485	CACA*ACTAGT*CGTTCTATCGCCACGATGAG	Fw	*yfpN* (2)
1486	TGTG*GAGCTCAAGCTT*TTATGCCATGATGTATACATTGTGTGA	Rv	*yfpN*
1487	AAGGTCATGAACCACGACAAACAAAAGAATGGAATC	Fw	*yfpC* (1)
1488	CACA*ACTAGT*AAACAGAAGGTCATGAACCACGACAAAC	Fw	*yfpC* (2)
1489	TGTG*GAGCTCAAGCTT*TTATTTGTATAGTTCATCCATGCC	Rv	*yfpC*

1507	ATATA*GAGCTCGTCGAC*TTAAAACTCTTTTCGCAGCCAAC	Rv	*ftsA*
MP17	CCC*AAGCTT*GTTATCCTCCGAACAAGCGTTTGAGGAAGC	Rv	*minD*
MP18	CCC*AAGCTTGGATCC*ATGTTTGAACCAATGGAACTTACCAATGAC	Fw	*ftsZ*
MP24	GGTGGTCGTCCGCCCTGGAGTCTGCAACGT	Fw	*ftsA*
MP25	ACGTTGCAGACTCCAGGGCGGACGACCACC	Rv	*ftsA*
MP26	GGAAACAGA*CCATGG*GCAGCAGCC	Fw	*his$_6$::zipA*
MP27	*GGATCC*TCACATAACTGGAGCAGGTTCCGC	Rv	*zipA*(1-552 bp)
MP28	*GGATCC*TCAACGAGCAGCCTCATGCTCCTG	Rv	*zipA*(1-255 bp)
MP29	*GGATCC*TCATACCTGCATAAAGATAGTGACACC	Rv	*zipA*(1-816 bp)
MP31	*GGATCC*TCATACCTGCGCTTCAGG	Rv	*zipA*(1-339 bp)
MP32	GGAAACAGA*CCATGG*ATAAACCGAAGCGC	Fw	*zipA*(553-987 bp)
MP33	*GGATCC*TCAGGCGTTGGCGTCTTT GAC	Rv	*zipA*(553-987 bp)
MP34	AA*CATATG*GCATTACTCGATTTCTTTCTC	Fw	*minE*
MP35	TTT*GAATTC*CTTATTTCAGCTCTTCTGC	Rv	*mine*
MP36	AAATATA*TCTAGA*ATGATCAAGGCGACGG	Fw	*ftsA*
MP37	ATATTA*CTGCAG*TTAAAACTCTTTTCGC	Rv	*ftsA*
MP38	TATA*CCATGG*ATGAAAGAACCGGATTATCTGGAT	Fw	*ftsZ* (1099-1152 bp)
MP39	TATA*CCATGG*ATGCCGCCTCGTCCGGCAGGC	Fw	*venus*
MP40	TATAGTCGACTTAGCCACCAAACAGGCGTTTCAG	Rv	*mind*
PN1	GGTGGT*CCATGG*TCAAGGCGACG	Fw	*ftsA*
PN2	GGTGGT*GTCGAC*TTAAAACTCTTTTCG	Rv	*ftsA*

[a] Reverse (Rv) [b] Forward (Fw) [c] *yfpN* = *eyfp* 1-462 bp [d] *yfpC* = *eyfp* 463-717 bp; bp starting from ATG start codon

(1) 1st PCR (2) 2nd PCR using 1st as template; italics bp in the sequences indicate the endonuclease restriction site

1.5. Chemical and reagents

Chemical and reagents used in this work are listed in the Table 5.

Table 5. Chemical and reagents used in this work

Product	Utility	Supplier
4', 6-diamidino-2-phenylindole (DAPI)	Visualization of DNA	Molecular Probes
Acrilamide: N, N´-methyl-bisacrylamide	Protein electrophoresis	Bio Rad
Agar	Preparation of LB plates / Microscopy	Pronadisa
Agarose	DNA electrophoresis	Pronadisa
Antibiotics (ampicillin, cloramphenicol, kanamycin, spectinomycin, tetracycline)	Selection marker	Roche

Arabinose	Protein overproduction	Merck
Alexa594-conjugated anti-rabbit goat serum	Secondary antibody for immunofluorescence	Molecular Probes
BM Chemiluminiscence Blotting Substrate (POD)	Immunoblotting	Roche
D-Cycloserine	Maxicells preparation	Sigma
Deoxinucleotides triphosphate	PCR	Roch
Isopropyl β-D-1-thiogalactopyranoside (IPTG)	Induction of protein overproduction	Roche
Kodak Biomax XAR film	Immunoblotting	Sigma
Marker X DNA	DNA electrophoresis	Roche
Miniprep kit	Plasmid DNA isolation	Qiagen, Promega
Nylon membrane positively charged	Immunoblotting	Roche
Phusion® High-Fidelity DNA Polymerase	PCR	New England Biolabs
Precision Plus Protein Standars Dual Color	Protein electrophoresis	Bio Rad
Protein A-Horseradish peroxidase conjugate	Immunoblotting	Bio Rad
Inmobilon-P membrane, PVDF	Immunoblotting	Millipore
PWO DNA polymerase	PCR	Roche
Site-directed Mutagenesis kit	Site-directed mutagenesis	Stratagene
Sodium citrate	P1 transduction	Merck
Sodium salicylate	Induction of protein overproduction	Sigma
Taq DNA polymerase	PCR	Roche
Vectashield	Fluorescence microsocopy	Vector Laboratories

1.6. Others

The available filters mounted on the Olympus BX61 microscope used in this work are listed in the Table 6.

Table 6. Available filters mounted on Olympus BX61 microscope

Filter name	Excitation band (nm)	Emission Band (nm)	Extra	Application
HQ:CY3r	530-545	610-675	Beam splitter 565LP	Phase-contrast
U-MNU2	360-370	420	Dichromatic filter: 400 nm	DAPI fluorescence
U-MNIBA2	470-490	515-550	Dichromatic filter: 505 nm	GFP, Venus and YFP fluorescence
U-MWIY2	545-580	610	Dichromatic filter: 600 nm	Alexa Fluor® 594 fluoresence

2. Methods

2.1. Bacterial growth conditions

E. coli strains, if not indicated otherwise, were cultured at 37ºC in Luria Bertani broth (LB) or LB agar plates (Sambrook *et al.*, 1989), supplemented with antibiotics when required (ampicillin [100 µg/ml], tetracycline [20 µg/ml], kanamycin [50 µg/ml], chloramphenicol [50 µg/ml], spectinomycin [50 µg/ml]). Liquid cultures were grown in an orbital shaker at 250 rpm. The optical density at 600 nm (OD_{600}) was measured using a CO8000 Cell Density Meter from WPA biowave. To measure the FtsZ levels in WM1074 and WM1657 growing cells, cells were grown overnight at 37ºC in a shaking water bath with aeration and then diluted 1:100. The optical density was measured periodically and kept below 0.3 by serial dilutions with prewarmed medium. In this way, the growth rate remained constant. After at least ten mass doublings samples were taken. After that the cultures were allowed to reach to an OD of aprox. 0.8, and samples were taken again and processed for SDS-PAGE and immunoblot.

2.2. Preparation of *E. coli* maxicells

E. coli CSR603 maxicells were prepared, with minor modifications, as reported by Sancar *et al.* (Sancar *et al.*, 1979). Briefly, the *E. coli* strain CSR603 was grown overnight in a shaker at 37ºC in Luria Bertani broth (LB) supplemented with antibiotics depending of the carrying plasmid (Table 2). Next day, 20 ml of fresh LB, supplemented with antibiotics if necessary, was inoculated 1:100 with the grown overnight cell culture an incubated in a shaker at 37ºC until the cell culture reached an cell number of 1 x 10^8 cells/ml. 10 ml of the bacterial suspension was irradiated in complete darkness with ultraviolet light (UV) (UV dose at 254 nm: 105.98 J/m^2) and incubated for 3 hours in a shaker at 37ºC in complete darkness to induce the degradation of UV-damaged chromosomal DNA (Sancar *et al.*, 1979). It is important to note that the UV irradiation dose is variable for each maxicell strain and UV-lamp setup and should be individually determined (our lamp is TUV TL D 15W SLV, Philips). 3 hours after UV irradiation, D-cycloserine at a final concentration of 200 µg/ml was added to the culture and it was left for additional 16 hours in a shaker at 37ºC in complete darkness. D-cycloserine inhibits the condensation of the pentapetide peptidoglycan precursors during peptidoglycan synthesis and therefore lyses actively dividing bacterial cells that escaped UV damage (Lovering *et al.*, 2012). The obtained maxicells were directly processed for phase-contrast, immunofluorescence microscopy, sodium-dodecyl-sulfate polyacrylamide gel electrophoresis (SDS-PAGE) or immunoblot.

If not indicated otherwise, maxicells overproducing a plasmid-encoded gene of interest were induced by the addition of the inductor at 3 hours after UV irradiation. Maxicells obtained

from CSR603 bearing the plasmid pJPV50 were performed at 30ºC, and shifted to 42ºC to allow overproduction of plasmid-encoded $FtsZ^+$ from lambda P_R.

2.3. Complementation plate assay of *E. coli* VIP2 and PAT84

Overnight cultures at similar OD_{600} of *E. coli* VIP2 (Pla *et al.*, 1991) or PAT84 (Koppes *et al.*, 1978) carrying either pPZV42, pPZV129, pPZV133 or the empty vector control pTrc99A grown at 30ºC were spotted in a 10-fold dilution series on LB plates supplemented with kanamycin, chloramphenicol and ampicillin in case of VIP2 cells, and LB plates supplemented with ampicillin for PAT84 cells. These plates further contain 0, 10 and 25 μM IPTG and were incubated overnight at 30ºC and 42ºC.

2.4. Production of FtsZ-VM and FtsZ*-VM in *E. coli* VIP2 and maxicells

For FtsZ-VM- and FtsZ*-VM-ring localization in *E. coli* VIP2, the strain carrying either pPZV42 or pPZV129 was grown overnight in LB supplemented with antibiotics at 30ºC. Next day it was reinoculated at 1:100 in fresh pre-warmed LB and grown in a shaker at 30°C. At an optical density OD_{600} of 0.3 cell cultures were was shifted to 42ºC for 180 minutes to deplete FtsZ (Plá *et al.*, 1993). Upon depletion of FtsZ the overproduction of either FtsZ-VM or FtsZ*-VM was induced for 120 minutes by the addition of 0.5 mM IPTG and cells were subsequently prepared for phase-contrast and fluorescence microscopy. For FtsZ-VM- and FtsZ*-VM-ring localization in maxicells, CSR603 bearing either the plasmid pPZV42 or plasmid pPZV129 was grown in LB supplemented with ampicillin in a shaker at 37 °C until they reached a cell number of 1×10^8 cells ml^{-1}. At this point cells were either converted into maxicells (see "Preparation of *E. coli* maxicells") or processed as a non UV-irradiated *wild-type* control. The overproduction of either FtsZ-VM or FtsZ*-VM was induced for 16 hours by the addition of 0.5 mM of IPTG at 3 hours after UV irradiation and Z-ring formation was observed by fluorescence microscopy.

2.5. BiFC in growing cells and in maxicells

In non UV-irradiated CSR603 and WM1074 strains, cells bearing the corresponding plasmids were grown over night at 37º C in LB broth supplemented with ampicillin and chloramphenicol. Next day they were reinoculated (1:100) in new LB broth supplemented with both antibiotics at 37º C until OD600 reached to 0.3. Overproduction of the plasmid-encoded proteins was induced by the addition of 100 μM sodium salicylate and 1mM IPTG. After 180 minutes, cultures were shifted to room temperature over night. Next day samples were observed by fluorescent microscopy. Maxicells carrying BiFC plasmids were prepared as described (see "Preparation of *E. coli* maxicells"). Overproduction of the plasmid-encoded proteins was induced simultaneously with the addition of D-cycloserine. After 180 minutes at 37º C, cultures were

shifted to room temperature during 13 hours and subsequently observed by fluorescent microscopy. The strain PB143/pDB346 carrying the corresponding BiFC plasmids were grown over night at 42º C in LB broth supplemented with ampicillin, chloramphenicol and spectinomycin. Next day cultures were reinoculated 1:100 in LB broth supplemented with antibiotics and incubated at 42º C until OD600 of the culture reached 0.3. Then cultures were shifted to 30º C and overproduction of BiFC plasmid-encoded proteins was induced as described for non UV-irradiated cells.

2.6. Overproduction of GFP-MinD and MinE-GFP

E. coli CSR603 carrying either plasmid pDR113 (P_{Lac}::*minE-gfpmut2*) (Raskin & de Boer, 1997) or pDR119 (P_{Lac}::*gfpmut2-minD*) (Raskin & de Boer, 1999b), was grown in LB-broth supplemented with ampicillin in a shaker at 37°C to a cell number of 1 x 10^8. At this point cells were either converted into maxicells or processed as a non UV-irradiated *wild-type* control. Overproduction of either MinE-GFP or GFP-MinD in maxicells was induced by the addition of 25 μM IPTG at 3 hours after UV irradiation simultaneously with the addition of D-cycloserine and incubated for 16 hours in a shaker at 37ºC in complete darkness. This amount of IPTG is sufficient for the induction of expression of the GFP fusions, but not toxic for cell growth (Raskin & de Boer, 1997). The light exposures of the fluorescence images were corrected for bleaching of the GFP fluorescence by the incident light.

2.7. P1 transduction

Donor strains P1*vir* lysate preparation of strains JW0427 (*clpP::kan*) and JW0428 (*clpX::kan*) was performed according to Miller *et al.* (Miller, 1972) and transducted into *E. coli* CSR603. The obtained transductant were screened on LB plates supplemented with 0.2% citrate together with 10 μg/ml kanamycin and 30 μg/ml nalidixic acid and incubated overnight at 37ºC. Positive candidates were checked by PCR as described by Baba *et al.* using specific set of primers for *kan*, *clpP* and *clpX* (Baba *et al.*, 2006).

2.8. Plasmids

Characteristics of the plasmids used in this work are listed in Table 2. All the PCR products were confirmed by sequence analysis (Parque Científico, UAM, Madrid; GENEWIZ, South Plainfield, NJ). The PCR annealing temperature, if not indicated otherwise, is 55ºC. The descriptions of constructs are grouped as following their appearance in the "*Results"* sections:

- *Selection of FtsZ placement in nucleoid-free bacterial cells.* The gene encoding for FtsZΔ366-383-Venus-mts (FtsZ*-VM) was transferred by PCR from pETFtsZ-mts (Osawa *et al.*, 2008) to the pGEM-T vector. Using the restriction endonucleases *NcoI* and *SalI* the gene was introduced

into the IPTG inducible expression vector pTrc99A. The resulting plasmid pPZV42 was used to overproduce FtsZ*-VM in strains VIP2 and CSR603. PCR was performed according to standard conditions (Sambrook *et al.*, 1989) using primers MP17, MP18, Taq DNA polymerase and pETFtsZ-mts as template. The gene coding for FtsZ-Venus-mts (*ftsZ-VM*) was *in vitro* synthesized (GeneArt AG). The delivered plasmid pZV130 was cut with *Nco*I-*Sal*I to transfer the 1953 bp carrying fragment into pTrc99A, producing plasmid pZV129. Plasmid pKFV37 was cut with *Sac*I-*Hin*dIII to transfer the *ftsZ* gene into pTrc99A, producing plasmid pZV133. The PCR product carrying the gene coding for the Venus-MinDmts protein (VM) was obtained using primers MP38 and MP40, plasmid pPZV129 as template, with a primer annealing temperature of 65 ºC, and was cloned into vector pTrc99A to construct pPZV134. The PCR product carrying the gene coding for ZC-VM (FtsZ C-terminal end-Venus-MinDmts) protein was obtained using primers MP39 and MP40, plasmid pPZV129 as template, with a primer annealing temperature of 65 ºC and was cloned into vector pTrc99A to construct pPZV135.

- *A specific role for ZipA in cell division.* The *ftsA* gene of pPNV40 was obtained by PCR using primers PN1 and PN2 and plasmid pMFV12 as a template and cloned into plasmid pTrc99A. pPZV23 was constructed by subcloning the *his::zipA* containing a *Nco*I-*Bam*HI fragment of pET-15ZIP into the plasmid pTrc99A. pPZV24 was constructed by the removal of an 477 bp KpnI fragment of plasmid pPZV23. pPZV29, pPZV30, pPZV32, pPZV36 were constructed by cloning the PCR products obtained using primer MP26 in combination with MP27, MP29, MP28 or MP31, respectively, and pPZV23 as a template. pPZV33 was obtained according the site-directed mutagenesis kit (Stratagene) using primers MP24 and MP25 and pPNV40 as template. pPZV38 was constructed by cloning the PCR product obtained using primers MP32 and MP33 and pPZV23 as template. pPZV43 was constructed by subcloning the *his::zipA Nco*I-*Xba*I fragment of pPZV23 into pBAD24. pPZV128 was constructed by subcloning the *his::zipA Nhe*I-*Sal*I fragment of pPZV43 into pBAD33. pPZV131 and pPZV132 were constructed by subcloning the obtained PCR products using primers MP36 and MP37 with template pPNV40 or pPZV33 respectively.

- *Bimolecular Fluorescence Complementation to study protein-protein interations of the early divisome assembly event.* PCR using Phusion® High-Fidelity DNA polymerase (NewEngland Biolabs) and an oligonucleotide primer annealing temperature of 55º C was performed according to standard procedure (Sambrook *et al.*, 1989). The PCR template for the amplification of the cell division genes was prepared from *E. coli* MC4100 cells as described by Baele *et al.* (Baele *et al.*, 2001), with exception of plasmids pDSW208-Z338-yfp (from WM3308 strain) and pKG110-CFP-ftsA* (from WM3229 strain) that were used as template for the amplification of *yfpN* (1-462bp) and *yfpC* (463-717bp) sequences of the enhanced yellow fluorescent protein gene *eyfp* and for

*ftsA**, respectively. The construction of the individual YFPN and YFPC fusion proteins (Table 8) was designed on two basic plasmid constructs with an interchangeable cassette strategy. Each cell division protein was connected to YFPN or YFPC bridged by a linker peptide: TAISR or RSIAT when *yfpN* is fused to the cell division gene by its 3' or 5' end respectively, and HNMVKQK or KQKVMNH when *yfpC* is fused by its 3' or 5' end respectively (Hu *et al.*, 2002a). Those linkers were added to *yfpN* and *yfpC* in two steps by two consecutives PCRs, using the following primers: 1478 with 1479 or 1480; 1481 with 1482 or 1483; 1486 with 1484 or 1485; 1489 with 1487 or 1488. *ftsA**, *ftsA*, *minC*, *ftsZ*, *sulA* and *slmA* were fused to the C-terminal end of the *yfp* halves. Each cassette was cloned into pKG110 plasmid: the cell division genes were amplified by PCR using upstream primers containing a SpeI endonuclease restriction site (1456, 1456, 1457, 1455, 1458 and 1459) and downstream primers containing a HindIII and SacI endonuclease restriction sites (1470, 1470, 1471, 1469, 1472 and 1473) to constructs the plasmids pPZV49, pPZV50, pPZV53, pPZV54, pPZV56 and pPZV57 respectively, whereas *yfpN* and *yfpC* were amplified using upstream primers containing a NsiI and BamHI endonuclease restriction sites (1478 and 1481) and downstream primers containing a SpeI endonuclease restriction site (1480 and 1483) to construct the plasmids pPZV58 and pPZV59). Following, these cell division genes cloned into pKG110 were digested with the restriction endonucleases SpeI and SacI and ligated to the plasmids containing each half of *yfp*, previously digested with the same enzymes, yielding the plasmids pPZV68, pPZV69, pPZV70, pPZV71, pPZV72, pPZV73, pPZV83, pPZV84, pPZV85, pPZV86, pPZV87 and pPZV88. The genes *zipA*, *zapA* and *zapB* were fused to the N-terminal end of the *yfp* halves. Each cassette was also cloned into pKG110 plasmid: the cell division genes were amplified by PCR using upstream primers containing a NdeI and BamHI endonuclease restriction sites (1453, 1466 and 1468) and downstream primers containing a SpeI endonuclease restriction site (1467, 1452 and 1454) to construct the plasmids pPZV51, pPZV52 and pPZV55 respectively, whereas *yfpN* and *yfpC* were cloned using upstream primers containing a SpeI endonuclease restriction site (1485 and 1488) and downstream primers containing a HindIII and SacI endonuclease restriction sites (1486 and 1489) to construct the plasmids pPZV60 and pPZV61 respectively. Following, the *yfp* halves cloned into pKG110 (pPZV60 and pPZV61) were digested by the restriction endonucleases SpeI and SacI and ligated to pPZV51, pPZV52 or pPZV55 previously digested with the same enzymes, yielding the plasmids pPZV74, pPZV75, pPZV76, pPZV92, pPZV93 and pPZV94.

To allow the coexpression of different BiFC constructs in the same cell, all the *yfp*C fusions were cloned also in pDSW210. They were obtained, excepting those containing *ftsA** and *ftsA*, by digestion of the respective pKG110 clones with BamHI and HindIII, and were cloned in

pDSW210 previously digested with the respective enzymes to produce the plasmids pPZV98, pPZV99, pPZV100, pPZV101, pPZV102, pPZV103, pPZv104, pPZV113, pPZV114 and pPZV115. The constructs *yfpC*::*ftsA** and *yfpC*::*ftsA* were amplified by PCR using plasmids pPZV68 and pPZV69 as template, an upstream primer containing NsiI and BamHI endonuclease restriction sites (1481) and a downstream primer containing SalI and SacI endonuclease restriction site (1507), and were cloned using BamHI and SalI restriction enzymes to construct the plasmids pPZV118 and pPZV119 respectively.

2.9. Production of anti His-MinE antibody

The *minE* gene were amplified by PCR and cloned into the pET28-a vector fused to an N-terminal hexa-histidine tag, producing the plasmid pPZV46. The *minE* PCR fragment was obtained by standard PCR using oligonuclotide primers MP34 and MP35, *Taq* polymerase and chromosomal DNA as template with an annealing temperature of 55ºC. The chromosomal DNA of *E. coli* MC4100 was isolated according to Baele *et al.* (Baele *et al.*, 2001). His-MinE was overproduced and purified according to the pET-vector expression systems in combination with nickel-affinity chromatography (His-Bind Resin) according to manufacturers manual (Novagen Biochemicals). Purified His-MinE was blotted on a nylon blotting membrane and send for the production of rabbit blood serum (PickCell Laboratories BV, Lelystad, The Netherlands) containing polyclonal antibodies that recognize His-MinE.

2.10. Phase-contrast and fluorescence microscopy

For phase-contrast and fluorescence microscopy, cells were spotted on an agarose-padded microscope slide and imaged with an Olympus DP70 camera coupled to an Olympus BX61 microscope, equipped with an 100 x immersion oil lens and the filters (Table 6). The images were captured with the analySIS imaging software (Olympus) and further processed with Adobe Photoshop CS and the Huygens professional deconvolution software package (Scientific Volume Imaging bv, Hilversum, The Netherlands). For BiFC microscopy, 5 µl of cell sample was mixed 1:1 with 2% low-melting agarose, spotted onto a coverslip, and imaged.

Immuno-fluorescence microscopy of cells was prepared as described by Addinall *et al.* (Addinall *et al.*, 1996), using antibodies against FtsZ, FtsA and ZipA as primary antibody and Alexa Fluor®-594 labelled goat anti-rabbit IgG, as secondary antibody. The cover slip was mounted together with the addition of Vectashield Mounting medium and DAPI on a microscope slide and sealed with transparent nail polish to protect sample from drying during microscopy. Three-dimensional reconstitution of individual optical sections (n= 55) was performed after deconvolution using the Huygens Professional software package and using the Bitplane Imaris

Software package. The elongation along the z-axis introduced by the optical system was corrected in the deconvoluted stacks by multiplying the vertical scale by 0.42 (the correction factor calculated from the measurement of control spherical particles).

2.11. SDS-PAGE and immunoblots

SDS-PAGE (Laemmli, 1970) and immunoblot analysis (Towbin *et al.*, 1979) were performed according to standard procedures. For SDS-PAGE, bacterial culture pellets were resuspended in SDS-PAGE sample buffer and boiled for 5 minutes at 95ºC and 0.1 OD_{600} of bacterial cells was loaded per lane. For the experiment in Figure 24, cells corresponding to 0.3 OD_{600} were loaded per lane. Blood sera or purified primary antibodies (Table 3) were used for specific protein detection, and horseradish peroxidase coupled protein A, the BM chemiluminescence blotting substrate and either BioRAD ChemDoc XRS+ Imaging System or Kodak Biomax XAR film were used for the development of the luminescence signals on PVDF or Nitrocellulose membranes. Quantification of the immunoblotted protein levels was performed using ImageJ software package (Wayne Rasband, NIH).

2.12. Protein structural data

Protein crystal structures were visualized and imaged using MacPyMOL software (2006, DeLano Scientific LLC) and Adobe Photoshop software. The Protein Data Bank (PDB) (Bernstein *et al.*, 1977) entry code of each crystal structure is indicated in the respective figure legend. Structures of FtsA and ZipA in Figure 31 were aligned according to Szwedziak *et al.* (2012).

Results

1. Maxicells: proof of principle

1.1. Screening of *recA* mutant strains for maxicell production

An important requirement for maxicell production is the availability of a suitable *Escherichia coli recA* mutant strain. We tested strains COLE1, BHB2688, CC118, CGSC4280, CSR603, DH5α, DIH101, JA221, JBS983, JBS1001, N100, NM530, RYC1000 and XL1 (Table 1) for mortality upon ultraviolet light (UV) irradiation. These strains carry different *recA* mutations.

All strains were tested on LB agar plates, which were divided into three zones corresponding to UV exposure of the plated strain for 0, 5 and 10 seconds. After UV irradiation the plates were incubated overnight at 37ºC in complete darkness. Nine of these fourteen strains respond to 5 seconds of UV irradiation (Figure 9A). The COLE1 strain was used as a control strain carrying the temperature sensitive *recA* (*tif-1*) mutation and only UV sensible at 42° C (Castellazzi *et al.*, 1972). Next screening was performed in liquid cultures exposed to UV during 9 seconds (Figure 9B). Strains CSR603, RYC1000 and DH5α were chosen in this screen as they responded well in plates and are described suitable maxicells strains (Sancar *et al.*, 1979, Genilloud *et al.*, 1989, Verkamp & Chelm, 1989). Upon UV-irradiation of these three strains only CSR603 cell cultures showed a significant mortality (~ $1x10^4$ surviving cell). Sancar *et al.* defines the UV dose necessary to induce DNA degradation but not lysis for the maxicells preparation to be equivalent to the reduction of a starting culture of $1x10^8$ cell/ml to $5x10^2$–$1x10^3$ cells/ml. In order to obtain the suitable dose, CSR603 liquid cultures were irradiated with UV for different periods (Figure 9C), showing the desired cell mortality at 45 seconds of UV exposure time with our setup. The UV exposure time was fixed to 60 seconds to ensure an homogeneous irradiation of a shaked liquid culture of CSR603.

1.2. Loss of nucleoid in *E. coli* maxicells

Phase-contrast and 4'-6-diamidino-2-fenilindol (DAPI) stained fluorescence images (for bacterial nucleoid detection) of *E. coli* CSR603 cells collected at 3 hours after the UV irradiation show that the DAPI fluorescence intensity decreases and is hardly detectable in maxicells indicating the absence of nucleoid, while their morphology is largely maintained (Figure 10). Cell length of each sample taken during the procedure shows that maxicells are ~ 30% longer than non-irradiated cells.

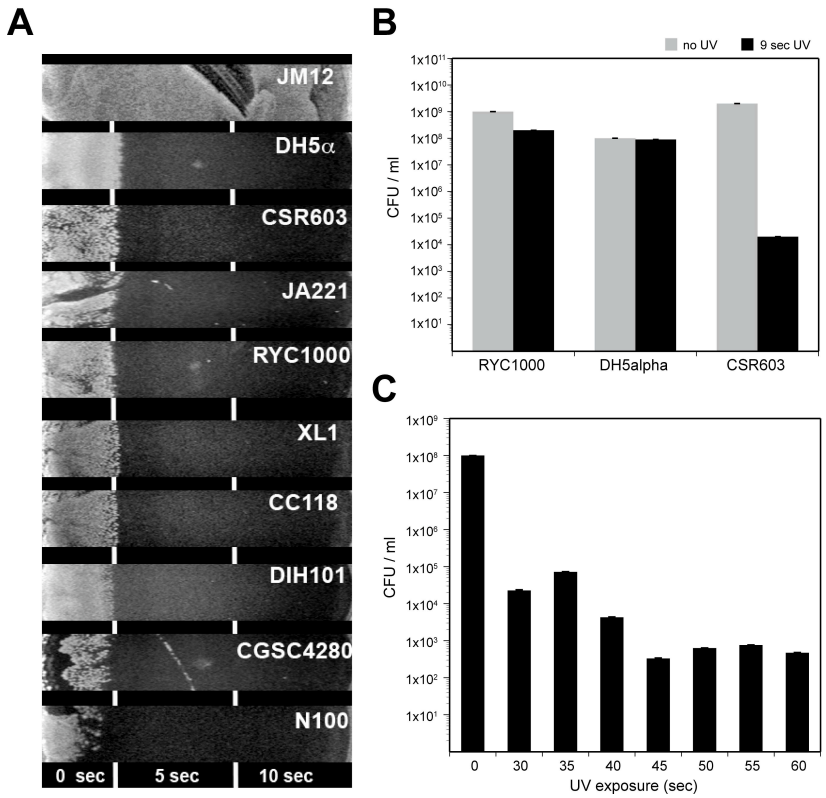

Figure 9. Sensitivity to UV irradiation of different recA strains grown on solid or liquid cultures at different exposures times.

(A) Growth of different *recA* strains after 0, 5 and 10 seconds (sec) of ultraviolet light (UV) irradiation on LB agar plates. JM12 strain was used as control (see text for details). (B) Survival cells (measured as Colony Formation Units per mililiter; CFU/ml) of RYC1000, DH5α and CSR603 strains liquid cultures before and after 9 sec of UV irradiation. (C) Survival cells of CSR603 liquid cultures irradiated for different UV exposure times (0, 30-60 sec).

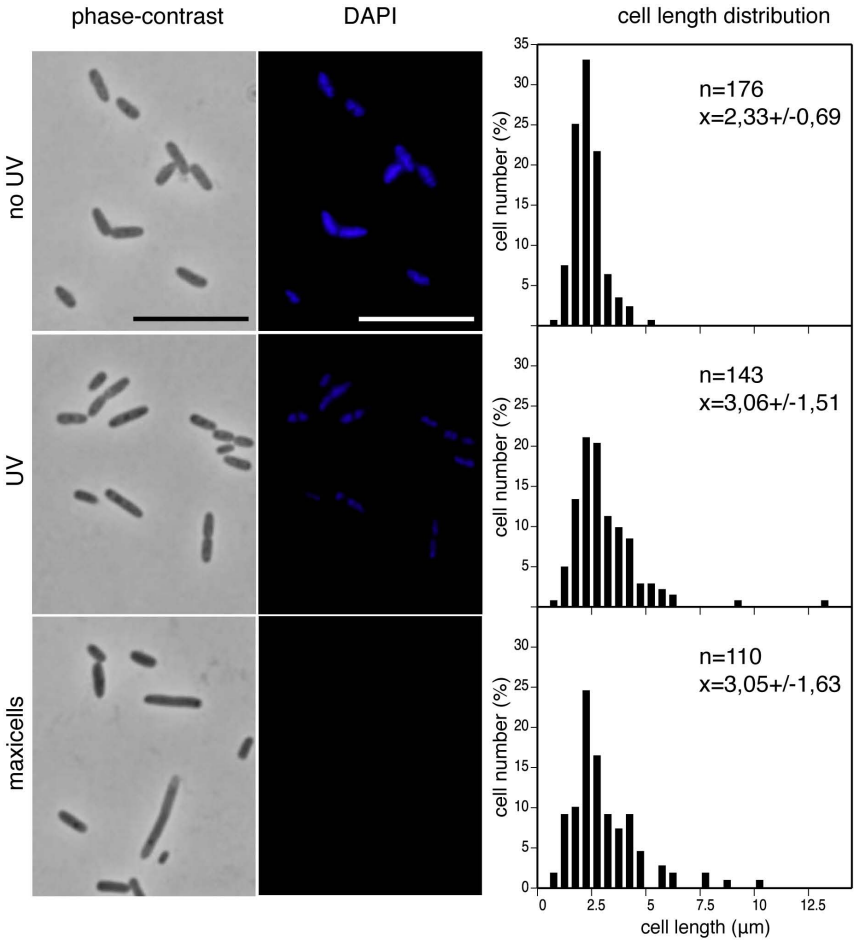

Figure 10. Morphological parameters of maxicells.

Maxicells were obtained from *E. coli* CSR603 as described in the text. Samples were taken at different stages in the maxicell production procedure as indicated in the figure. Namely, normal growing cells (no UV); irradiated cells observed 3 hr after irradiation (UV); and UV irradiated cells further incubated for 3 hr in the absence of cycloserine plus 16 additional hr in its presence (maxicells), see text for details. Panels at the left-hand side show phase contrast images of representative fields. The panels at the middle show DAPI fluorescence images of the same fields. Scale bars represent 10 μm. The panels at the right hand-side show cell length distributions for each stage measured as described in the text. The number of cells measured, n, the mean cell length, x, and the standard deviation are indicated.

2. Selection of FtsZ placement in nucleoid-free bacterial cells

2.1. MinD and MinE oscillate in the absence of NO

Protein levels of the components of both septum placement machineries (MinCDE and SlmA) were analysed by immunoblot. The nucleoid occlusion (NO) effector protein SlmA was shown to be present both in non UV-irradiated cells and 3 hours after UV irradiation, but was absent from maxicells (Figure 11A). The absence of SlmA together with the disappearance of the nucleoid is likely to completely deprive maxicells of the NO septum selection mechanism. MinC, MinD and MinE remained unchanged protein levels in maxicells than in non-irradiated cells (Figure 11A).

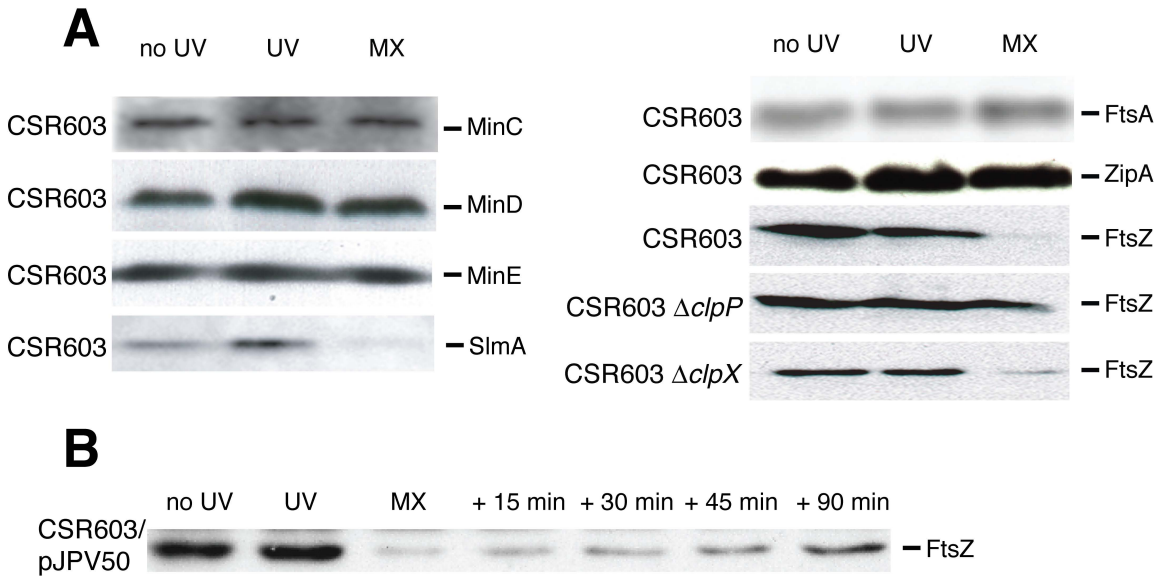

Figure 11. Levels of septum site-selection and proto-ring proteins, and kinetics of plasmid-encoded FtsZ production in maxicells.

(A) Samples from cultures of *E. coli* CSR603, CSR603 Δ*clpP* and CSR603 Δ*clpX* were withdrawn at different stages: normal growing cells (no UV); irradiated cells observed 3 hr after irradiation (UV); and UV irradiated cells further incubated for 3 hr in the absence of cycloserine plus 16 additional hr in its presence (MX). The amounts of MinC, MinD, MinE, SlmA, FtsA, ZipA and FtsZ were measured by immunoblot using antibodies raised against each protein. All the proteins were analysed in the case of CSR603, while only the FtsZ levels were measured in CSR603 Δ*clpP* and CSR603 Δ*clpX*. (B) CSR603 maxicells contaning an inducible copy of *ftsZ*$^{+}$ in pJPV50 were obtained, expression from the plasmid was induced for the times indicated in the figure and the FtsZ levels were detected by immunoblot with antibodies against FtsZ.

To test the MinCDE functionality we studied if they were able to maintain their pole-to-pole oscillation in maxicells. The minimal requirements for the oscillation to take place is the presence of MinD and MinE (Raskin & de Boer, 1997) since MinC is not itself attached to the membrane and it oscillates passively due to its high affinity binding to MinD (Lutkenhaus, 2007). To independently monitor the position of MinD and MinE in maxicells we overproduced GFP-

fusion protein variants of MinD and MinE (Raskin & de Boer, 1999b, Rowland *et al.*, 2000). A pole-to-pole oscillation of the GFP-MinD or MinE-GFP fluorescence signals was observed (Figure 12) with an oscillation frequency of 40 to 60 seconds, which is comparable to the value found in non-irradiated cells (Raskin & de Boer, 1999b).

GFP-MinD oscillated as a spiral-like structure placed in the proximity of the membrane while MinE-GFP oscillated as a sharp ring. Oscillation of both proteins indicates that ATP is likely to be available at sufficient levels to drive MinD dimerization and association to the cytoplasmic membrane in maxicells. Moreover, as in maxicells GFP-MinD was not co-overproduced with MinE, nor MinE-GFP with MinD, our results indicate that the endogenous amounts of MinD and MinE retained by maxicells are sufficient to maintain the oscillation. As the MinC levels remained unchanged in maxicells and MinC attaches to MinD we can infer that the observed oscillation of MinDE should also involve the displacement of the MinD-attached MinC and therefore that a functional Min system is present in the absence of NO.

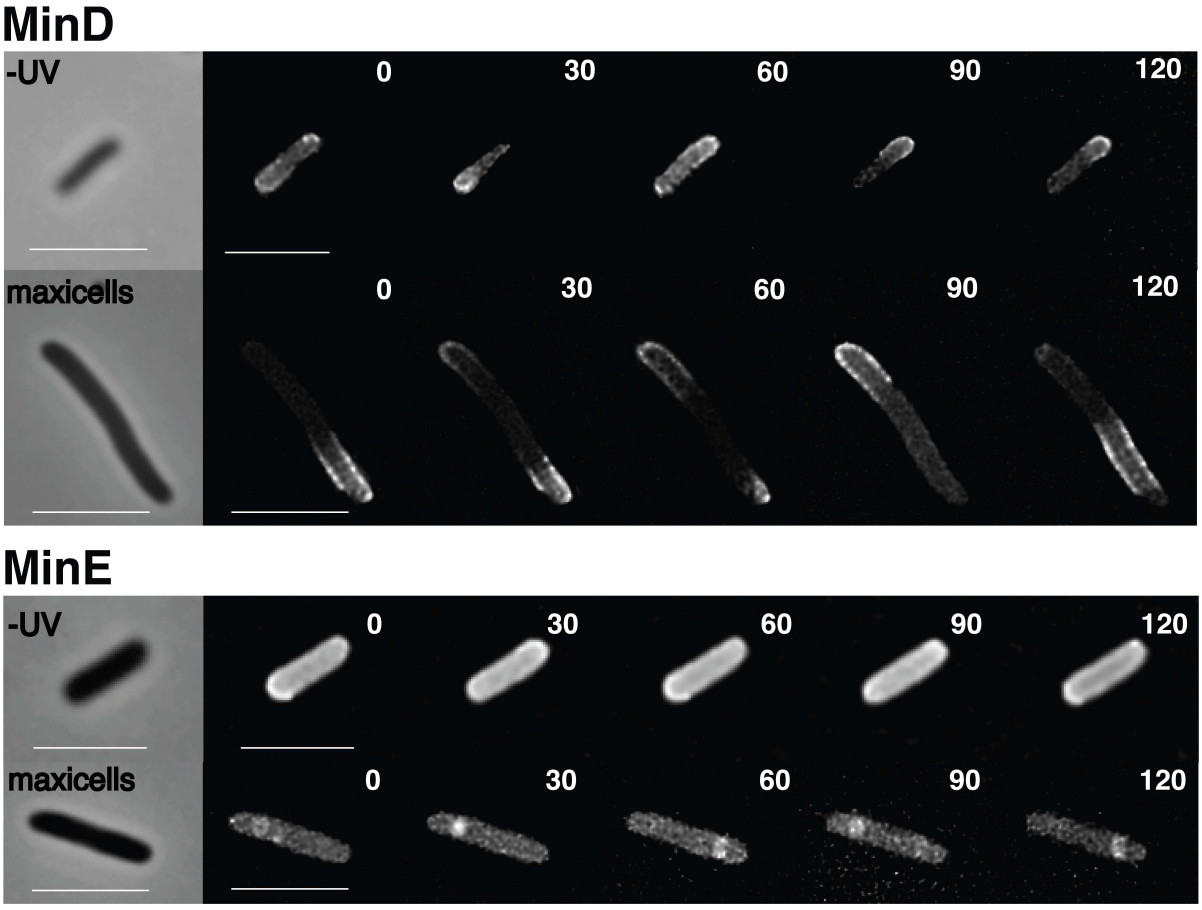

Figure 12. Oscillation of MinD and MinE in the absence of the bacterial nucleoid.

Phase-contrast and deconvoluted GFP-fluorescence microscopy images of non-UV irradiated CSR603 cells (-UV) and CSR603 maxicells carrying plasmid producing either GFP-MinD or MinE-GFP were recorded at the time intervals (seconds) indicated in the different frames. A phase contrast image, taken at time zero, has been included for each case (left hand side frames). The scale bars represent 10 μm.

2.2. Stability of FtsZ in maxicells

To study the positioning of FtsZ rings in the absence of NO and presence of Min, we determined the protein levels of the proto-ring components FtsZ, FtsA and ZipA in maxicells. The FtsZ protein levels, relative to non-irradiated cells, remained unchanged 3 hours after UV irradiation and dropped to a low residual amount, in maxicells (Figure 11A). This drop is specific for FtsZ and was not observed for FtsA or ZipA. In growing cells the ClpXP protease complex has been reported to be responsible for FtsZ degradation (Camberg *et al.*, 2009, Weart *et al.*, 2005), where the protein degradation is directed by the presence of a ClpX-recognition signal, which is not present in FtsA or ZipA, but it is contained within the last eighteen amino acids of the FtsZ carboxyl terminal (C-terminal) end (Camberg *et al.*, 2009), although the exact sequence of this motif is not known. The ClpX moiety unfolds and transfers its substrate to ClpP, the protease moiety responsible for the degradation (Camberg *et al.*, 2009). To check if the loss of FtsZ in maxicells is due to the action of ClpXP, *E. coli* strains carrying insertional inactivations in either *clpX* (VIP979) or *clpP* (VIP978) were constructed. Data in Figure 11A show that the FtsZ levels remained unchanged in CSR603 Δ*clpP* maxicells, relative to unirradiated cells, indicating that the protease moiety ClpP is required for degradation. Surprisingly, the absence of ClpX had no effect on preventing the degradation of FtsZ in CSR603 Δ*clpX* maxicells, although in this case we cannot discard that a different recognition unfoldase, as ClpA (Hoskins *et al.*, 2000) may take over the role of ClpX in maxicells.

2.3. The positioning of $FtsZ^+$ in maxicells.

The absence of NO and the presence of a functional Min system prompted us to study the placement of FtsZ in maxicells. We have shown that in maxicells FtsZ is degraded to a low residual amount by the ClpXP system. This allows to specifically synthesize plasmid encoded *ftsZ de novo* and monitor its localization or eventual Z-ring formation in the absence of the chromosomal encoded protein. When produced from plasmid pJPV50 at 30ºC, where *ftsZ* expression is controlled by lambda CI_{857} (Plá *et al.*, 1993), lambda CI_{857} is functional and represses *ftsZ* expression. Maxicells prepared at 30 ºC showed the decrease of FtsZ levels (Figure 11B; lanes no UV, UV and MX). At 42ºC the lambda CI_{857} repressor becomes inactivated and a gradual increase of the FtsZ levels is detected (Figure 11B; lanes from 15 to 90min). Deconvolved immunofluorescence images of $FtsZ^+$-producing maxicells show that the $FtsZ^+$ protein has no preferred localization along the entire length. Inspection of these images suggests, nevertheless,

that FtsZ$^+$ localizes as diffuse arc or spiral patterns in the proximity of the membrane, although the resolution does not allow for more detail (Figure 13B).

2.4. Localization of membrane-bound FtsZ variants depending on the presence of its C-terminal domain.

FtsZ membrane binding depends on the interaction with ZipA and FtsA. Osawa *et al.* (Osawa *et al.*, 2008) constructed an FtsZ variant in which the Venus protein (Nagai *et al.*, 2002) was used to reveal the protein and the membrane targeting sequence of MinD (MinDmts) (Szeto *et al.*, 2002) provided an anchor to the cytoplasmic membrane independent of FtsA and ZipA (Osawa *et al.*, 2008). This protein (referred in this work as FtsZ*-VM) lacks the amino acid residues 367-383 at the FtsZ C-terminal end that interact with MinC, ZipA, FtsA or ClpX (Shen & Lutkenhaus, 2009, Ma & Margolin, 1999, Mosyak *et al.*, 2000, Szwedziak *et al.*, 2012, Camberg *et al.*, 2009) (Figure 13A). We have constructed FtsZ-VM, a variant of FtsZ*-VM where the full length FtsZ protein, including its C-terminal end, is fused to Venus and MinDmts (Figure 13A), and studied the localization of either FtsZ*-VM or FtsZ-VM produced in maxicells

FtsZ*-VM localizes along the cell length as multiple membrane bound bands or rings (Figure 13B). As NO is absent and FtsZ*-VM lacks the sequence sensitive to MinC this result indicates that these structures adopted in maxicells do not respond to any septum site placement machinery. This also occurs in artificial vesicles as it was described by Osawa *et al.* (2008). From our results it can be observed that the membrane-bound FtsZ*-VM does not form a wide continuous band along the cell length, instead discete narrow bands are found separated by dark spaces where the protein is either absent or at levels below those allowing detection.

The effect of the Min septum site selection mechanism on FtsZ-VM was then analyzed in maxicells. Different from FtsZ*-VM, the protein containing the full C-terminal region localizes as a belt at midcell and as caps at both poles (Figure 13B). Localization at midcell would be consequent with the action of the Min proteins in growing cells. FtsZ-VM localization found at the cell poles was unexpected as in growing cells FtsZ$^+$ is cleared from them by the action of Min. This polar localization might occur due to a cumulative effect of MinD-mts together with ZipA or FtsA, both present in maxicells (Figure 11) on membrane anchoring of FtsZ-VM. As controls, the Venus protein fused to MinD-mts (VM) or the FtsZ C-terminal end fused to Venus and MinDmts (ZC-VM) when overproduced in maxicells did not accumulate as rings, belts or polar caps (data not shown), and moreover, these two proteins failed to associate to the membrane. It is already known that at least two MinDmts are needed for the *E. coli* MinD dimer to remain attached to the

membrane (Szeto *et al.*, 2002) that explains why the non dimerizing proteins VM or ZC-VM are not found attached to the membrane. In contrast, as both FtsZ*-VM and FtsZ-VM protein can interact through their FtsZ domains, they can adopt a structure in which at least two MinD-mts segments target the proteins to the membrane.

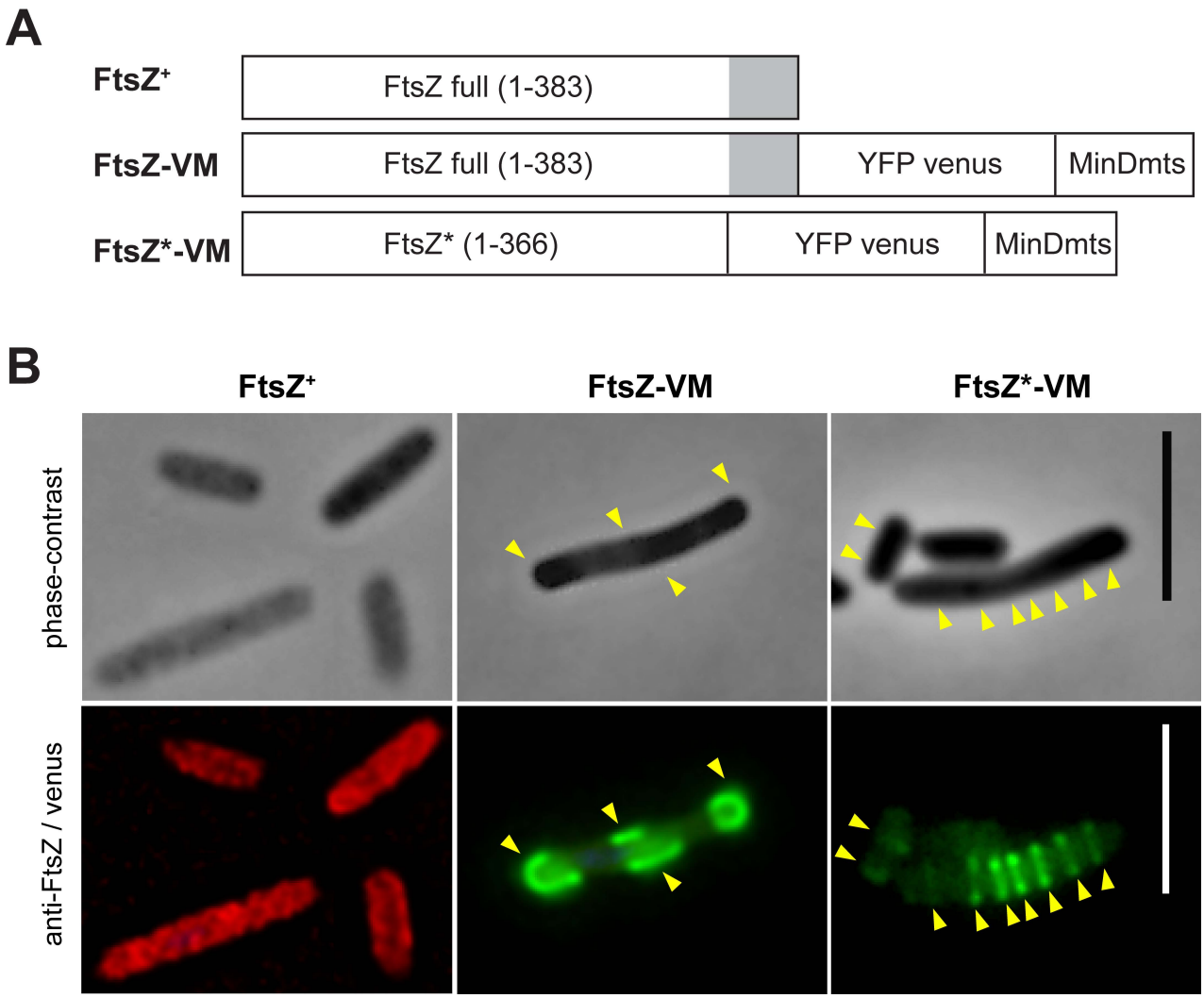

Figure 13. Localization of FtsZ variants in maxicells.

(A) The FtsZ fusion proteins localized in maxicells in panel B are schematized. The grey shaded square representes the C-terminal domain (17 residues) of FtsZ. This domain is not present in FtsZ*-VM. (B) Maxicells obtained from CSR603 cells containing plasmids pJPV50 ($FtsZ^+$), pPZV42 (FtsZ*-VM) or pPZV129 (FtsZ-VM) were observed after 16hr induction of the plasmid encoded genes by 0.5 mM IPTG. The $FtsZ^+$ protein was revealed by immunostainig with Alexa Fluor-594 labeled MCV2 purified antibody against FtsZ as indicated in Materials and Methods. The fluorescence signal of the Venus fusions was observed as indicated in Experimental Procedures. Scale bars represent 10 μm.

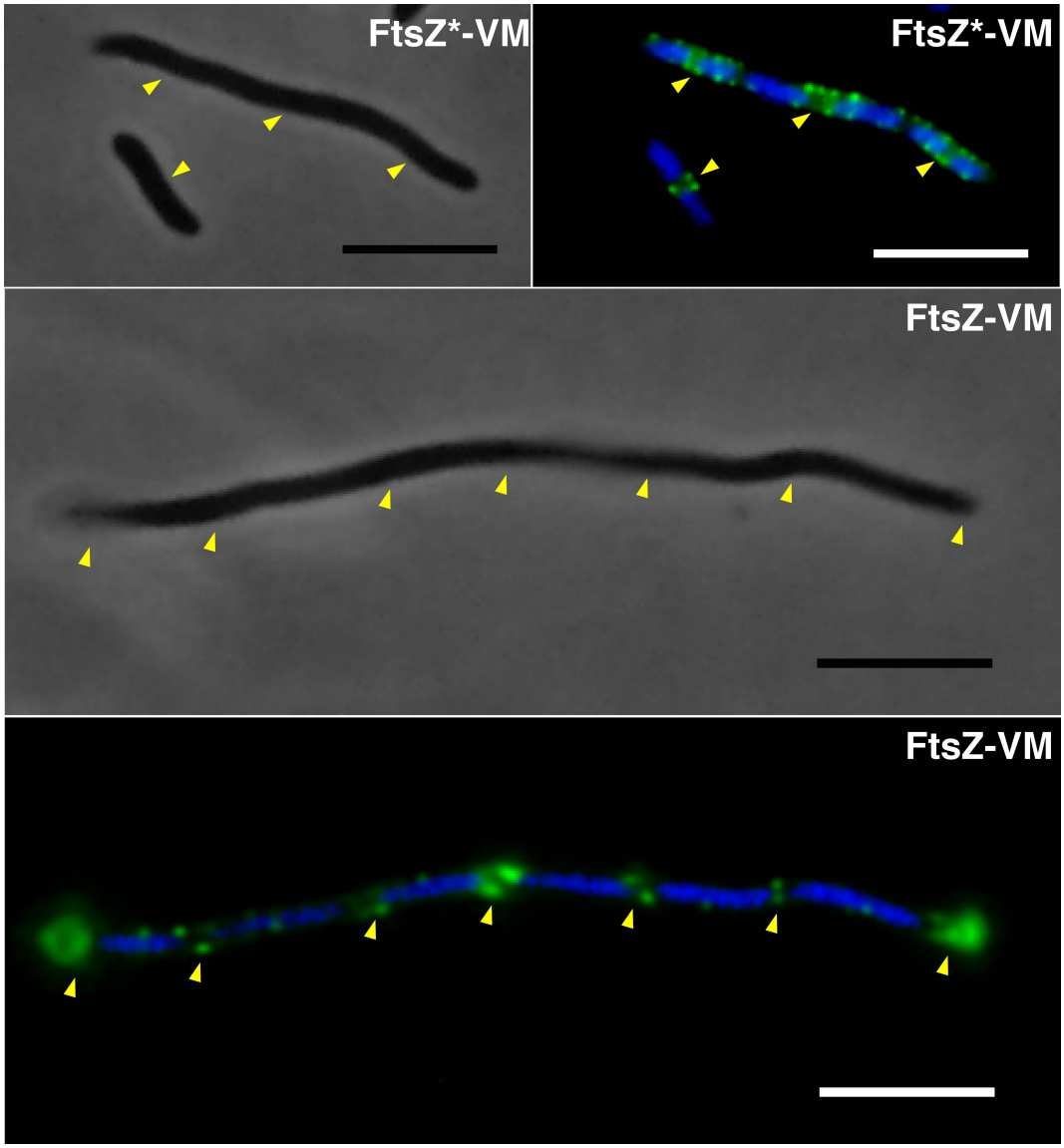

Figure 14. Localization of FtsZ-VM and FtsZ*-VM in FtsZ-depleted VIP2 cells.

Cultures of VIP2 cells harbouring plasmids pPZV42 (FtsZ*-VM) or pPZV129 (FtsZ-VM) growing exponentially at 30ºC were shifted to 42ºC and incubated for 180 min to deplete the amount of $FtsZ^{+}$. Production of each plasmid-encoded FtsZ variant was then achieved by addition of 0.5 mM IPTG during 120 min. Samples from each culture were then stained with DAPI to reveal nucleoids and observed. Phase-contrast and fluorescence merged micrographs of DAPI staining and Venus-fluorescence signal are shown for each strain. Arrowheads highlight the position of the Z-rings. Scale bars represent 10 μm.

2.5. The bacterial nucleoid is necessary for the midcell positioning of FtsZ.

VIP2 is an *ftsZ* thermonull strain containing an insertional inactivation of the *ftsZ* chromosmal copy together with a replication thermosensitive plasmid carrying $ftsZ^{+}$ (Pla *et al.*, 1991). It displays a filamentous phenotype at 42ºC, the non-permissive temperature, caused by the cessation of cell division due to the depletion of FtsZ following the loss of the plasmid. This strain allows to probe the localization of FtsZ-VM or FtsZ*-VM in the absence of wild type endogenous FtsZ, but in the presence of the nucleoid.

A concentration of 500 μM IPTG was used to induce expression from plasmids encoding FtsZ-VM or FtsZ*-VM to achieve protein levels sufficient for their detection by fluorescence microscopy. Results in Figures 14 and 15 show that the position of the FtsZ*-VM or FtsZ-VM fluorescence signals coincide with the positions of potential septation sites in between nucleoids. FtsZ*-VM localized as multiple bands producing images that could be compatible with either parallel individual rings or helical structures. Besides forming single ring or foci between nucleoids (Figure 14), FtsZ-VM localized in U-shaped caps at the poles, similar to maxicells (Figure 13). We do not observe minicells at the poles, suggesting that this fusion of YFP to FtsZ is not fully functional, as has been reported for other similar constructs (Ma *et al.*, 1996).

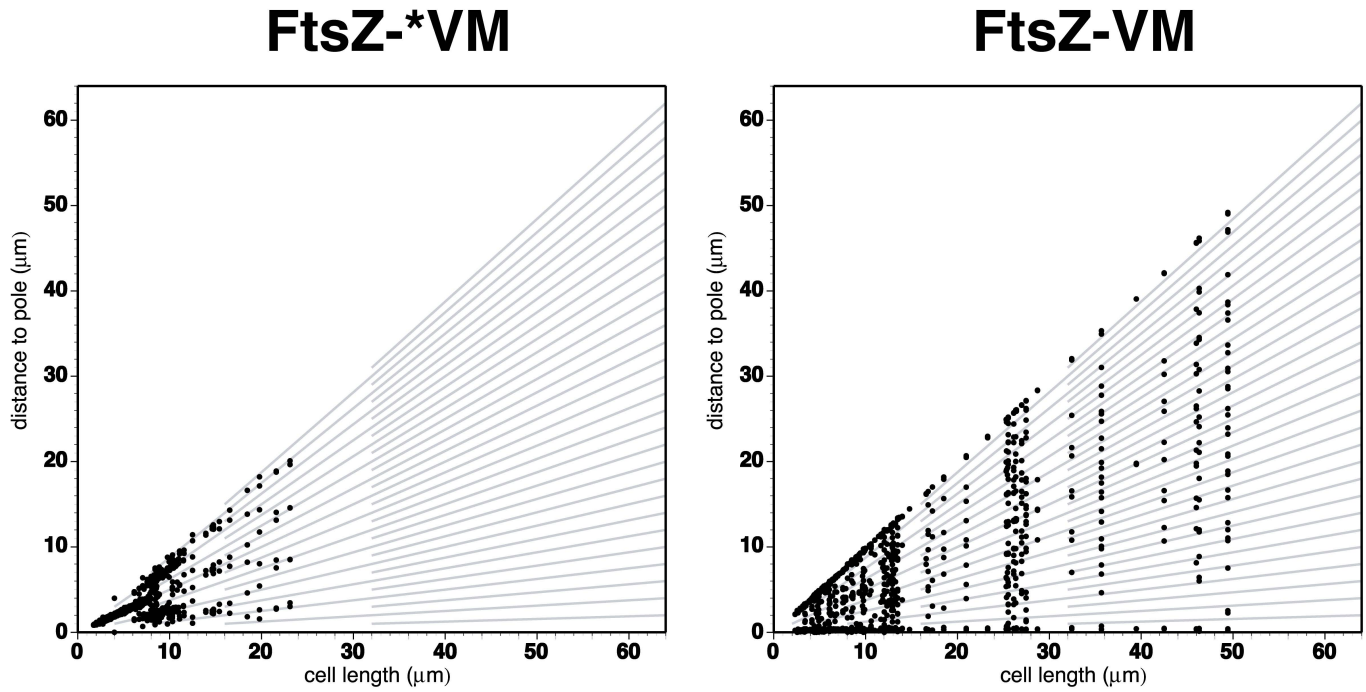

Figure 15. FtsZ*-VM and FtsZ-VM localization at potential cell division sites in VIP2 under FtsZ-depletion conditions.

The position of FtsZ*-VM- (left panel**)** and FtsZ-VM-rings (right panel) in the cell are represented as described in Tormo & Vicente (Tormo & Vicente, 1984). Each position occupied by a fluorescent ring was assigned to two values representing its distance from one of each of the cell poles. Straight lines mark the theoretical positions of potential division sites contained within filaments of different lengths.

Functionality of FtsZ-VM and FtsZ*-VM was tested, compared to the wild type, regarding their ability to support the growth of VIP2 (Figure 16). At 30ºC we found that pPZV133 containing *ftsZ*$^{+}$ blocks the growth of VIP2 on plates both when inducing expression with 25 or 10 μM IPTG (higher induction levels as those used for visualizing the proteins are obviously lethal). Under these expression conditions FtsZ protein levels are higher than in untransformed VIP2 due to the *trc* promoter on the plasmid, which is stronger than the natural promoters used in VIP2 to

complement the insertional inactivation of *ftsZ*, and to the higher copy number of the cloning vectors. These high FtsZ levels can titrate out other essential divisome components what can be the reason for our results. On the other hand, pPZV129 encoding FtsZ-VM blocks the growth of VIP2 on plates at 30ºC when 25 but not when 10 μM IPTG is added. Finally, pPZV42 encoding FtsZ*-VM does not have any effect on the growth of VIP2 either at 25 or 10 μM IPTG concentration. This suggests that the FtsZ*-VM protein is likely to be inert both in division and in the interaction with other proto-ring elements. Unexpectedly we observe no complementation of VIP2 by any of these proteins at 42 ºC. To show then if the $FtsZ^{+}$ encoded by pPZV133 was functional we checked its ability to complement strain PAT84 (*ftsZ84*, Ts) at 42 ºC (Figure 16).

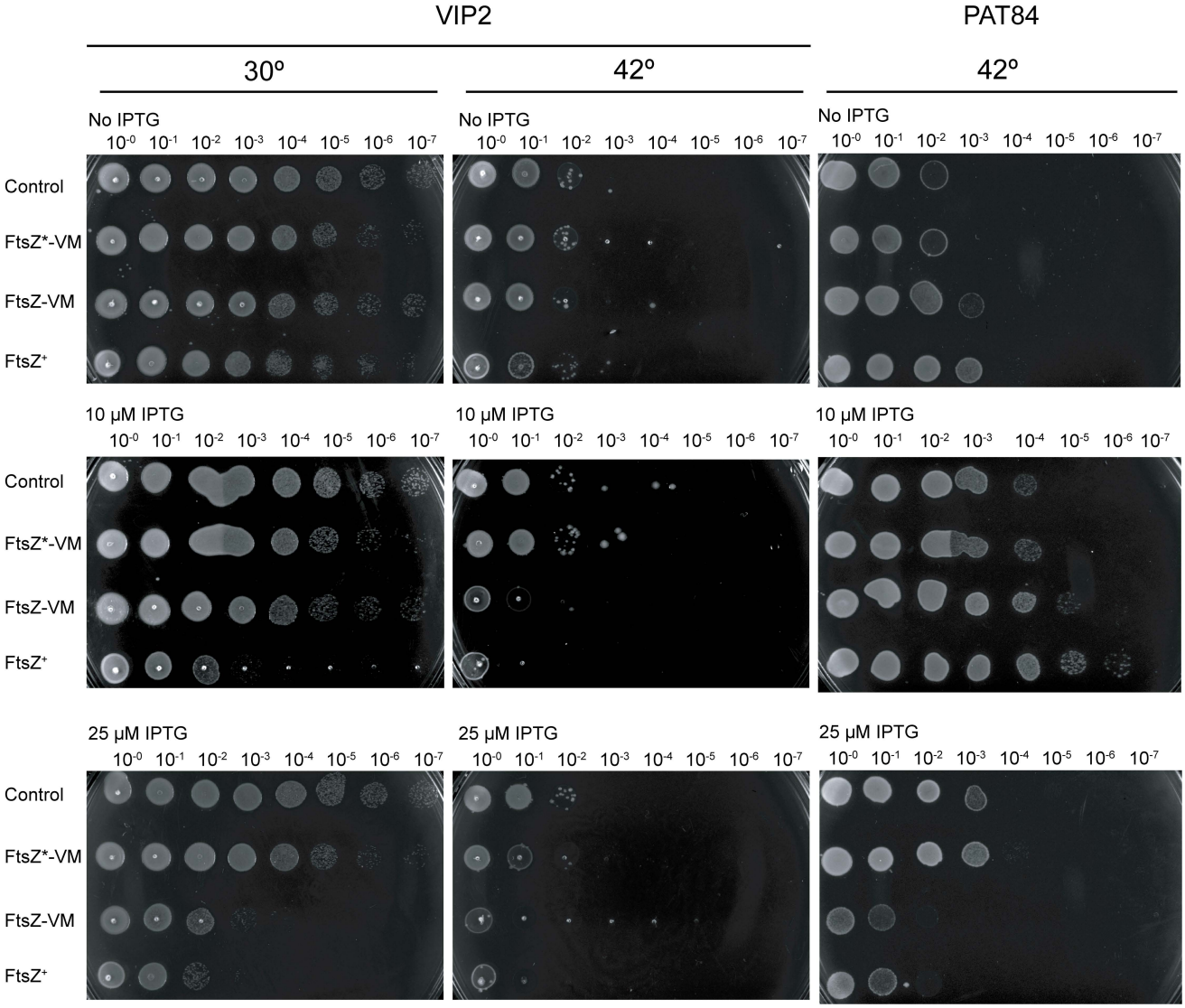

Figure 16. Effect of the overproduction of FtsZ variants on the growth of thermonull (VIP2) and thermosensitive (PAT84) *E. coli ftsZ* strains.

VIP2 and PAT84 strains carrying either plasmid pPZV42 (FtsZ*-VM), pPZV129 (FtsZ-VM), pPZV133 (FtsZ+) or pTrc99A (control) were grown overnight at 30ºC. Serial dilutions from each culture were spotted onto LB plates in the presence of two different concentrations of IPTG as indicated in the figure. The results were read after overnight incubation at the indicated temperatures.

Induction at 25 μM IPTG blocked growth, but the lower 10 μM concentration supported growth. While the FtsZ*-VM protein had no effect on the growth of PAT84 at 42 ºC at any inducer concentration, corroborating that it may be inert, FtsZ-VM did show a low complementation ability (one order of magnitude lower than FtsZ+) at low induction levels (10 μM) and blocked growth at 25 μM IPTG what agrees well with the prediction that it should be partly but not fully functional in septation.

3. A specific role for ZipA in cell division

3.1. ZipA protects FtsZ from degradation

In order to study the effect of the two other proto-ring components, FtsA and ZipA, protein levels on the stability of FtsZ, we induced the production of different forms of ZipA at 3 hours after UV irradiation (the time of D-cycloserine addition) and measured the amount of FtsZ present in maxicells. Results shown in Figure 17 (and Figure 34) indicate that the overproduction of His-ZipA reduced FtsZ degradation. As a control, the production of the His-ZipA3 mutant, a C-terminal truncate of His-ZipA that lacks most of its FZB domain (from amino acids 114 to 272, Figure 18A), showed no stabilization of the FtsZ levels as it also occurred in maxicells carrying an empty vector as a control (Figure 17). The fact that maxicells retain a basal level of ZipA, even when they contain no plasmid encoded copy of *zipA*, could contribute to maintain the low residual amount of FtsZ found after the D-cycloserine treatment. The FZB domain has been described to interact directly with the C-terminal end of FtsZ (Mosyak *et al.*, 2000), this is the same FtsZ domain recognized by ClpX (Camberg *et al.*, 2009). ClpX is an unfoldase that facilitates the access of ClpP to the substrate, although other unfoldases as ClpA may be also active. Our results could be due to an steric hindrance from the excess of ZipA blocking the access of ClpX to the recognition signal present at the C-terminal end of FtsZ. In the presence of ZipA the accesibility of the ClpP protease to FtsZ would be reduced and degradation would then proceed at a lower rate. Nevertheless, FtsZ would never be fully protected from degradation by ClpP as the other unfoldases together with the intrinsic protease activity of ClpP, may remain active.

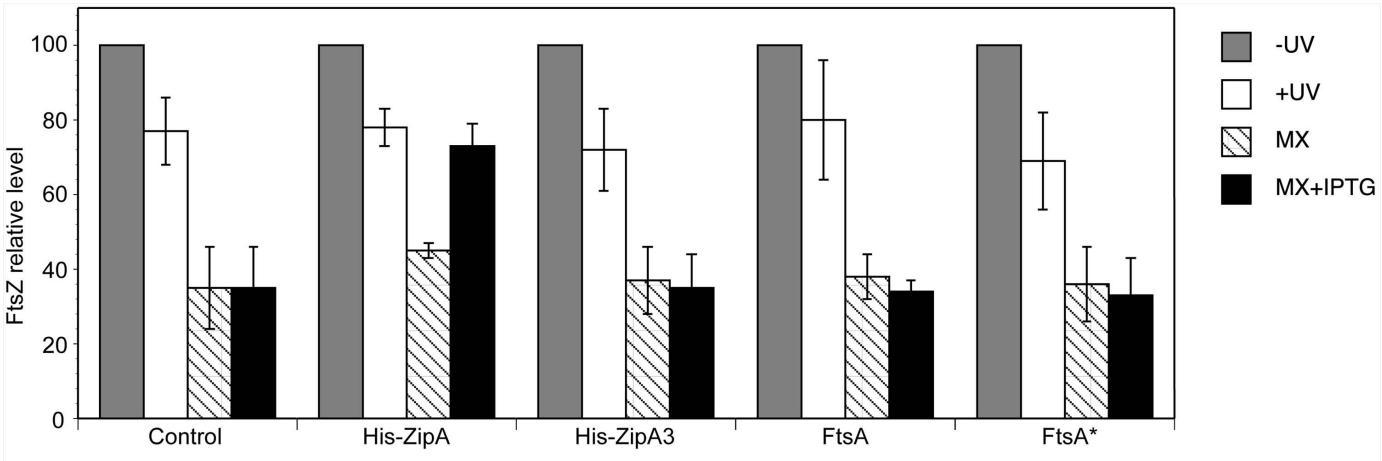

Figure 17. Protection of FtsZ from degradation by overproduction of ZipA in maxicells.

FtsZ protein level during the maxicell production procedure of *E. coli* CSR603 cells bearing empty plasmid (control) and overproducing His-ZipA (pPZV23), His-ZipA3 (pPZV24), FtsA (pPNV40) or FtsA* (pPZV33). (-UV) non-UV irradiated cells, (+UV) 3 hours after irradiation, (MX) 16 hours after D-cycloserine addition and (MX+IPTG) 16 hours after addition of D-cycloserine and IPTG. Black bars indicate the standard deviation in each case.

3.2. Protection of FtsZ by ZipA only requires the FZB domain

To find which subdomains of ZipA are involved in FtsZ protection, different ZipA deletion mutants containing an intact N-terminal transmembrane domain were constructed as shown in Figure 18A. In addition, the isolated cytoplasmic FZB domain that has been described to interact with FtsZ (Mosyak *et al.*, 2000) was also constructed. Overproduction in maxicells shows that only the full length His-ZipA, the entire FZB domain and the His-ZipA4 mutant (lacking part of the FZB domain from Pro-273 to Ala-328) were able to protect FtsZ from degradation (Figure 18B and Figure 35). This result indicates that the isolated FZB domain, or even a shorter form in which the last 55 C-terminal amino acids are missing, is sufficient for FtsZ protection from proteolysis and that the rest of the ZipA protein is not involved in it.

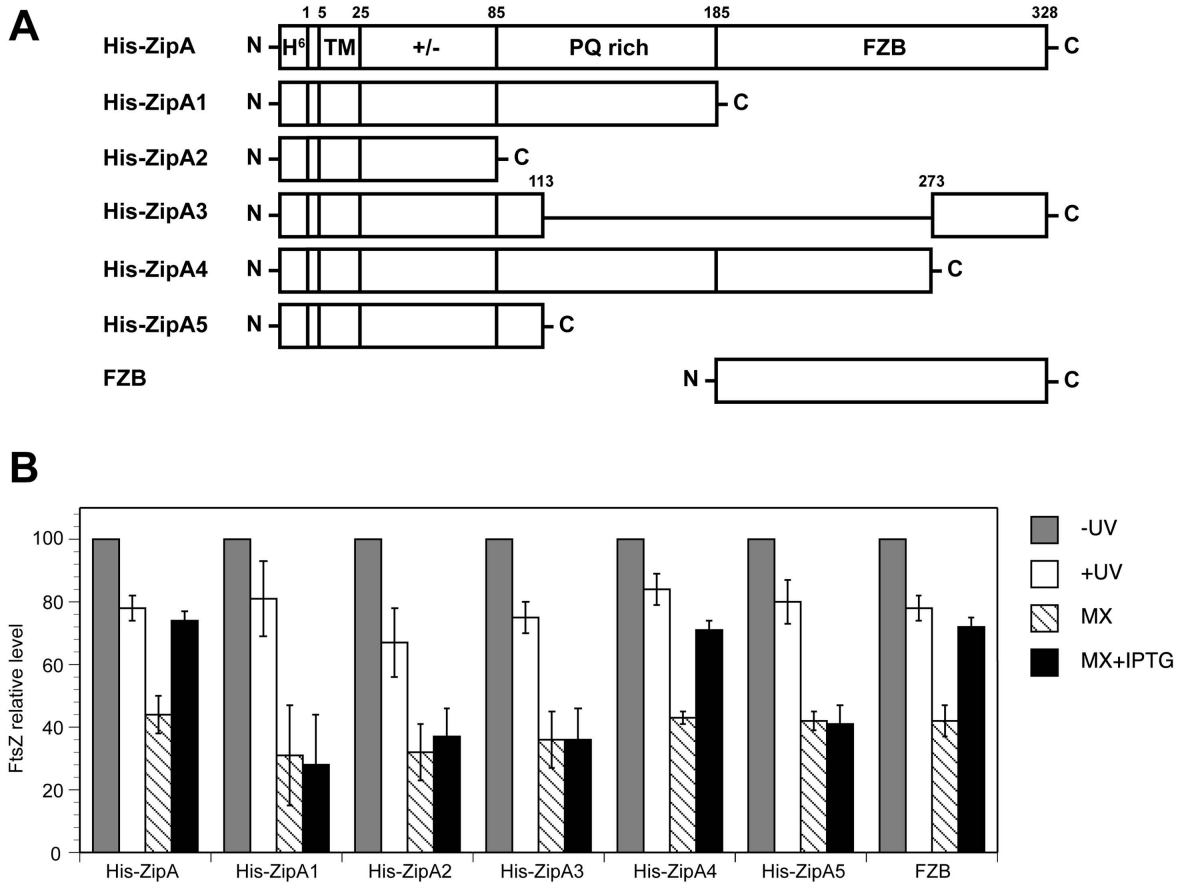

Figure 18. FtsZ-protective properties of different ZipA mutants.

(A) ZipA structural domains (TM, transmembrane domain; +/-, charged domain; PQ rich, proline/glutamine rich domain; FZB, FtsZ binding domain) and the different mutants used in the present work. (B) FtsZ protein levels during the maxicell production procedure of *E. coli* CSR603 cells overproducing the different ZipA mutants. (-UV) non-UV irradiated cells, (+UV) 3 hours after irradiation, (MX) 16 hours after D-cycloserine addition and (MX+IPTG) 16 hours after addition of D-cycloserine and IPTG. Black bars indicate the standard deviation in each case.

3.3. Neither FtsA nor FtsA* can protect FtsZ from proteolysis

The essentiality of the role of ZipA in *E. coli* divison has been questioned as it can be bypassed by gain-of-function FtsA mutants. Among them, FtsA* has been described to allow the late divisome assembly steps in the absence of ZipA (Geissler *et al.*, 2003, Geissler & Margolin, 2005). To test if FtsA or FtsA* can exert the protective role on the stability of FtsZ that we have observed, we have overproduced FtsA or FtsA* in maxicells. The *ftsA* or *ftsA** genes were placed under the control of an IPTG inducible P_{trc} promoter (pPNV40 and pPZV33 respectively) and expression was induced at 3 hours after UV-irradiation at the time of D-cycloserine addition. The results in Figure 17 (and Figure 34) show that when FtsA or FtsA* were overproduced the FtsZ levels diminished in a similar way as in the control. This indicates that, contrary to ZipA, neither FtsA nor FtsA* protect FtsZ from degradation. Similarly to ZipA, FtsA interacts with the C-terminal end of FtsZ (Ma & Margolin, 1999, Szwedziak *et al.*, 2012) and this interaction was postulated to stabilize and tether the FtsZ-ring to the inner membrane (Pichoff & Lutkenhaus, 2005). Moreover, a decrease of 5% in the FtsZ protein levels was found in an exponentially growing culture of a *ftsA** Δ*zipA* strain (WM1657) relative to the wild type cells (WM1074) growing under similar conditions (Geissler *et al.*, 2003) (Table 7). Our results suggest that stabilization of the ring by FtsA may be exerted at the stages from FtsZ polymerization to ring assembly, but is very unlikely that it takes place on monomeric FtsZ. We therefore conclude that ZipA has a role on the stability of the FtsZ protein itself and that this role cannot be replaced by either FtsA or FtsA*.

Table 7. FtsZ relative level

OD_{600nm}	WM1074 (WT)	WM1657 (*ftsA** Δ*zipA*)
0.2	100 % ± 14.4[a]	94.7 % ± 15.7
0.8	100 % ± 15.1	95.1 % ± 18.4

[a] SD: standard deviation

3.4. FtsA or FtsA* do not interfere with ZipA in the protection of FtsZ

As both ZipA and FtsA can interact with the same region of FtsZ, namely the C-terminal end, we have tested if the protective role of ZipA on FtsZ stability could be hindered by the presence of FtsA or even more by FtsA* (Geissler *et al.*, 2007). We overproduced ZipA (pPZV128, arabinose induced) together with either FtsA (pPNV40, IPTG induced) or FtsA* (pPZV33, IPTG induced) in maxicells, inducing expression at the time of D-cycloserine addition, and measured the levels of FtsZ after 16 hours. In these conditions, overproduction of FtsA or

FtsA* together with ZipA had no effect on decreasing the FtsZ levels significantly relative to those attained when ZipA was produced in isolation (Figure 19 and supplemental Figure 36). We conclude that the presence of FtsA or FtsA* had no effect either to increase or diminish the protective action exerted by ZipA on FtsZ stability.

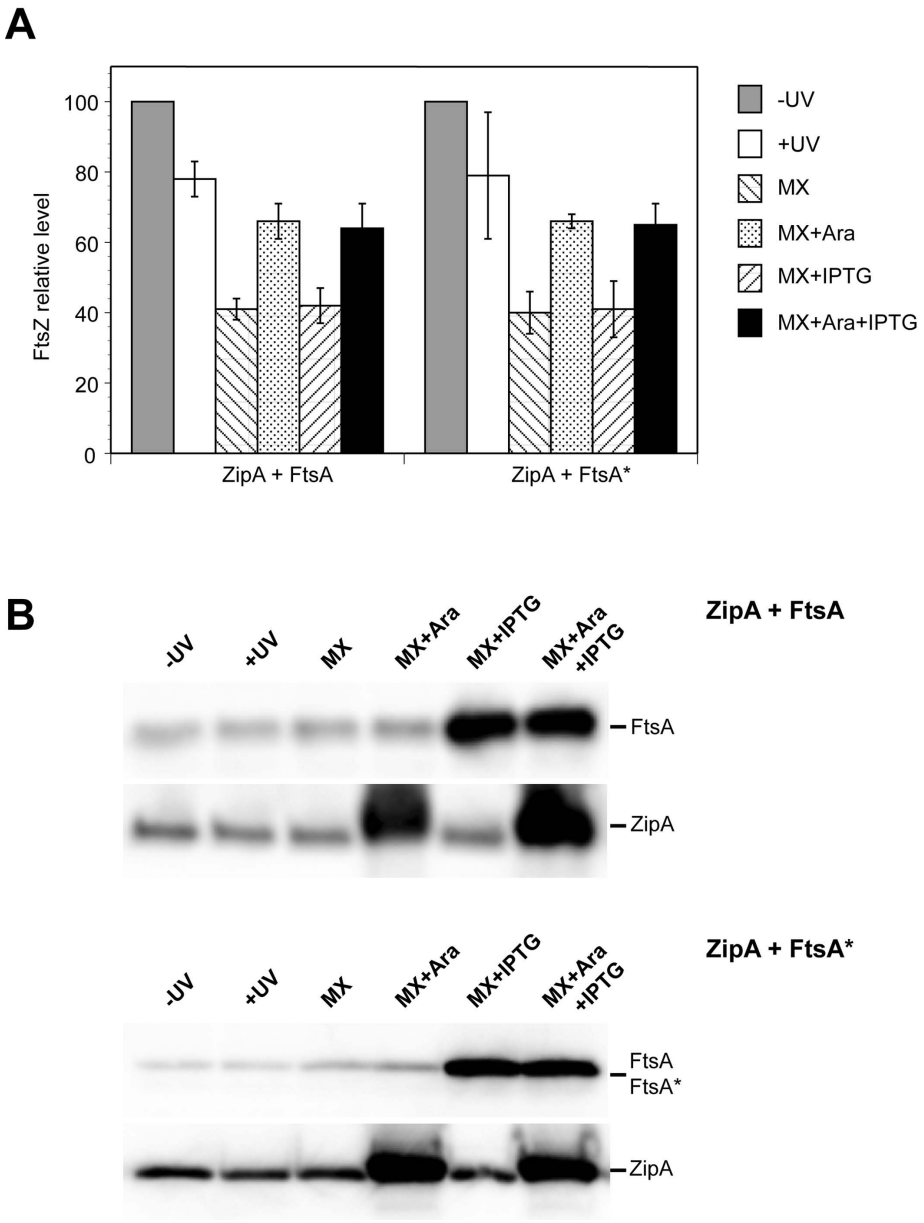

Figure 19. FtsZ-protection under ZipA and FtsA or FtsA* overproducing conditions.

(A) FtsZ protein levels during the maxicell production procedure of *E. coli* CSR603 cells overproducing ZipA (pPZV128), FtsA (pPNV40) or FtsA* (pPZV33) or a combination of ZipA with FtsA or with FtsA*. Black bars indicate the standard deviation in each case. (B) Levels of ZipA, FtsA and FtsA* on maxicells overproducing separately ZipA, $FtsA^+$ or FtsA*, or pairwise combinations of $ZipA^+$ together with $FtsA^+$ or with FtsA*. (-UV) non-UV irradiated cells, (+UV) 3 hours after irradiation, (MX) 16 hours after D-cycloserine addition and (MX+Ara), (MX+IPTG) and (MX+Ara+IPTG) 16 hours after addition of arabinose, IPTG or both, respectively, and D-cycloserine.

To exclude that FtsA or FtsA* may lose their activity if they were mislocalised at inclusion bodies under overproduction conditions we checked their localization inside the maxicells. Under these experimental conditions the overproduced FtsA or FtsA* proteins localized along the cell membrane suggesting that their lack of action on ZipA-mediated protection of FtsZ is not an artifact caused by the formation of aggregates (Figure 20).

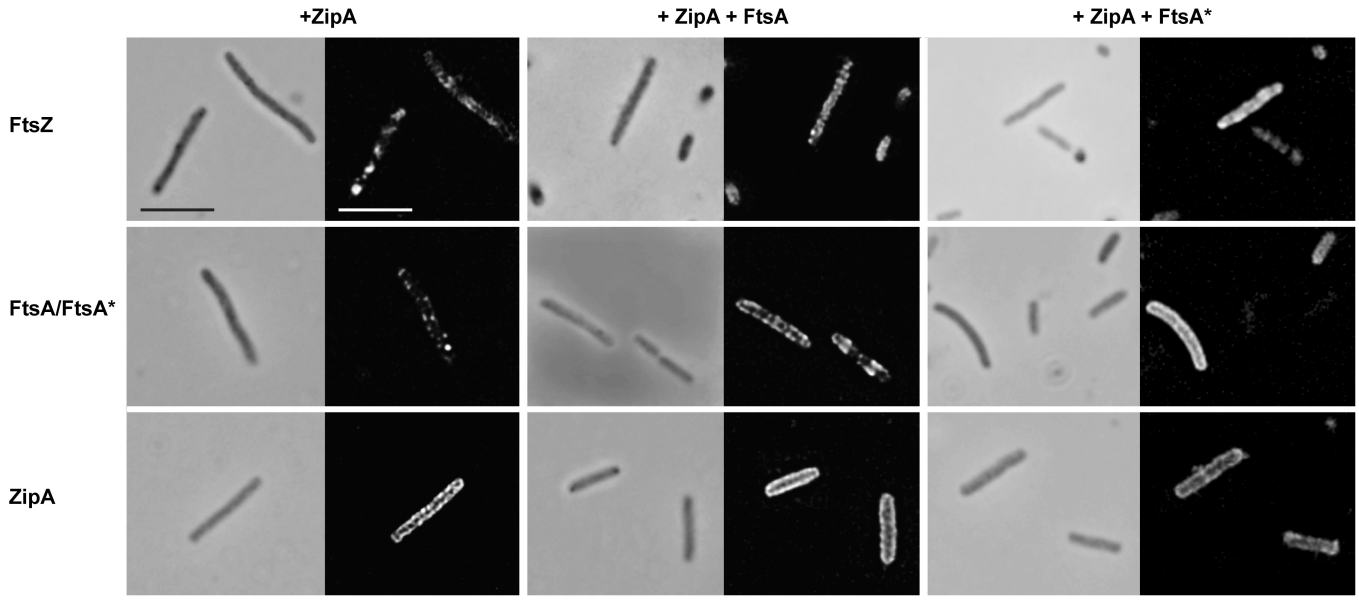

Figure 20. Localization of FtsZ, FtsA/FtsA* and ZipA in ZipA+FtsA or ZipA+FtsA* cooverproduced maxicells.

Phase contrast and fluorescence merged micrographs of DAPI staining and FtsZ (upper), FtsA/FtsA* (middle) and ZipA (lower) immunolocalization images of maxicells overproducing ZipA alone (+ZipA), and in combination with FtsA (+ZipA+FtsA) or FtsA* (+ZipA+FtsA*). Samples imaged correspond to 16 hours after addition of IPTG (+ZipA) or arabinose and IPTG (+ZipA+FtsA and ZipA+FtsA*) at time-point +UV (3 hours after UV-irradiation). Scale bars represent 10 μm.

As expected, neither FtsA nor FtsA* were able to exert any protective action on FtsZ when they were combined with the His-ZipA1 protein, itself unable to protect FtsZ from degradation (Figure 21 and supplemental Figure 37). Equally, the protective effect of the His-ZipA4 and FZB proteins on FtsZ was not interfered or increased by the simultaneous presence of either FtsA or FtsA*. These results further support our conclusion indicating that in maxicells the ZipA FZB domain can by itself protect FtsZ from degradation and that it cannot be replaced by either FtsA or FtsA*.

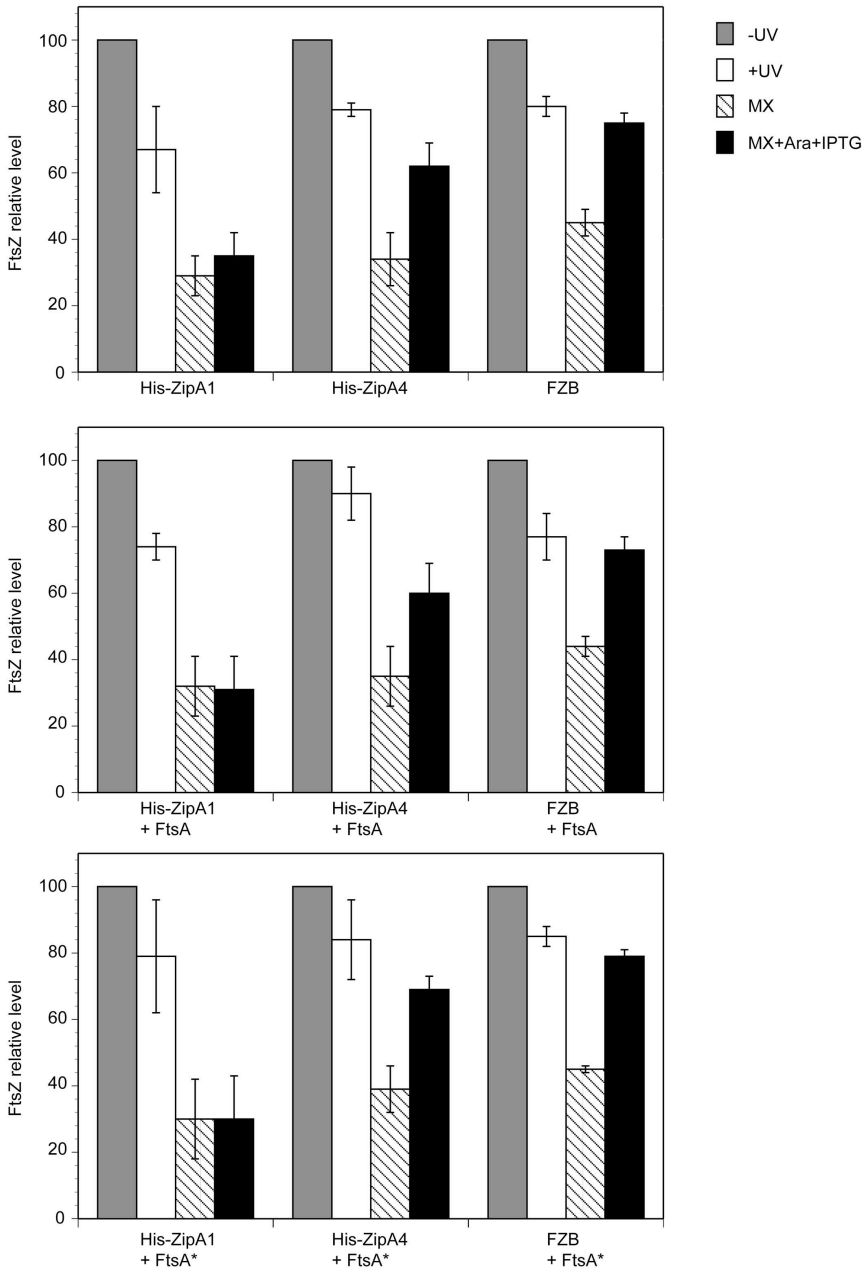

Figure 21. FtsA or FtsA* cannot substitute or interfere with FZB in FtsZ protection.

FtsZ levels on maxicells overproducing His-ZipA1 (pPZV29), His-ZipA4 (pPZV30) and FZB (pPZV38) alone (upper pannel), or in combination with FtsA (pPZV131) (middle pannel) or FtsA* (pPZV132) (bottom pannel). (-UV) non-UV irradiated cells, (+UV) 3 hours after irradiation, (MX) 16 hours after D-cycloserine addition and (MX+Ara+IPTG) 16 hours after addition of arabinose, IPTG and D-cycloserine. Black bars indicate the standard deviation in each case.

3.5. ZipA overproduction promotes ordered FtsZ structures in maxicells

Biochemical data have previously shown that ZipA is able to promote FtsZ polymerization, bundling and sheet formation *in vitro* (RayChaudhuri, 1999). Immuno-fluorescence microscopy images of maxicells show that FtsZ localized from pole-to-pole as

regularly spaced foci when His-ZipA was overproduced, whereas no foci were detected in the non-ZipA overproducing control (Figure 22). A three-dimensional reconstruction of deconvoluted FtsZ images identified the regular spaced FtsZ foci as being part of a wide helical structure within the maxicell (Figure 23).

As expected, the ZipA contained in maxicells was localized along the cytoplasmic membrane (Hale & de Boer, 1999). Besides lining the membrane, ZipA accumulated at several discrete points along the membrane length when overproduced (Figure 20). These local accumulations of overproduced ZipA were more evident when observing the three-dimensional reconstruction of deconvoluted images (Figure 23). Although ZipA may have an effect on the topology of FtsZ assemblies, we have not investigated further if the ZipA foci may coincide with specific regions within the FtsZ helix. ZipA was able to maintain the localization pattern of FtsZ and its own one even in the presence of overproduced FtsA or FtsA* (Figure 20). No FtsZ helical spirals were observed when FtsA, FtsA* (Figure 22) or His-ZipA3 (data not shown) were overproduced what is in agreement with their inability to protect FtsZ from degradation.

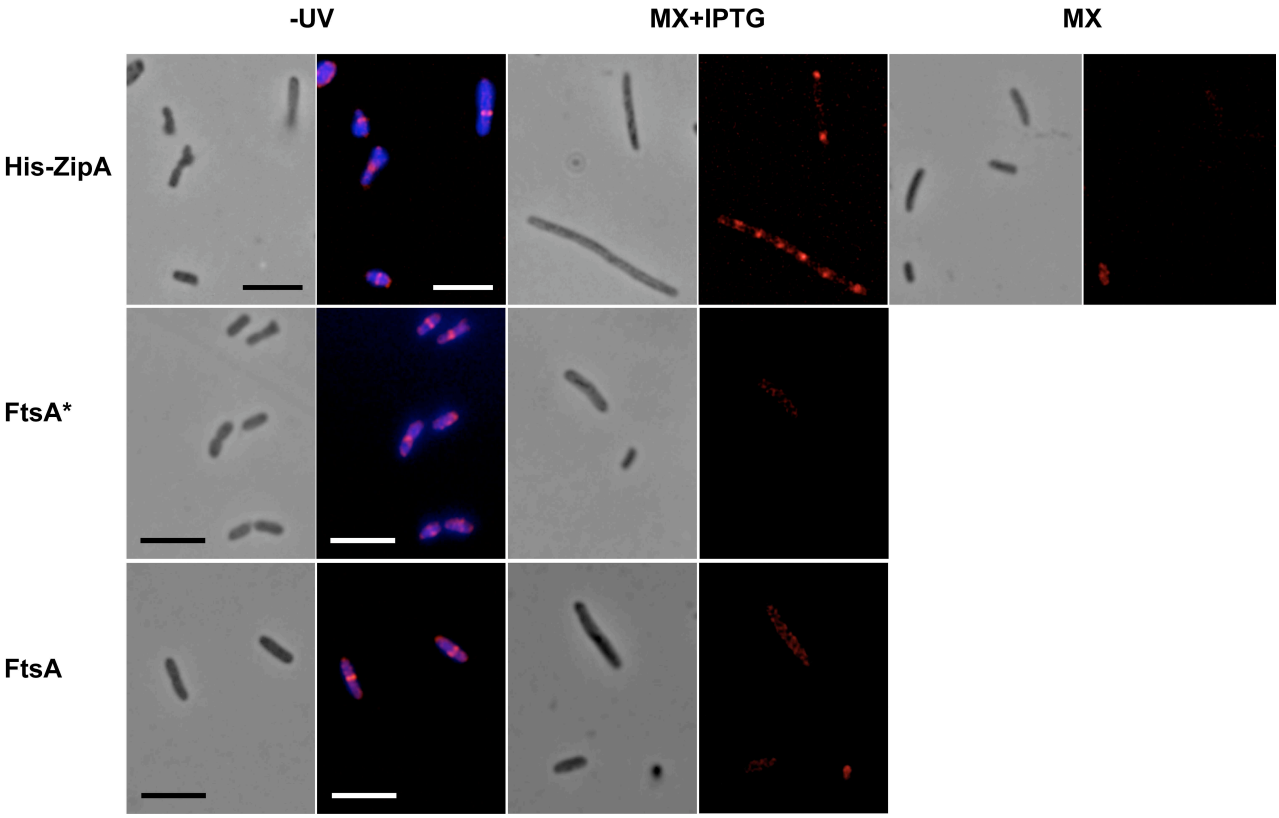

Figure 22. Localization of FtsZ stabilized by ZipA.

Phase contrast and fluorescence merged micrographs of DAPI staining and FtsZ immunolocalization images showing FtsZ location in CSR603/pPZV23 (His-ZipA), CSR603/pPZV33 (FtsA*) and CSR603/pPNV40 (FtsA) maxicells. (-UV) non-UV irradiated cells, (MX+IPTG) 16 hours after addition of IPTG at time-point +UV and (MX) 19 hours after irradiation. Scale bars represent 10 μm.

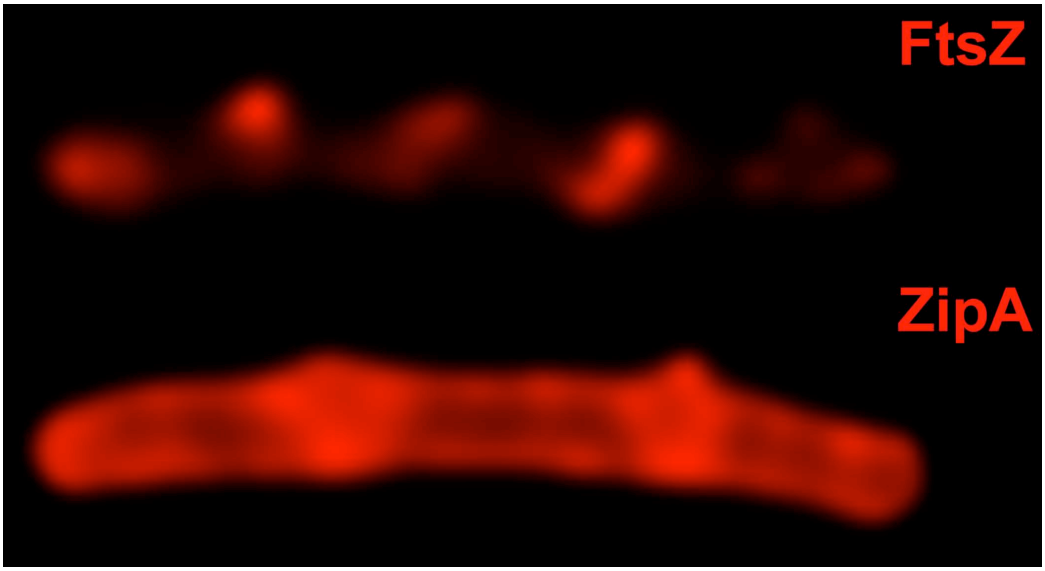

Figure 23. FtsZ helical-like structures formed by ZipA.

Snapshots of a 3D reconstitution of deconvoluted immunofluorescent image stacks of FtsZ and ZipA in CSR603/pPZV23 (His::*zipA*) 16 hours after addition of D-cycloserine and IPTG.

4. Bimolecular Fluorescence Complementation to study protein-protein interations of the early divisome assembly event

4.1. Assay setup and screening

To get a better understanding of the individual protein-protein interactions during proto-ring formation we performed bimolecular fluorescence complementation (BiFC) in growing cells and maxicells. BiFC assay is based on the irreversible reconstitution of the fluorescence signal upon association of two non-fluorescent fragments of the green fluorescent protein or its derivatives once they are brought into close proximity (Kerppola, 2008). We used the enhanced yellow fluorescent protein (YFP), which was split into YFPN (N-terminal part, amino acid residues 1 to 154) and YFPC (C-terminal part, amino acid residues 155 to 238). Both YFP fragments were fused to the proteins of interest with flexible linker sequences in order to facilitate the association between both fragments and avoid steric constrains (Hu *et al.*, 2002a). YFPN or YFPC were fused to the proto-ring components (FtsZ, FtsA and ZipA), and to FtsZ-associating proteins (MinC, SlmA, SulA, ZapA and ZapB) (Table 8).

Upon protein-protein interaction between cell division proteins, YFPN and YFPC reconstitute and produce a bright fluorescent signal in comparison with the non-specific fluorescent background (Hu *et al.*, 2002a, Hu & Kerppola, 2003, Rackham & Brown, 2004, Shyu *et al.*, 2006). YFP fragments were fused to the N-terminal end of FtsZ as it was shown for GFP-FtsZ to properly localize at midcell in growing cells (Hale & de Boer, 1999) without interfering with described FtsZ interactions via its C-terminal end (Flynn *et al.*, 2003, Camberg *et al.*, 2009). FtsA was fused via its N-terminal end as GFP-FtsA localizes at midcell (Hale & de Boer, 1999) and purified N-terminal histidine-tagged FtsA* was shown to interact *in vitro* with FtsZ (Beuria *et al.*, 2009). ZipA carries the YFP fragments fused to its C-ter end as ZipA-GFP is known to localized at midcell in growing cells (Hale & de Boer, 1999). MinC was fused by its N-terminal end to the YFP fragments as fusions at the C-terminal perturbed the MinC function (Shiomi & Margolin, 2007). The YFP fragments were fused to the N-terminal end of SulA as N-terminal Protein A-tagged SulA remains active (Trusca *et al.*, 1998). SlmA was fused by its N-terminal end as fluorescent or histidine-amino-tagged SlmA localizes properly in growing cells and interacts with FtsZ (Bernhardt & de Boer, 2005). ZapA was fused N-terminally to not interfere with the C-terminal homo-tetramer interface (Low *et al.*, 2004). Finally, ZapB was fused to the YFP fragments by its C-terminal end as ZapB-GFP was described to localize properly in growing cells (Ebersbach *et al.*, 2008). All the constructs were cloned into low copy number plasmids under the control of weak promoters, inducing an attenuated expression to avoid experimental artifacts or

toxic effects due to high protein levels. As negative controls, each single construct was overproduced individually or only YFPN together with YFPC. No fluorescence signal was obtained for these controls (data not shown).

Thirty-five combinations were asssayed for fluorescence in the *E. coli* strain WM1074 (Table 8) and the reconstitution of the YFP fluorescent signal was detected for six protein pairs, i.e. ZipA-FtsZ, ZipA-ZapA, ZapB-FtsZ, ZapB-ZapA, ZapB-ZipA and ZapB-ZapB, but not for the 29 remaining combinations.

To confirm the overexpression of each pair of proteins assayed, samples from the positive combinations were immunoblotted using anti-GFP antibody and the fusion proteins were identified at their expected molecular weights (Figure 24), indicating that the stability of the fusion proteins is similar for all cases and no degradation events take place. Note that due to the weak overproduction induced, proteins gels were overloaded for the detection of the fusion proteins (See *Methods*, 2.11).

Table 8. Overview of the BiFC screening results

	YFPC-FtsA	YFPC-FtsA*	YFPC-FtsZ	YFPC-MinC	YFPC-SlmA	YFPC-SulA	ZapA-YFPC	ZapB-YFPC	ZipA-YFPC
YFPN-FtsA	-	-	-	ND	ND	ND	ND	ND	-
YFPN-FtsA*	-	-	-	ND	ND	ND	ND	ND	-
YFPN-FtsZ	-	-	-	-	-	-	-	+	+
YFPN-MinC	ND	ND	ND	ND	ND	ND	ND	ND	ND
YFPN-SlmA	ND	ND	ND	ND	ND	ND	ND	ND	ND
YFPN-SulA	ND	ND	ND	ND	ND	ND	ND	ND	ND
ZapA-YFPN	-	-	-	ND	ND	ND	-	+	+
ZapB-YFPN	-	-	-	ND	ND	ND	-	+	-
ZipA-YFPN	-	-	-	ND	ND	ND	-	+	-

- : negative fluorescence reconstitution of YFP; + : positive fluorescence reconstitution of YFP; ND : Not determined; YFPN: enhanced yellow fluorescent protein (1-154 aa); YFPC: enhanced yellow fluorescent protein (155-238 aa)

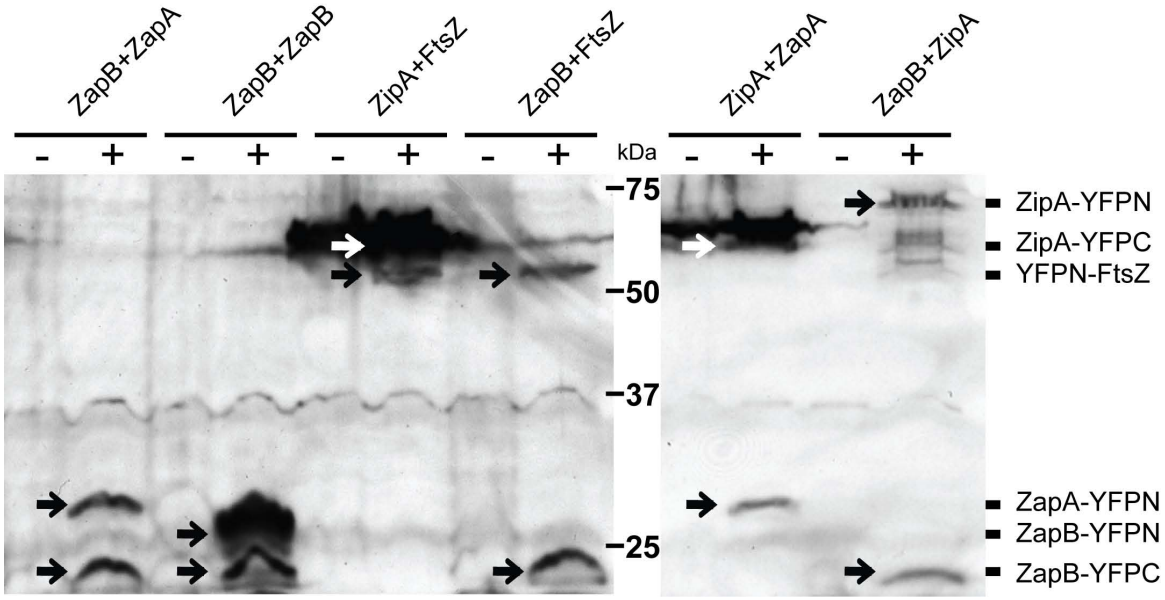

Figure 24. Protein levels of the overproduced YFPN and YFPC fusion proteins.

Immunoblot of WM1074 cell extracts non-overproducing (-) and overproducing (+) YFPN and YFPC fusion proteins. YFPN and YFPC fusion proteins were specifically detected with anti-GFP antibody at their expected molecular weights (arrows).

Table 9. Percentage of cells with positive YFP fluorescence signal reconstitution

Protein pairs overproduced	CSR603 [a]		CSR603 maxicells		PB143/pDB346 [b]	
	n	%	n	%	n	%
YFPN-FtsZ + ZipA-YFPC	1086	7.8	105	11.4	ND	ND
ZapA-YFPN + ZipA-YFPC	848	6.6	100	2	228	1.8
YFPN-FtsZ + ZapB-YFPC	2383	2.9	136	5.9	ND	ND
ZapA-YFPN + ZapB-YFPC	1358	2.9	250	5.2	ND	ND
ZipA-YFPN + ZapB-YFPC	220	10	252	0.8	223	39
ZapB-YFPN + ZapB-YFPC	496	53.4	245	40	ND	ND

[a] growing cells; [b] FtsZ-depleted growing cells; n = total of counted cells; % = cell percentage with YFP fluorescent signal; ND = not determined

The ZipA-FtsZ, ZipA-ZapA, ZapB-FtsZ, ZapB-ZapA, ZapB-ZipA and ZapB-ZapB protein combinations that resulted in fluorescence complementation in strain WM1074 were reproduced in *E. coli* CSR603 cells (showing the same localization patterns), in CSR603 maxicells and in PB143/pDB346 FtsZ-depleted growing cells (Raskin & de Boer, 1997) to test FtsZ-free backgrounds in growing and non-growing cells (Table 9). These experiments will indicate the FtsZ or cell growth implication on the observed BiFC protein-protein interaction.

4.2. ZipA-FtsZ forms fluorescent rings

The overproduction of YFPN-FtsZ and ZipA-YFPC showed fluorescence signal in growing cells and in maxicells. In both setups we observed the presence of membrane-attached fluorescent rings (Figure 25A) localized at potential cell division sites (Figure 25B), indicating that ZipA interacts with FtsZ and tethers it to the cytoplasmic membrane. The presence of rings implicates FtsZ-FtsZ interactions to form oligomeric structures, which probably involves a mixture of YFPN-FtsZ and endogenous FtsZ in growing cells, and only YFPN-FtsZ in maxicells.

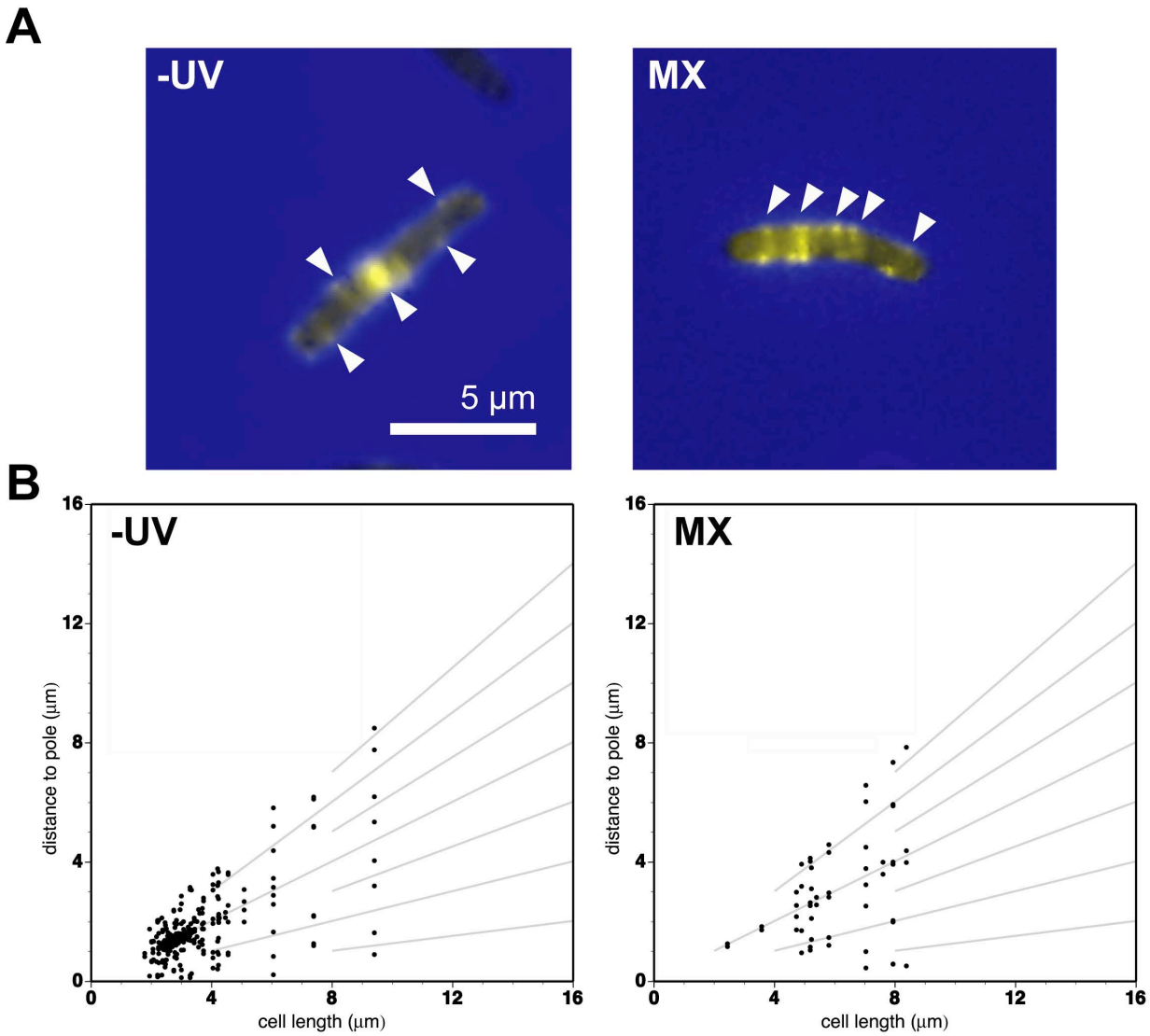

Figure 25. Localization of the YFPN-FtsZ•ZipA-YFPC complex.

(A) Merged phase contrast and fluorescence microscopy images of CSR603 growing cells (-UV) and CSR603 maxicells (MX). Yellow fluorescence signal displays the reconstituted YFPN•YFPC (eYFP) upon the simultaneous overproduction of YFPN-FtsZ and ZipA-YFPC. (B) Plot of the fluorescence signal position versus bacterial cell length of YFPN•YFPC fluorescence signal (black dots) in non UV-irradiated CSR603 growing cells (-UV) and CSR603 maxicells (MX). Grey lines mark the theoretical positions of potential septation sites contained within cells of different lengths (Tormo & Vicente, 1984).

4.3. The interaction of ZipA with ZapA requires FtsZ

Overproducing ZapA-YFPN and ZipA-YFPC we observed reconstituted fluorescence signal in growing cells as rings or as membrane-attached spots (Figure 26A) at midcell or potential cell division sites (Figure 26B). The ring structures must be FtsZ dependent, as in maxicells no or very few rings were found (Figure 26A and B). To test if this interaction is FtsZ dependent, both proteins were overproduced in the *ftsZ* thermonull strain under FtsZ-depleted conditions. No significant fluorescence reconstitution was observed (Figure 26C), indicating that ZapA-YFPN and ZipA-YFPC are not able to directly interact in the absence of FtsZ.

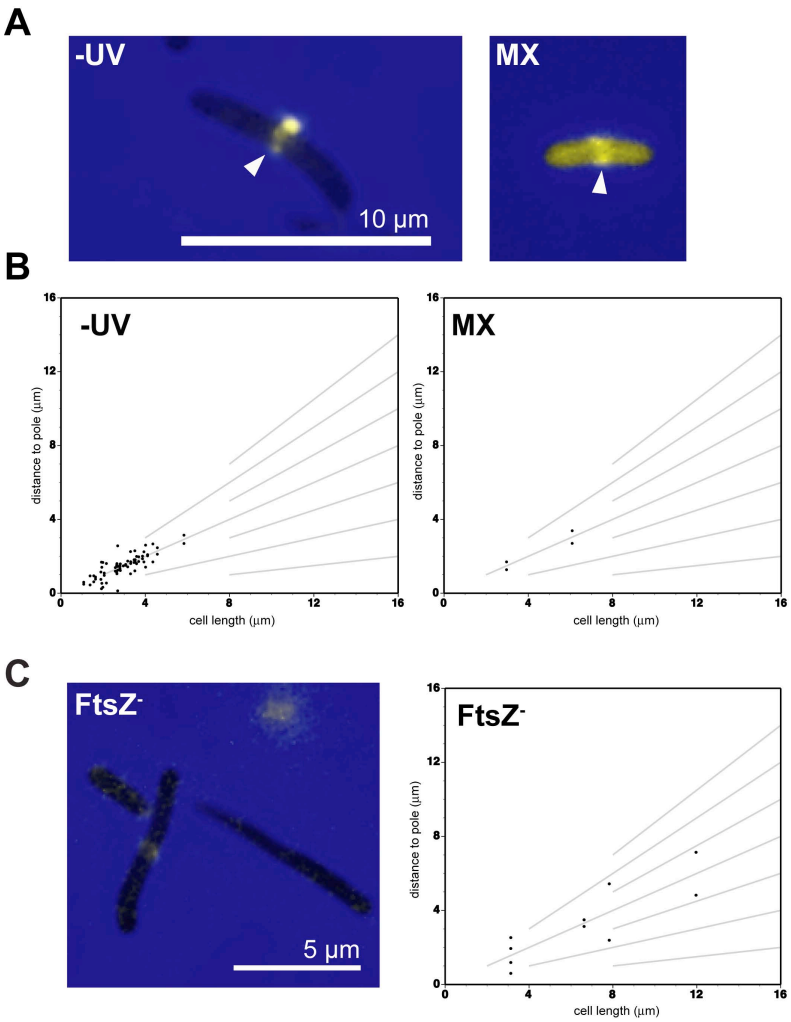

Figure 26. Localization of the ZapA-YFPN•ZipA-YFPC complex.

(A) Merged phase contrast and fluorescence microscopy images of CSR603 growing cells (-UV) and CSR603 maxicells (MX). Yellow fluorescence signal displays the reconstituted YFPN•YFPC (eYFP) upon simultaneous overproduction of ZapA-YFPN and ZipA-YFPC. **(B)** Plot of fluorescence signal position versus bacterial cell length of YFPN•YFPC fluorescence signal (black dots) in non UV-irradiated CSR603 growing cells (-UV) and CSR603 maxicells (MX). **(C)** Merged phase contrast and fluorescence microscopy image of FtsZ-depleted PB143/pDB346 growing cells (left panel), and the position of the observed fluorescence signal upon simultaneous overproduction of ZapA-YFPN and ZipA-YFPC (right panel). Grey lines mark the theoretical positions of potential septation sites contained within cells of different lengths.

4.4. ZapB self interacts at midcell and cell poles

The overproduction of ZapB-YFPN and ZapB-YFPC showed fluorescent YFP signal in growing cells and in maxicells. In both systems the fluorescent signal localized as single foci (Figure 27A) at midcell, potential cell division sites and cell poles (Figure 27B). This localization coincides with previous reports under ZapB-overproducing conditions (Ebersbach *et al.*, 2008). The interaction and placement of the fluorescent signal is FtsZ-independent as it was found in the presence and absence of FtsZ. Next to the localization, our results also support the fact that ZapB self-interacts and functions at least as a dimer (Ebersbach *et al.*, 2008).

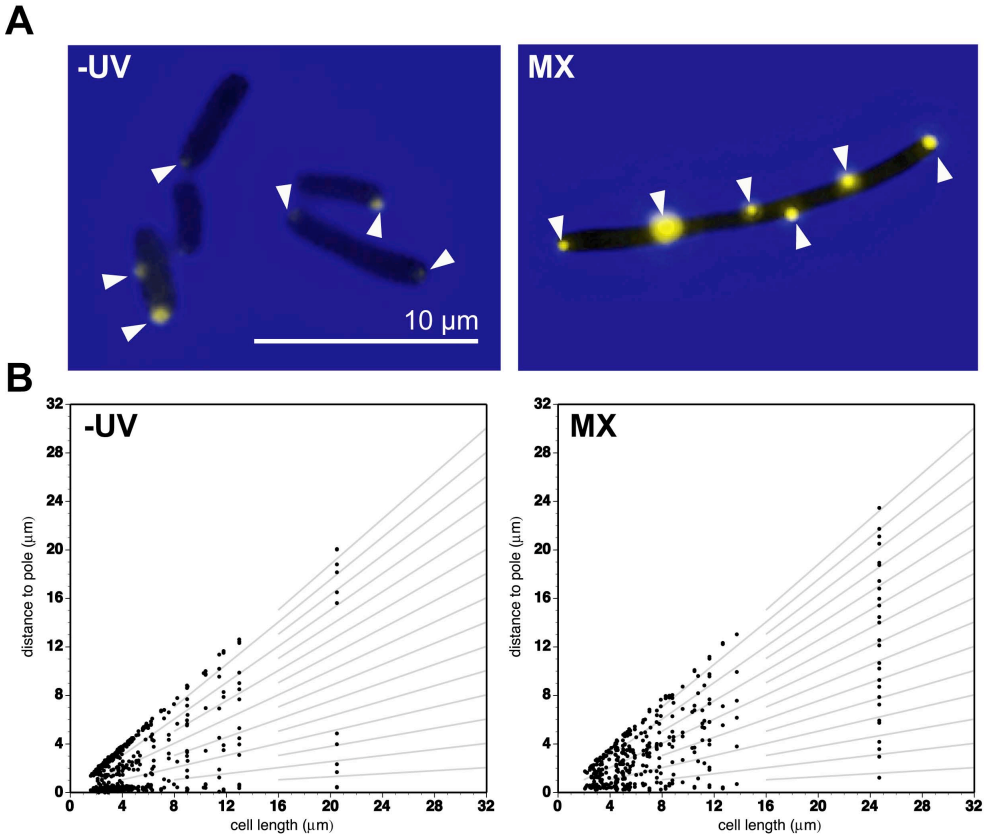

Figure 27. Localization of the ZapB-YFPN•ZapB-YFPC complex.

(A) Merged phase contrast and fluorescence microscopy images of CSR603 growing cells (-UV) and CSR603 maxicells (MX). Yellow fluorescence signal displays the reconstituted YFPN•YFPC (eYFP) upon simultaneous overproduction of ZapB-YFPN and ZapB-YFPC (arrows). **(B)** Plot of fluorescence signal position versus bacterial cell length of YFPN•YFPC fluorescence signal (black dots) in non UV-irradiated CSR603 growing cells (-UV) and CSR603 maxicells (MX). The grey lines in the plot mark the theoretical positions of potential septation sites contained within cells of different lengths.

4.5. ZapB-FtsZ interaction as single foci

The YFPN-FtsZ and ZapB-YFPC overproduction in growing cells and in maxicells displayed reconstituted YFP fluorescent foci placed close to the cytoplasmic membrane (Figure

28A), and positioned at midcell, potential division sites or close to the cell poles (Fig. 28B). These foci did not span the entire cell width, but located at one side of the cytoplasm or at the cytoplasm center without contacting the lateral cytoplasmic membrane.

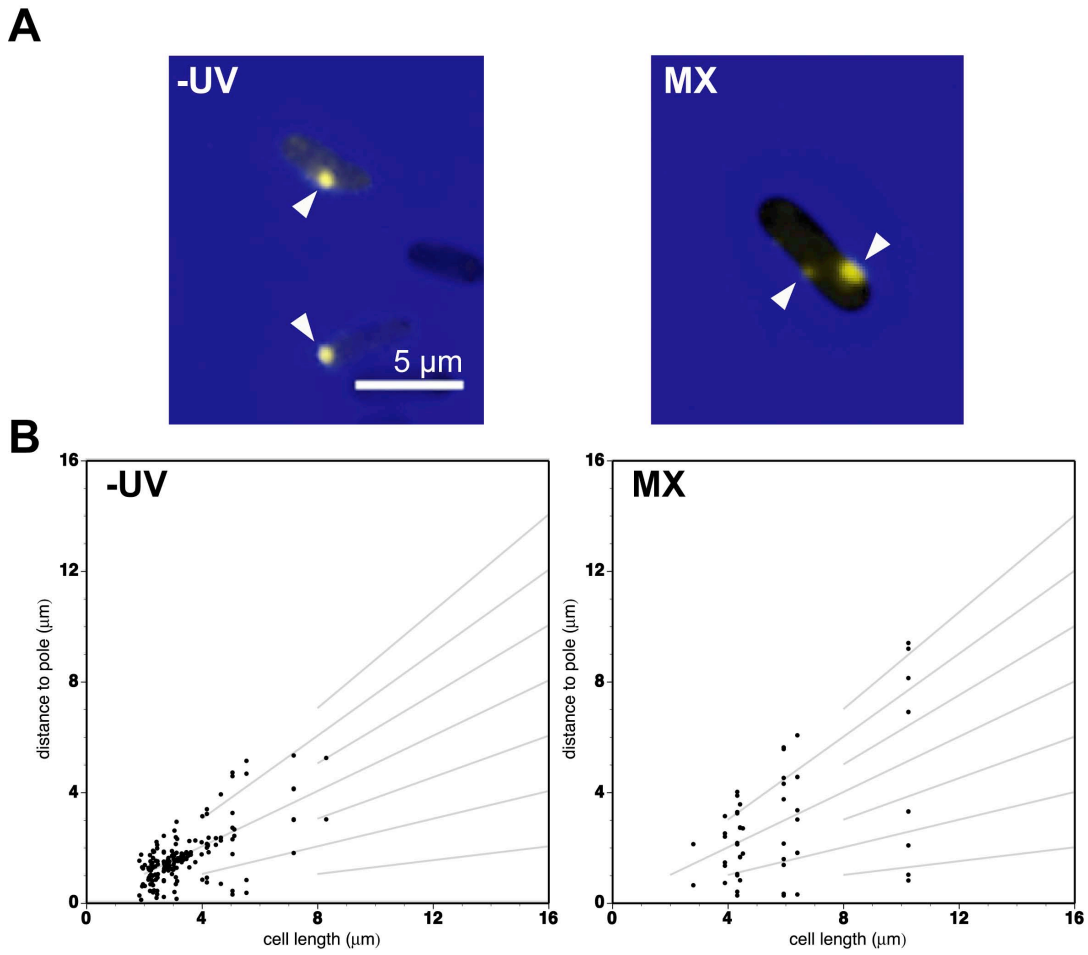

Figure 28. Localization of the YFPN-FtsZ•ZapB-YFPC complex.

(A) Merged phase contrast and fluorescence microscopy images of CSR603 growing cells (-UV) and CSR603 maxicells (MX). Yellow fluorescence signal displays the reconstituted YFPN•YFPC (eYFP) upon simultaneous overproduction of YFPN-FtsZ and ZapB-YFPC (arrows). **(B)** Plot of fluorescence signal position versus bacterial cell length of YFPN•YFPC fluorescence signal (black dots) in non UV-irradiated CSR603 growing cells (-UV) and CSR603 maxicells (MX). Grey lines mark the theoretical positions of potential septation sites contained within cells of different lengths.

4.6. ZapB recruits ZapA to the cell poles

The overproduction of ZapA-YFPN together with ZapB-YFPC showed fluorescence foci in growing cells and in maxicells (Fig. 29A), localized at midcell, potential cell division sites and close to the cell poles (Fig. 29B). While in growing cells the midcell and the potential cell division site-located foci suggests that ZapA and ZapB are recruited to the FtsZ-ring, in maxicells this

localization is Z-ring independent. The polar location of ZapB-ZapA foci suggests that ZapB may recruit ZapA to the cell poles, as suggested by Galli & Gerdes (Galli & Gerdes, 2012).

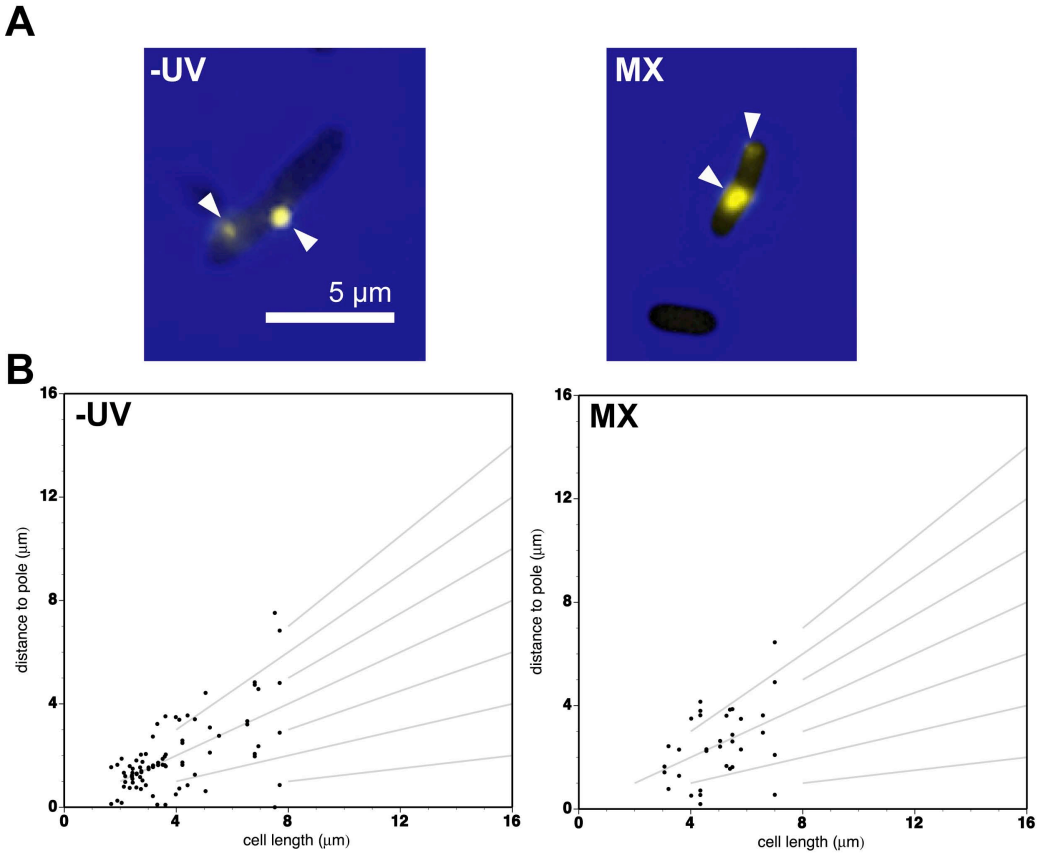

Figure 29. Localization of the ZapA-YFPN•ZapB-YFPC complex.

(A) Merged phase contrast and fluorescence microscopy images of CSR603 growing cells (-UV) and CSR603 maxicells (MX). Yellow fluorescence signal displays the reconstituted YFPN•YFPC (eYFP) upon simultaneous overproduction of ZapA-YFPN and ZapB-YFPC (arrows). **(B)** Plot of fluorescence signal position versus bacterial cell length of YFPN•YFPC fluorescence signal (black dots) in non UV-irradiated CSR603 growing cells (-UV) and CSR603 maxicells (MX). Grey lines mark the theoretical positions of potential septation sites contained within cells of different lengths.

4.7. The interaction of ZapB with ZipA occurs at the potential division sites

The overproduction of ZipA-YFPN together with ZapB-YFPC showed fluorescent ring structures or single foci at midcell, potential cell division sites and cell poles in growing cells (Figure 30B and 30C, -UV). Furthermore CSR603, as WM1074 (data not shown) displayed an aberrant phenotype. These cells present tight and elongated constrictions at the potential cell division sites that avoid cell separation (Figure 30A). Within these cells the fluorescent signal was located at the cell poles surrounding the tight constrictions, and in some cases within it (Figure 30A). In maxicells neither aberrant phenotype nor significant number of cells showing reconstituted YFP signal were found (Figure 30B and 30C, MX). To probe the FtsZ-dependency

of the ZapB-ZipA interaction in growing cells, both constructs were overproduced together in the *ftsZ* thermonull strain under FtsZ-depleted conditions. The fluorescent signal localized at midcell, potential cell division sites and cell poles (Figure 30D), but neither constrictions nor aberrant phenotype were found.

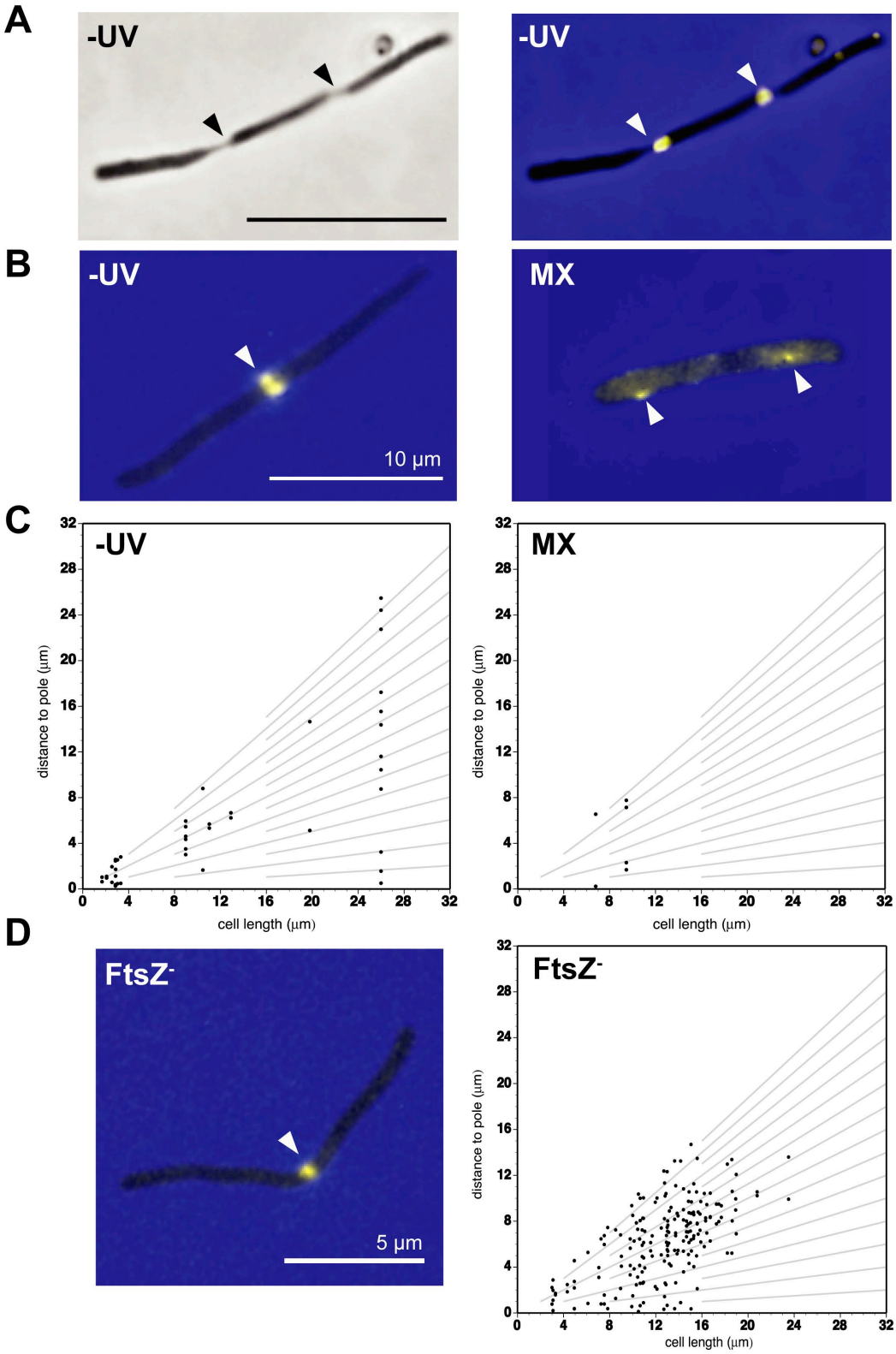

Figure 30. Localization of the ZipA-YFPN•ZapB-YFPC complex.

(A) Phase contrast (left) and merged phase contrast and fluorescence microscopy images (right) of CSR603 growing cells (-UV) showing the aberrant phenotype. Yellow fluorescence signal displays the reconstituted YFPN•YFPC (eYFP) upon simultaneous overproduction of ZipA-YFPN and ZapB-YFPC (arrows). **(B)** Merged phase contrast and fluorescence microscopy images of CSR603 growing cells (-UV) and CSR603 maxicells (MX). Yellow fluorescence signal displays the reconstituted YFPN•YFPC (eYFP) upon simultaneous overproduction of ZipA-YFPN and ZapB-YFPC (arrows). **(C)** Plot of fluorescence signal position versus bacterial cell length of YFPN•YFPC fluorescence signal (black dots) in non UV-irradiated CSR603 growing cells (-UV) and CSR603 maxicells (MX). **(D)** Merged phase contrast and fluorescence microscopy image of FtsZ-depleted PB143/pDB346 growing cells (left panel), and the position of the observed fluorescence signal upon simultaneous overproduction of ZipA-YFPN and ZapB-YFPC (right panel). The grey lines in the plot mark the theoretical positions of potential septation sites contained within cells of different lengths.

Discussion

The absence of nucleoid is accompanied by the degradation of SlmA in maxicells. This allows to dissociate the two mechanisms that operate to place the septum in *E. coli*, as the Min system is operative as evidenced by its ability to oscillate. Using maxicells we have investigated the complementary roles of Min and NO, the effect of the ZipA protein on the prevention of FtsZ degradation and the interactions of FtsZ with the proteins that have an accesory role in its assembly into a Z-ring at midcell.

1. FtsZ placement does not depend of Nucleoid Occlusion

1.1. MinCDE oscillation is independent of Nucleoid Occlusion

Analysis of maxicells has evidenced a different stability of the FtsZ and SlmA proteins relative to other divisome and septum positioning proteins, namely FtsA, ZipA and MinCDE when harboured in these cells deprived of nucleoid. The finding that FtsZ and SlmA are degraded in maxicells has allowed us to study the effect of Min in the absence of Nucleoid Occlusion (NO) and to focus on the fate of *de novo* synthesis of the FtsZ protein in the absence of endogenous FtsZ background. The oscillation of the GFP-fusion protein variants of MinD and MinE indicates that maxicells contain sufficient amount of at least ATP, MinD and MinE to support it (Hu & Lutkenhaus, 2001), and therefore that the Min system is totally independent from the nucleoid. Placement of the Z-rings at the cell center of nucleoid-less cells had been previously evidenced using segregation defective mutants (Sun *et al.*, 1998), however the Min oscillation was not studied in those cells.

1.2. Placement of the Z-ring by Min is dependent of the FtsZ C-terminal end

We have found that Min and NO, although complementary, have some specific effects on the placement of FtsZ. We have used three forms of FtsZ protein: one, $FtsZ^+$ contains no artificial domain to attach it to the membrane; the other two carry a short amphipatic helix mediating attachment with one of them, FtsZ*-VM, lacking the domain sensitive to MinC that is present in the last one, FtsZ-VM. While, in the absence of NO and presence of Min, the membrane-attached FtsZ-VM protein is confined to the poles and to a central belt, the $FtsZ^+$ protein shows a diffuse localization along the entire length. This localization may reflect a different strength in the binding of $FtsZ^+$ to the anchoring ZipA and FtsA protein relative to the strength of the direct binding of FtsZ-VM to the membrane. FtsZ-MV contains two motifs potentially able to anchor it to the membrane, the MinD-mts that provides a direct anchoring and the FtsZ C-terminal region that can associate to ZipA or FtsA providing an indirect anchoring. As the binding of $FtsZ^+$ to ZipA has been reported to be weak (Hernandez-Rocamora *et al.*, 2012) and the FtsZ polymers have been shown to displace the membrane-attached FtsA when assayed in giant vesicles (Jimenez *et al.*,

2011) we can speculate that binding of FtsZ-VM to the membrane may be stronger than $FtsZ^+$ to FtsA and ZipA. In addition, the MinD-mts has been reported to show a binding preference for the cardiolipin rich polar regions of the cell (Mileykovskaya *et al.*, 2003), in which some residual amounts of FtsA and ZipA may remain as remnants from the previous division event (Teather *et al.*, 1974). Together this could be a reasonable explanation to account for the preferential polar localization of the FtsZ-VM protein observed in maxicells and in VIP2 filaments, while the FtsZ*-VM protein, the third assayed FtsZ variant attached to the membrane by the MinDmts but lacking the C-terminal region of FtsZ would not bind with sufficient strength to accumulate at those locations.

Interestingly, in *E. coli* growing cells NO still affects the localization of membrane-attached FtsZ*-VM that, instead of appearing uniformly distributed along the membrane length, is organized as discrete rings or short spirals located preferentially at potential septation sites (Figure 12 and 13). On the contrary, the pattern adopted by this protein in maxicells show a succession of bands uniformly spaced along the cell length (Figure 14), indicating that the protein is insensitive to the action of the Min system.

In *E. coli* the MinDmts domain only functions as a membrane targeting sequence when at least two MinDmts sequences are in close proximity, on the contrary no membrane binding is observed (Szeto *et al.*, 2002). While FtsZ-VM and FtsZ*-VM form membrane-attached ring, belt or cap structures, the Venus protein fused to MinDmts (VM) or the FtsZ C-terminal end fused to Venus-MinDmts (ZC-VM) show a cytoplasmic localization. From these results we can infer that the attachment of the MinDmts-fused proteins to the inner membrane is promoted by the ability of the FtsZ motif to polimerize, as shown for FtsZ-VM and FtsZ*-VM, that connects and brings close the MinDmts sequences.

Using strains in which the Min system, the nucleoid occlusion or both have been genetically abolished in *Bacillus subtilis*, it has been recently proposed that nucleoid occlusion and Min may not have a role in determining the cell centre but promote a more efficient use of the midcell position to assemble a Z-ring (Rodrigues & Harry, 2012). This has led to the proposal that an additional undiscovered mechanism has to operate in marking the *B. subtilis* cell centre. In maxicells where NO is abolished, the analysis of the distribution of Z-rings formed by the Min insensitive protein FtsZ*-VM shows that this protein is not proficient at finding the cell centre (Figure 14), indicating that if a center marking device different from NO and Min exists in *E. coli* it may operate on the FtsZ C-terminal end that also mediates the interaction of FtsZ with MinC, FtsA or ZipA.

2. The cell division role of ZipA involves the protection of FtsZ

2.1. ZipA stabilizes the FtsZ protein levels

Out of the three components of the proto-ring (Vicente & Rico, 2006), we found that FtsZ is specifically degraded in maxicells, while the other two, FtsA and ZipA, are stable. Our results show that FtsZ is present at low levels due to both the specific degradation of FtsZ by ClpP and to the absence of *de novo* synthesis. Although the FtsZ degradation seems to be independent of the ClpX moiety, we cannot exclude that a different recognition unfoldase, as ClpA (Hoskins *et al.*, 2000a, Hoskins *et al.*, 2000b) may take over the role of ClpX in maxicells.

To further find if the two other components of the proto-ring, FtsA and ZipA, could prevent FtsZ degradation, we overproduced them in maxicells. While overproduction of ZipA reduces the degradation of FtsZ in maxicells, the overproduction of the other proto-ring component $FtsA^+$ or the gain-of-function mutant FtsA* (Geissler *et al.*, 2007) do not. As all but one of the last FtsZ eighteen C-terminal amino acid residues (Ala-366) that are needed for its recognition by ClpX (Camberg *et al.*, 2009) coincide with the sequence that interacts with ZipA (Mosyak *et al.*, 2000), we propose that masking of the C-terminal end of FtsZ by the ZipA FZB domain underlies the observed protection. Although FtsA, and presumably FtsA*, also bind to the same C-terminal end of FtsZ as ZipA, the nature of each interaction is different (Figure 30). The FtsZ C-terminal end is embedded into a hydrophobic pocket of the ZipA FZB and is folded as an extended α-helix exposing its hydrophobic residues at one side of the helix towards the binding interface (Mosyak *et al.*, 2000). On the other hand, the binding of the C-terminal α-helix of FtsZ to FtsA is electrostatic, the hydrophobic residues are buried inside the bent allowing the peptide chain to create a water-bound flat polar interface with FtsA (Szwedziak *et al.*, 2012). These differences in binding may be invoked to explain the different behaviour of ZipA or FtsA in FtsZ protection but the specific details of each interaction need to be investigated further.

The protection of FtsZ by ZipA is not affected by the simultaneous presence of either FtsA or FtsA* (Figure 19). Detailed examination of the structures adopted by the ZipA FZB or FtsA when interacting with FtsZ suggests that due to steric impediments it is not possible for both proteins to bind simultaneously to the same FtsZ molecule (Figure 31B).

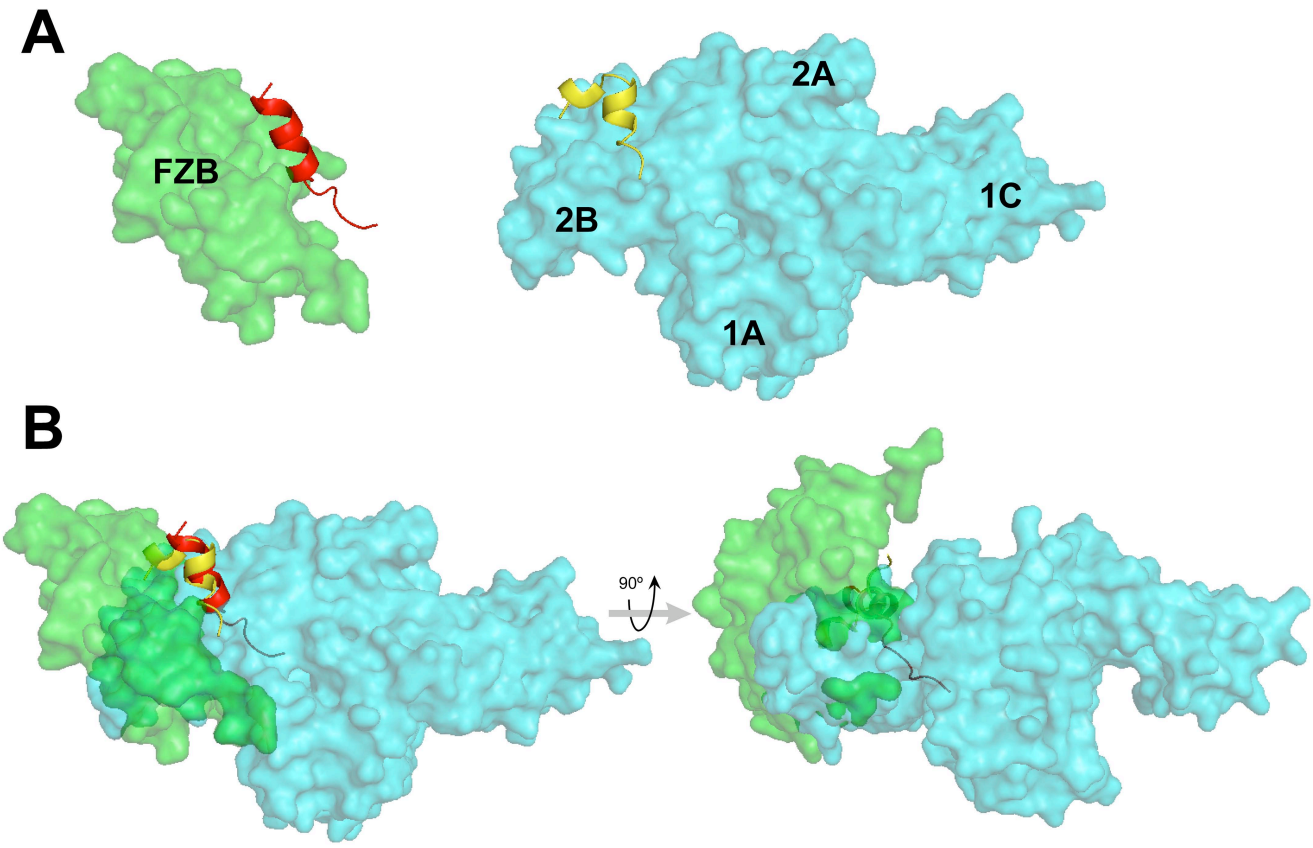

Figure 31. Structure of the ZipA and FtsA regions involved in the binding to the FtsZ C-terminal end.

(A) At the left-hand side *E. coli* ZipA (green) and FtsZ C-terminal end (red; adapted from PDB 1F47) (Mosyak *et al.*, 2000). At the right-hand side the *T. maritima* FtsA (cyan) and FtsZ C-terminal end (yellow; adapted from PDB 4A2A) (Szwedziak *et al.*, 2012). (B) The structures shown in panel A have been oriented to maintain the overlap of the two conformations of the FtsZ C-terminal end as published by Szwedziak *et al.* (Szwedziak *et al.*, 2012) (colours as in panel A).

FtsA* has been shown to bypass some of the functions exerted by ZipA in the assembly and stability of the divisome, among them the need for ZipA in the assembly of late divisome proteins (Geissler *et al.*, 2003, Geissler & Margolin, 2005, Geissler *et al.*, 2007), and therefore we expected that it could act by protecting FtsZ from degradation. Instead, we found that neither FtsA nor FtsA* protect FtsZ in maxicells. Similarly to our observations on $FtsZ^{+}$, while overproduction of ZipA has been shown to stabilize the rings formed by FtsZ84 at the non-permissive temperature (RayChaudhuri, 1999), FtsA* has no effect on the stability of the FtsZ84 rings at 42ºC (Geissler *et al.*, 2007). These published results did not include data on the effects of either ZipA or FtsA* on the protection of FtsZ84. It is possible then that the effects of ZipA take place on the stability of the FtsZ protein, while those of FtsA* are exerted on the stability of the FtsZ ring rather than on the protein itself. According to that a model for the mechanism of the FtsA gain-of-function mutants has been described (Pichoff *et al.*, 2012). The finding that most of these mutants have

reduced ability to self-interact may indicate that only FtsA monomers would be involved in the recruitment of late assembly proteins during the divisome formation. However, Pichoff and co-workers also mention that maybe it is not the unique mechanism by which FtsA mutants bypass the ZipA requirement, as almost 20% of the FtsA gain-of-function mutants described do not have impairment in self-interaction.

2.2. The C-terminal end of FtsZ, a central hub during the divisome assembly

In addition to the interactions with FtsA, ZipA and ClpX (Wang *et al.*, 1997, Ma & Margolin, 1999, Liu *et al.*, 1999, Mosyak *et al.*, 2000, Haney *et al.*, 2001, Szwedziak *et al.*, 2012, Camberg *et al.*, 2009), the C-terminal end of FtsZ also interacts with the C-terminal domain of MinC, the FtsZ polymerization inhibitor of the Min system (Shen & Lutkenhaus, 2009). Depending on which molecule is accepted for the interaction the fate of the FtsZ molecule will be directed to the production of a division ring or prevented from acting in cytokinesis (Figure 32). In *Bacillus subtilis* SepF and EzrA, positive and negative modulators of the FtsZ polymerization respectively, also bind to FtsZ at this site (Singh *et al.*, 2008, Krol *et al.*, 2012, Singh *et al.*, 2007). This suggests a role for the C-terminal end of FtsZ as a central hub to integrate different signals that modulate the efficiency and progress of divisome assembly and for ZipA as having a dual role in the anchoring and the stability of FtsZ.

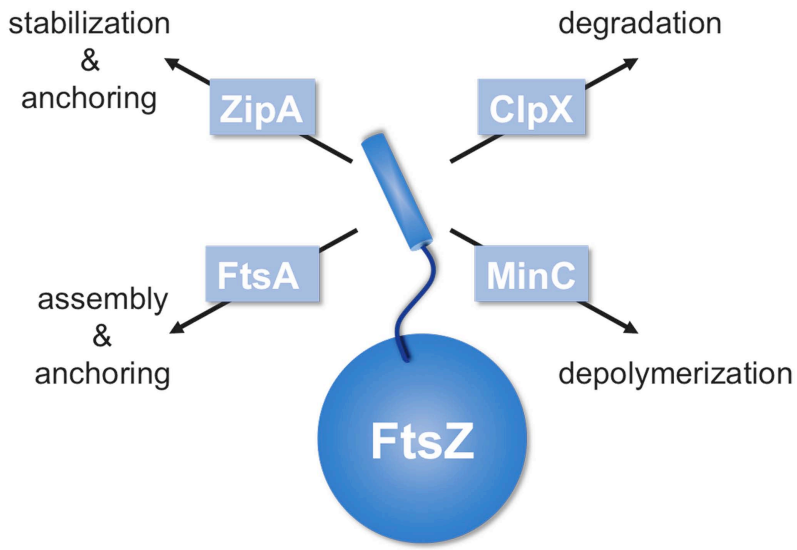

Figure 32. The C-terminal end of FtsZ as a central hub to integrate signals that modulate divisome assembly in *E. coli*.

The C-terminal end of FtsZ is represented as a cilinder protruding from the bulk of the protein on which different modulators can exert their action. FtsA and ZipA would promote septation while ClpX and MinC would prevent it.

3. Identification and visualization of *E. coli* divisome interactions by bimolecular fluorescence complementation

3.1 Topology of the protein-protein interactions, a key factor

In addition to the main three components of the proto-ring, a set of accessory proteins as ZapA, ZapB, MinC, SlmA or SulA have been described to play a role on the Z-ring assembly. They are not individually essential, but their loss is additive on the functionality of the cell division. Multiple interactions between the *E. coli* divisome components have been described suggesting the formation of multiprotein complexes at midcell (Rothfield *et al.*, 1999, Di Lallo *et al.*, 2003, Karimova *et al.*, 2005). Bimolecular Fluorescence Complementation (BiFC) (Hu *et al.*, 2002a, Kerppola, 2008) has been used to study *in vivo* the interactions between different proteins involved in the Z-ring formation. YFP fluorescence was observed for a specific combination of the YFP fragment fusions, e.g YFPN fused to FtsZ and YFPC to ZipA, but not if YFPC is fused to FtsZ and YFPN to ZipA, perhaps because a specific topology of the fused YFP fragments is necessary for the fluorescence reconstitution. Further progress in the study of proto-ring interactions using BiFC will require to combine fusions to both N- and C-terminal ends of the proteins due to, as shown, is not frequent that fluorescent protein reconstitution could be detected using both configurations, exchanging the fragments from one partner to the other. Moreover different length linkers could be also used in order to minimize possible steric constrains.

Using BiFC we have not detected some interactions, as FtsZ-FtsZ, FtsZ-FtsA, FtsA-FtsA and ZapA-ZapA that have been previously published. This discrepancy can be due to the topology and orientation of the YFP fragments in the fusion constructs. In the case of FtsZ-FtsZ or ZapA-ZapA, the absence of fluorescence reconstitution probably is due to their interaction involving a head-to-tail or an anti-parallel manner respectively (Figure 2 and 5) (Mingorance *et al.*, 2010, Low *et al.*, 2004). These conformations would not allow the fluorescent protein fragments fused at the N-terminal end of FtsZ or at the C-terminal end of ZapA to be close enough to associate. The expected interactions between FtsZ and MinC, SlmA or SulA were not observed and this could also happen due to the YFPN-YFPC topology not allowing the interaction. In these cases the partners involved in the interaction are known to inhibit the Z-ring, what would perhaps be the primary cause for the lack of a positive result in the BiFC test.

3.2. Physiological localization of the protein-protein interactions

A great advantage of BiFC over other visualization methods to study protein interactions in living cells is that proteins assayed can be produced at levels comparable to the endogenous ones. Under mild overproducing conditions, cells appear slightly filamented, but they mostly do not show aberrant phenotypes. This allows to study protein-protein interactions under physiological conditions that it can reveal some of the interactions that have not been evidenced when other techniques were used. In all the pair of proteins that show a reconstituted fluorescent signal, with exception of ZapB-ZapA, the YFP signal is found where there is a coincidence of localization patterns of both proteins (Figure 33). This supports that the YFP signal found reflects the physiological location of each interaction during the cell cycle.

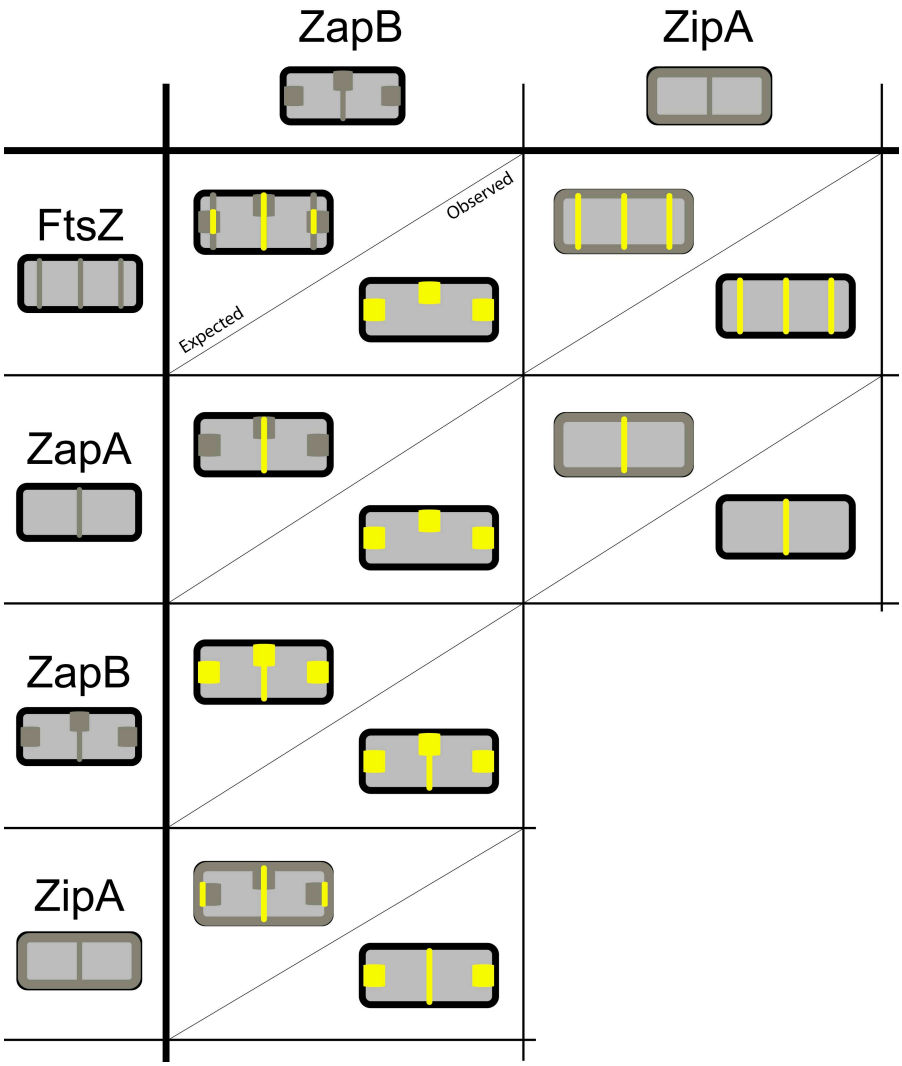

Figure 33. Overview of the expected and observed localization pattern of the reconstituted YFPN•YFPC fluorescent signals obtained.

Header of columns and rows represent the localization pattern of the individual proteins (Vicente *et al.*, 2006, Ebersbach *et al.*, 2008). The expected and observed fluorescent signal localization pattern for the positive combinations obtained in this work is drawn in the intersection of the respective column and row.

3.3. FtsZ interaction with ZapA and ZapB at the cell poles

It has been described that the interaction of ZapB with FtsZ, at midcell, requires the previous binding of ZapA to FtsZ (Ebersbach *et al.*, 2008, Galli & Gerdes, 2010). Whereas the interaction between FtsZ and ZapA has been described to occur preferentially at midcell, the ZapB protein localize both at midcell and at cell poles. We have observed that ZapA besides localizing at midcell also localizes at the cell poles where it interacts with ZapB. This result supports the suggested inhibitory role of ZapB over the ZapA capacity of binding to and bundling FtsZ at midcell (Galli & Gerdes, 2012). Surprisingly we find that ZapB can direct FtsZ to localize at the cell pole, which has been already suggested based on the observation that overproduction of ZapB in a *ΔzapAΔzapB* strain stimulated the Z-ring assembly (Galli & Gerdes, 2010). As in the presence of ZapB we find ZapA to be also at the poles, we cannot exclude a role of ZapA to participate in the polar localization of FtsZ.

3.4. The interaction of ZapB with ZipA occurs at the potential cell division sites

The mild overproduction of the proteins ZipA and ZapB provokes an aberrant phenotype of *E. coli* growing cells, with tight and elongated constrictions linking the potential daughter cells, suggesting a cell division blockage at late stages of the cell division cycle. This phenotype resembles the phenotype showed under high ZapB overproduction conditions (Ebersbach *et al.*, 2008), in cells carrying an FtsK mutation (Diez *et al.*, 1997) or in cells carrying mutations in the periplasmic amidase AmiC or the peptidase EnvC (Bernhardt & de Boer, 2003, Hara *et al.*, 2002). AmiC and EnvC are peptidoglycan modifying enzymes involved in the separation of the daughters cells at the end of the cell cycle. The found ZipA-ZapB interaction most likely visualizes a transient trapped protein-protein interaction that does not depend on the FtsZ concentration, but leads to the aberrant phenotype when FtsZ is present in growing cells (Figure 30). The tight and elongated constrictions suggest impairment on the cell separation process that might be produced by a potential effect of the BiFC-trapped interaction of ZipA with ZapB over AmiC, EnvC or FtsK, or maybe by an overstabilization of the Z-ring that would avoid the disassembly of the cell division ring and the correct cell separation.

The ZipA-ZapB interaction was not detected in maxicells, suggesting that it requires the active growth of the cell or perhaps the presence of a nucleoid. *E. coli* cell growth involves cell elongation and cell division, in which different protein complexes direct the synthesis of the peptidoglycan cell wall. A transitional step between them, the preseptal peptidoglycan synthesis, incorporates new peptidoglycan forming a ring at the midcell. FtsZ and ZipA are the only two proteins necessary to direct the preseptal peptidoglycan synthesis to midcell (185). The BiFC-

trapped ZipA-ZapB interaction may interfere with this action, producing the aberrant phenotype. Although our results show that the ZipA-ZapB interaction does not depend on the FtsZ concentration (Figure 30D), ZipA and ZapB might both stabilize and nucleate the residual amount of FtsZ in growing cells under FtsZ-depleted conditions (less than 20%) (Raskin & de Boer, 1997), and consequently be localized at the potential cell division sites.

4. Stability, placement and interactions of the divisome components in nucleoid-deprived *Escherichia coli* cells

In this study we have used maxicells as a convenient and potent tool to study some crucial aspects of bacterial division. Among them we have found that both septum positioning mechanisms, Min and NO, may complement each other to fine tune the localization of Z-rings. In its turn, the FtsZ protein becomes degraded by a mechanism involving ClpP protease and it can be protected by ZipA from this degradation. This is a role that cannot be substituted by FtsA or even by FtsA*. We have evidenced an undescribed interaction between the accesory proteins ZapB and ZipA. Finally the ZapB protein, by itself or in combination with ZapA may place FtsZ at the poles and together with a modified ZipA may contribute to alter the maturation of the septum. Maxicells may then be considered as an excellent system to bridge *in vivo* and *in vitro* studies and to discover new molecular mechanisms that participate in bacterial division.

Conclusions

- The only presence of the Min system is able to restrict the location of the Z-ring. The Min oscillatory movement is maintained from pole-to-pole in the absence of the Nucleoid Occlusion (NO) system, indicating that it does not depend on the chromosomal DNA. Both septum placement systems have synergic effects on the FtsZ placement, as shown by the localization of the FtsZ variants FtsZ-VM and FtsZ*-VM in maxicells and growing cells under FtsZ-depletion. Maxicells are able to maintain the energy systems as can be inferred by the Min oscillation and the Z-ring formation, which are ATP and GTP-dependent respectively.

- The proto-ring component ZipA stabilizes FtsZ. This stabilization avoids the ClpP-mediated FtsZ degradation. The carboxyl globular domain of ZipA (FZB) is the unique region of the protein necessary to bind to and carry out the FtsZ protection. Neither FtsA nor its gain-of-function mutant FtsA* are able to protect FtsZ, indicating that it is a specific role of ZipA that cannot be substituted by them.

- The regulatory network between the Z-ring and its effector proteins is complex. The interaction of ZapB with ZapA at the cell poles supports the inhibitory role of ZapB on ZapA. The novel ZapB-FtsZ interaction at the cell poles indicates a direct interaction between the two proteins, although we cannot discard the presence of ZapA mediating this interaction. The trapped ZipA-ZapB interaction produced an aberrant phenotype by impairment on the cell separation process, in which may be involved the ZipA-directed preseptal peptidoglycan synthesis.

Conclusiones

- La sola presencia del sistema Min es capaz de restringir la localización del anillo de FtsZ. El movimiento oscilatorio del sistema Min desde un polo a otro de la célula se mantiene en ausencia del sistema de oclusión por nucleoide, lo cual indica que no es dependiente de la presencia del ADN cromosomal. Ambos sistemas de posicionamiento del septo tienen efectos sinérgicos sobre la localización del anillo de FtsZ, como se ha observado mediante la localización de las variantes FtsZ-VM y FtsZ*-VM en células en crecimiento carentes de FtsZ. Las maxicélulas son capaces de mantener los sistemas energéticos como se deduce de la observación de la oscilación de Min y de la formación de anillos de FtsZ, los cuales son procesos dependientes de ATP y GTP respectivamente.

- El componente del proto-anillo ZipA estabiliza a la proteína FtsZ. Esta estabilización evitando su degradación mediada por ClpP. El dominio globular carboxilo terminal de ZipA (FZB) es la única región necesaria para la unión y protección de FtsZ. Ni FtsA ni su mutante FtsA* son capaces de llevar a cabo dicha protección, indicando que es una función específica de ZipA la cual no puede ser compensada por ninguna de ellas dos.

- La red reguladora entre el anillo de FtsZ y sus proteínas efectoras es compleja. La interacción de ZapB con ZapA en los polos apoya la función inhibitoria de ZapB sobre ZapA. La nueva interacción ZapB-FtsZ en los polos indica una interacción directa entre ambas proteínas, aunque no se puede descartar la presencia y mediación de ZapA en dicha interacción. La interacción "atrapada" entre ZipA y ZapB produce un fenotipo aberrante provocado por un defecto en el proceso de separación de las células, en el cual podría estar implicada la sintésis de peptidoglicano preseptal.

References

Adams, D. W. & J. Errington, (2009) Bacterial cell division: assembly, maintenance and disassembly of the Z ring. *Nat Rev Microbiol* **7**: 642-653.

Addinall, S. G., E. Bi & J. Lutkenhaus, (1996) FtsZ ring formation in *fts* mutants. *J. Bacteriol.* **178**: 3877-3884.

Addinall, S. G., C. Cao & J. Lutkenhaus, (1997) FtsN, a late recruit to the septum in *Escherichia coli*. *Mol. Microbiol.* **25**: 303-309.

Addinall, S. G. & J. Lutkenhaus, (1996) FtsA is localized to the septum in an FtsZ-dependent manner. *J.Bacteriol.* **178**: 7167.

Amann, E., J. Brosius & M. Ptashne, (1983) Vectors bearing a hybrid trp-lac promoter useful for regulated expression of cloned genes in Escherichia coli. *Gene* **25**: 167.

Baba, T., T. Ara, M. Hasegawa, Y. Takai, Y. Okumura, M. Baba, K. A. Datsenko, M. Tomita, B. L. Wanner & H. Mori, (2006) Construction of Escherichia coli K-12 in-frame, single-gene knockout mutants: the Keio collection. *Mol Syst Biol* **2**: 2006 0008.

Baele, M., L. A. Devriese & F. Haesebrouck, (2001) Lactobacillus agilis is an important component of the pigeon crop flora. *J Appl Microbiol* **91**: 488-491.

Bagg, A., C. J. Kenyon & G. C. Walker, (1981) Inducibility of a gene product required for UV and chemical mutagenesis in Escherichia coli. *Proc Natl Acad Sci U S A* **78**: 5749-5753.

Beggs, J. D., (1978) Transformation of yeast by a replicating hybrid plasmid. *Nature* **275**: 104-109.

Bernhardt, T. G. & P. A. de Boer, (2005) SlmA, a nucleoid-associated, FtsZ binding protein required for blocking septal ring assembly over Chromosomes in E. coli. *Mol Cell* **18**: 555-564.

Bernstein, F. C., T. F. Koetzle, G. J. Williams, E. F. Meyer, Jr., M. D. Brice, J. R. Rodgers, O. Kennard, T. Shimanouchi & M. Tasumi, (1977) The Protein Data Bank: a computer-based archival file for macromolecular structures. *J Mol Biol* **112**: 535-542.

Bi, E. & J. Lutkenhaus, (1993) Cell division inhibitors SulA and MinCD prevent formation of the FtsZ ring. *J Bacteriol* **175**: 1118-1125.

Bolivar, F., R. L. Rodriguez, M. C. Betlach & H. W. Boyer, (1977) Construction and characterization of new cloning vehicles. I. Ampicillin-resistant derivatives of the plasmid pMB9. *Gene* **2**: 75-93.

Bork, P., C. Sander & A. Valencia, (1992) An ATPase domain common to prokaryotic cell cycle proteins, sugar kinases, actin, and hsp70 heat shock proteins. *Proc Natl Acad Sci U S A* **89**: 7290-7294.

Broome-Smith, J. K., A. Edelman, S. Yousif & B. G. Spratt, (1985) The nucleotide sequences of the ponA and ponB genes encoding penicillin-binding protein 1A and 1B of Escherichia coli K12. *Eur J Biochem* **147**: 437-446.

Broome-Smith, J. K. & B. G. Spratt, (1982) Deletion of the penicillin-binding protein 6 gene of Escherichia coli. *J Bacteriol* **152**: 904-906.

Bullock, W. O., J. M. Fernandez & J. M. Short, (1987) XL1-Blue: A high efficiency plasmid transforming *recA E.coli* strain with beta-galactosidase selection. *Biotechniques* **5** 376-378.

Busiek, K. K., J. M. Eraso, Y. Wang & W. Margolin, (2012) The early divisome protein FtsA interacts directly through its 1c subdomain with the cytoplasmic domain of the late divisome protein FtsN. *J Bacteriol* **194**: 1989-2000.

Camberg, J. L., J. R. Hoskins & S. Wickner, (2009) ClpXP protease degrades the cytoskeletal protein, FtsZ, and modulates FtsZ polymer dynamics. *Proc Natl Acad Sci U S A* **106**: 10614-10619.

Camberg, J. L., J. R. Hoskins & S. Wickner, (2011) The interplay of ClpXP with the cell division machinery in Escherichia coli. *J Bacteriol* **193**: 1911-1918.

Casadaban, M. J., (1976) Transposition and fusion of the lac genes to selected promoters in Escherichia coli using bacteriophage lambda and Mu. *J Mol Biol* **104**: 541-555.

Castellazzi, M., J. George & G. Buttin, (1972) Prophage induction and cell division in E. coli. I. Further characterization of the thermosensitive mutation tif-1 whose expression mimics the effect of UV irradiation. *Mol Gen Genet* **119**: 139-152.

Chen, Y. & H. P. Erickson, (2005) Rapid in vitro assembly dynamics and subunit turnover of FtsZ demonstrated by fluorescence resonance energy transfer. *J Biol Chem* **280**: 22549-22554.

Chen, Y., S. L. Milam & H. P. Erickson, (2012) SulA Inhibits Assembly of FtsZ by a Simple Sequestration Mechanism. *Biochemistry* **51**: 3100-3109.

Cho, H., H. R. McManus, S. L. Dove & T. G. Bernhardt, (2011) Nucleoid occlusion factor SlmA is a DNA-activated FtsZ polymerization antagonist. *Proc Natl Acad Sci U S A* **108**: 3773-3778.

Corbin, B. D., B. Geissler, M. Sadasivam & W. Margolin, (2004) Z-ring-independent interaction between a subdomain of FtsA and late septation proteins as revealed by a polar recruitment assay. *J.Bacteriol.* **186**: 7736.

Cordell, S. C., R. E. Anderson & J. Löwe, (2001) Crystal structure of the bacterial cell division inhibitor MinC. *Embo J* **20**: 2454-2461.

Cordell, S. C., E. J. Robinson & J. Löwe, (2003) Crystal structure of the SOS cell division inhibitor SulA and in complex with FtsZ. *Proc Natl Acad Sci U S A* **100**: 7889-7894.

Dai, K. & J. Lutkenhaus, (1992) The proper ratio of FtsZ to FtsA is required for cell division to occur in Escherichia coli. *J Bacteriol* **174**: 6145-6151.

Dajkovic, A., G. Lan, S. X. Sun, D. Wirtz & J. Lutkenhaus, (2008a) MinC spatially controls bacterial cytokinesis by antagonizing the scaffolding function of FtsZ. *Curr Biol* **18**: 235-244.

Dajkovic, A., A. Mukherjee & J. Lutkenhaus, (2008b) Investigation of regulation of FtsZ assembly by SulA and development of a model for FtsZ polymerization. *J Bacteriol* **190**: 2513-2526.

Davie, E., K. Sydnor & L. I. Rothfield, (1984) Genetic basis of minicell formation in Escherichia coli K-12. *J Bacteriol* **158**: 1202-1203.

de Boer, P. A., R. E. Crossley & L. I. Rothfield, (1988) Isolation and properties of minB, a complex genetic locus involved in correct placement of the division site in Escherichia coli. *J Bacteriol* **170**: 2106-2112.

de Boer, P. A., R. E. Crossley & L. I. Rothfield, (1989) A division inhibitor and a topological specificity factor coded for by the minicell locus determine proper placement of the division septum in E. coli. *Cell* **56**: 641-649.

de Boer, P. A., R. E. Crossley & L. I. Rothfield, (1990) Central role for the Escherichia coli minC gene product in two different cell division-inhibition systems. *Proc Natl Acad Sci U S A* **87**: 1129-1133.

de Boer, P. A., R. E. Crossley & L. I. Rothfield, (1992) Roles of MinC and MinD in the site-specific septation block mediated by the MinCDE system of Escherichia coli. *J Bacteriol* **174**: 63-70.

Diez, A. A., A. Farewell, U. Nannmark & T. Nystrom, (1997) A mutation in the ftsK gene of Escherichia coli affects cell-cell separation, stationary-phase survival, stress adaptation, and expression of the gene encoding the stress protein UspA. *J Bacteriol* **179**: 5878-5883.

Draper, G. C., N. McLennan, K. Begg, M. Masters & W. D. Donachie, (1998) Only the N-terminal domain of FtsK functions in cell division. *J Bacteriol* **180**: 4621-4627.

Durand-Heredia, J., E. Rivkin, G. Fan, J. Morales & A. Janakiraman, (2012) Identification of ZapD as a cell division factor that promotes the assembly of FtsZ in Escherichia coli. *J Bacteriol*. **194**: 3189-3198

Durand-Heredia, J. M., H. H. Yu, S. De Carlo, C. F. Lesser & A. Janakiraman, (2011) Identification and characterization of ZapC, a stabilizer of the FtsZ ring in Escherichia coli. *J Bacteriol* **193**: 1405-1413.

Ebersbach, G., E. Galli, J. Møller-Jensen, J. Löwe & K. Gerdes, (2008) Novel coiled-coil cell division factor ZapB stimulates Z ring assembly and cell division. *Mol Microbiol* **68**: 720-735.

Emmerson, P. T. & S. C. West, (1977) Identification of protein X of Escherichia coli as the recA+/tif+ gene product. *Mol Gen Genet* **155**: 77-85.

Erickson, H. P., (2001) The FtsZ protofilament and attachment of ZipA - structural constraints on the FtsZ power stroke. *Curr. Opin. Cell Biol.* **13**: 55-60.

Feucht, A., I. Lucet, M. D. Yudkin & J. Errington, (2001) Cytological and biochemical characterization of the FtsA cell division protein of *Bacillus subtilis*. *Mol. Microbiol.* **40**: 115-125.

Flynn, J. M., S. B. Neher, Y. I. Kim, R. T. Sauer & T. A. Baker, (2003) Proteomic discovery of cellular substrates of the ClpXP protease reveals five classes of ClpX-recognition signals. *Mol Cell* **11**: 671-683.

Fogliano, M. & P. F. Schendel, (1981) Evidence for the inducibility of the uvrB operon. *Nature* **289**: 196-198.

Frischauf, A. M., H. Lehrach, A. Poustka & N. Murray, (1983) Lambda replacement vectors carrying polylinker sequences. *J Mol Biol* **170**: 827-842.

Fu, G., T. Huang, J. Buss, C. Coltharp, Z. Hensel & J. Xiao, (2010) In vivo structure of the E. coli FtsZ-ring revealed by photoactivated localization microscopy (PALM). *PLoS One* **5**: e12682.

Galli, E. & K. Gerdes, (2010) Spatial resolution of two bacterial cell division proteins: ZapA recruits ZapB to the inner face of the Z-ring. *Mol Microbiol* **76**: 1514-1526.

Galli, E. & K. Gerdes, (2012) FtsZ-ZapA-ZapB interactome of Escherichia coli. *J Bacteriol* **194**: 292-302.

Geissler, B., D. Elraheb & W. Margolin, (2003) A gain-of-function mutation in *ftsA* bypasses the requirement for the essential cell division gene *zipA* in *Escherichia coli*. *Proc Natl Acad Sci U S A* **100**: 4197-4202.

Geissler, B. & W. Margolin, (2005) Evidence for functional overlap among multiple bacterial cell division proteins: compensating for the loss of FtsK. *Mol Microbiol* **58**: 596-612.

Geissler, B., D. Shiomi & W. Margolin, (2007) The *ftsA** gain-of-function allele of *Escherichia coli* and its effects on the stability and dynamics of the Z ring. *Microbiology* **153**: 814-825.

Genilloud, O., M. C. Garrido & F. Moreno, (1984) The transposon Tn5 carries a bleomycin-resistance determinant. *Gene* **32**: 225-233.

Gerding, M. A., Y. Ogata, N. D. Pecora, H. Niki & P. A. de Boer, (2007) The trans-envelope Tol-Pal complex is part of the cell division machinery and required for proper outer-membrane invagination during cell constriction in E. coli. *Mol Microbiol* **63**: 1008-1025.

Glynn, S. E., A. Martin, A. R. Nager, T. A. Baker & R. T. Sauer, (2009) Structures of asymmetric ClpX hexamers reveal nucleotide-dependent motions in a AAA+ protein-unfolding machine. *Cell* **139**: 744-756.

Gueiros-Filho, F. J. & R. Losick, (2002) A widely conserved bacterial cell division protein that promotes assembly of the tubulin-like protein FtsZ. *Genes Dev.* **16**: 2544-2556.

Guzman, L. M., D. Belin, M. J. Carson & J. Beckwith, (1995) Tight regulation, modulation, and high-level expression by vectors containing the arabinose PBAD promoter. *J Bacteriol* **177**: 4121-4130.

Hale, C. A. & P. A. de Boer, (1997) Direct binding of FtsZ to ZipA, an essential component of the septal ring structure that mediates cell division in *E. coli*. *Cell* **88**: 175-185.

Hale, C. A. & P. A. de Boer, (1999) Recruitment of ZipA to the septal ring of Escherichia coli is dependent on FtsZ and independent of FtsA. *J Bacteriol* **181**: 167-176.

Hale, C. A. & P. A. de Boer, (2002) ZipA is required for recruitment of FtsK, FtsQ, FtsL, and FtsN to the septal ring in *Escherichia coli*. *J. Bacteriol.* **184**: 2552-2556.

Hale, C. A., A. C. Rhee & P. A. de Boer, (2000) ZipA-induced bundling of FtsZ polymers mediated by an interaction between C-terminal domains. *J. Bacteriol.* **182**: 5153-5166.

Hale, C. A., D. Shiomi, B. Liu, T. G. Bernhardt, W. Margolin, H. Niki & P. A. de Boer, (2011) Identification of Escherichia coli ZapC (YcbW) as a component of the division apparatus that binds and bundles FtsZ polymers. *J Bacteriol* **193**: 1393-1404.

Hanahan, D., (1983) Studies on transformation of Escherichia coli with plasmids. *J Mol Biol* **166**: 557-580.

Haney, S. A., E. Glasfeld, C. Hale, D. Keeney, Z. He & P. de Boer, (2001) Genetic analysis of the Escherichia coli FtsZ-ZipA interaction in the yeast two-hybrid system. Characterization of FtsZ residues essential for the interactions with ZipA and with FtsA. *J Biol Chem* **276**: 11980-11987.

Hanson, P. I. & S. W. Whiteheart, (2005) AAA+ proteins: have engine, will work. *Nat Rev Mol Cell Biol* **6**: 519-529.

Haydon, D. J., N. R. Stokes, R. Ure, G. Galbraith, J. M. Bennett, D. R. Brown, P. J. Baker, V. V. Barynin, D. W. Rice, S. E. Sedelnikova, J. R. Heal, J. M. Sheridan, S. T. Aiwale, P. K.

Chauhan, A. Srivastava, A. Taneja, I. Collins, J. Errington & L. G. Czaplewski, (2008) An inhibitor of FtsZ with potent and selective anti-staphylococcal activity. *Science* **321**: 1673-1675.

Heidrich, C., M. F. Templin, A. Ursinus, M. Merdanovic, J. Berger, H. Schwarz, M. A. de Pedro & J. V. Holtje, (2001) Involvement of N-acetylmuramyl-L-alanine amidases in cell separation and antibiotic-induced autolysis of Escherichia coli. *Mol Microbiol* **41**: 167-178.

Hernandez-Rocamora, V. M., B. Reija, C. Garcia, P. Natale, C. Alfonso, A. P. Minton, S. Zorrilla, G. Rivas & M. Vicente, (2012) Dynamic interaction of the Escherichia coli cell division ZipA and FtsZ proteins evidenced in nanodiscs. *J Biol Chem* **287**: 30097-30104.

Hirota, Y., A. Ryter & F. Jacob, (1968) Thermosensitive mutants of E. coli affected in the processes of DNA synthesis and cellular division. *Cold Spring Harb Symp Quant Biol* **33**: 677-693.

Hoskins, J. R., S. K. Singh, M. R. Maurizi & S. Wickner, (2000) Protein binding and unfolding by the chaperone ClpA and degradation by the protease ClpAP. *Proc Natl Acad Sci U S A* **97**: 8892-8897.

Howard-Flanders, P. & L. Theriot, (1966) Mutants of Escherichia coli K-12 defective in DNA repair and in genetic recombination. *Genetics* **53**: 1137-1150.

Hu, C. D., Y. Chinenov & T. K. Kerppola, (2002a) Visualization of interactions among bZIP and Rel family proteins in living cells using bimolecular fluorescence complementation. *Mol Cell* **9**: 789-798.

Hu, Z., E. P. Gogol & J. Lutkenhaus, (2002b) Dynamic assembly of MinD on phospholipid vesicles regulated by ATP and MinE. *Proc Natl Acad Sci U S A* **99**: 6761-6766.

Hu, Z. & J. Lutkenhaus, (2000) Analysis of MinC reveals two independent domains involved in interaction with MinD and FtsZ. *J Bacteriol* **182**: 3965-3971.

Hu, Z. & J. Lutkenhaus, (2001) Topological regulation of cell division in E. coli. spatiotemporal oscillation of MinD requires stimulation of its ATPase by MinE and phospholipid. *Mol Cell* **7**: 1337-1343.

Hu, Z. & J. Lutkenhaus, (2003) A conserved sequence at the C-terminus of MinD is required for binding to the membrane and targeting MinC to the septum. *Mol Microbiol* **47**: 345-355.

Huisman, O. & R. D'Ari, (1981) An inducible DNA replication-cell division coupling mechanism in E. coli. *Nature* **290**: 797-799.

Huisman, O., R. D'Ari & S. Gottesman, (1984) Cell-division control in Escherichia coli: specific induction of the SOS function SfiA protein is sufficient to block septation. *Proc Natl Acad Sci U S A* **81**: 4490-4494.

Ish-Horowicz, D. & J. F. Burke, (1981) Rapid and efficient cosmid cloning. *Nucleic Acids Res* **9**: 2989-2998.

Iwasaki, H., A. Nakata, G. C. Walker & H. Shinagawa, (1990) The Escherichia coli polB gene, which encodes DNA polymerase II, is regulated by the SOS system. *J Bacteriol* **172**: 6268-6273.

Jimenez, M., A. Martos, M. Vicente & G. Rivas, (2011) Reconstitution and organization of Escherichia coli proto-ring elements (FtsZ and FtsA) inside giant unilamellar vesicles obtained from bacterial inner membranes. *J Biol Chem* **286**: 11236-11241.

Kannan, P. & K. Dharmalingam, (1990) Induction of the inhibitor of RecBCD enzyme in<i>Escherichia coli</i> is a<i>lexA</i>-independent SOS response. *Current Microbiology* **21**: 7-15.

Kerppola, T. K., (2008) Bimolecular fluorescence complementation (BiFC) analysis as a probe of protein interactions in living cells. *Annu Rev Biophys* **37**: 465-487.

Koppes, L. J., N. Overbeeke & N. Nanninga, (1978) DNA replication pattern and cell wall growth in Escherichia coli PAT 84. *J Bacteriol* **133**: 1053-1061.

Krol, E., S. P. van Kessel, L. S. van Bezouwen, N. Kumar, E. J. Boekema & D. J. Scheffers, (2012) Bacillus subtilis SepF binds to the C-terminus of FtsZ. *PLoS One* **7**: e43293.

Krupka, M., G. Rivas, A. I. Rico & M. Vicente, (2012) Key Role of Two Terminal Domains in the Bidirectional Polymerization of FtsA Protein. *J Biol Chem* **287**: 7756-7765.

Kuzminov, A., (1999) Recombinational repair of DNA damage in Escherichia coli and bacteriophage lambda. *Microbiol Mol Biol Rev* **63**: 751-813, table of contents.

Lackner, L. L., D. M. Raskin & P. A. de Boer, (2003) ATP-dependent interactions between Escherichia coli Min proteins and the phospholipid membrane in vitro. *J Bacteriol* **185**: 735-749.

Laemmli, U. K., (1970) Cleavage of structural proteins during the assembly of the head of bacteriophage T4. *Nature* **227**: 680-685.

Lara, B., A. I. Rico, S. Petruzzelli, A. Santona, J. Dumas, J. Biton, M. Vicente, J. Mingorance & O. Massidda, (2005) Cell division in cocci: localization and properties of the Streptococcus pneumoniae FtsA protein. *Mol Microbiol* **55**: 699-711.

Lee, C. A. & J. Beckwith, (1986) Suppression of growth and protein secretion defects in Escherichia coli secA mutants by decreasing protein synthesis. *J.Bacteriol.* **166**: 878.

Lee, S. & C. W. Price, (1993) The minCD locus of Bacillus subtilis lacks the minE determinant that provides topological specificity to cell division. *Mol Microbiol* **7**: 601-610.

Leung, A. K., E. Lucile White, L. J. Ross, R. C. Reynolds, J. A. DeVito & D. W. Borhani, (2004) Structure of Mycobacterium tuberculosis FtsZ reveals unexpected, G protein-like conformational switches. *J Mol Biol* **342**: 953-970.

Li, Z., M. J. Trimble, Y. V. Brun & G. J. Jensen, (2007) The structure of FtsZ filaments in vivo suggests a force-generating role in cell division. *Embo J* **26**: 4694-4708.

Little, J. W. & D. W. Mount, (1982) The SOS regulatory system of Escherichia coli. *Cell* **29**: 11-22.

Little, J. W., D. W. Mount & C. R. Yanisch-Perron, (1981) Purified lexA protein is a repressor of the recA and lexA genes. *Proc Natl Acad Sci U S A* **78**: 4199-4203.

Liu, G., G. C. Draper & W. D. Donachie, (1998) FtsK is a bifunctional protein involved in cell division and chromosome localization in Escherichia coli. *Mol Microbiol* **29**: 893-903.

Liu, Z., A. Mukherjee & J. Lutkenhaus, (1999) Recruitment of ZipA to the division site by interaction with FtsZ. *Mol. Microbiol.* **31**: 1853-1861.

Lloyd, R. G., S. M. Picksley & C. Prescott, (1983) Inducible expression of a gene specific to the RecF pathway for recombination in Escherichia coli K12. *Mol Gen Genet* **190**: 162-167.

Loose, M., E. Fischer-Friedrich, J. Ries, K. Kruse & P. Schwille, (2008) Spatial regulators for bacterial cell division self-organize into surface waves in vitro. *Science* **320**: 789-792.

Lovering, A. L., S. S. Safadi & N. C. Strynadka, (2012) Structural perspective of peptidoglycan biosynthesis and assembly. *Annual review of biochemistry* **81**: 451-478.

Low, H. H., M. C. Moncrieffe & J. Löwe, (2004) The crystal structure of ZapA and its modulation of FtsZ polymerisation. *J Mol Biol* **341**: 839-852.

Löwe, J. & L. A. Amos, (1998) Crystal structure of the bacterial cell-division protein FtsZ. *Nature* **391**: 203-206.

Lu, C., J. Stricker & H. P. Erickson, (1998) FtsZ from *Escherichia coli*, *Azotobacter vinelandii*, and *Thermotoga maritima*-quantitation, GTP hydrolysis, and assembly. *Cell Motil. Cytoskeleton* **40**: 71-86.

Lutkenhaus, J., (2007) Assembly dynamics of the bacterial MinCDE system and spatial regulation of the Z ring. *Annu Rev Biochem* **76**: 539-562.

Ma, L. Y., G. King & L. Rothfield, (2003) Mapping the MinE site involved in interaction with the MinD division site selection protein of Escherichia coli. *J Bacteriol* **185**: 4948-4955.

Ma, X., W. Ehrhardt & W. Margolin, (1996) Colocalization of cell division proteins FtsZ and FtsA to cytoskeletal structures in living Escherichia coli cells by using green fluorescent protein. *Proc.Natl.Acad.Sci.USA* **93**: 13003.

Ma, X. & W. Margolin, (1999) Genetic and functional analyses of the conserved C-terminal core domain of Escherichia coli FtsZ. *J.Bacteriol.* **181**: 7531-7544.

Mateos-Gil, P., I. Marquez, P. Lopez-Navajas, M. Jimenez, M. Vicente, J. Mingorance, G. Rivas & M. Velez, (2012) FtsZ polymers bound to lipid bilayers through ZipA form dynamic two dimensional networks. *Biochim Biophys Acta* **1818**: 806-813.

Mayo, O., C. Hernandez-Chico & F. Moreno, (1988) Microcin B17, a novel tool for preparation of maxicells: identification of polypeptides encoded by the IncFII minireplicon pMccB17. *J Bacteriol* **170**: 2414-2417.

McKenney, K., H. Shimatake, D. Court, U. Schmeissner, C. Brady & M. Rosenberg, (1981) Gene amplification and analysis. In: Structural analysis of nucleic acid. J. G. Chirikjian & T. S. Papas (eds). New York: Elsevier/North-Holland Publishing Co., pp. 383.

Meinhardt, H. & P. A. de Boer, (2001) Pattern formation in Escherichia coli: a model for the pole-to-pole oscillations of Min proteins and the localization of the division site. *Proc Natl Acad Sci U S A* **98**: 14202-14207.

Mendieta, J., A. I. Rico, E. Lopez-Vinas, M. Vicente, J. Mingorance & P. Gomez-Puertas, (2009) Structural and functional model for ionic (K(+)/Na(+)) and pH dependence of GTPase activity and polymerization of FtsZ, the prokaryotic ortholog of tubulin. *J Mol Biol* **390**: 17-25.

Michel, B., (2005) After 30 years of study, the bacterial SOS response still surprises us. *PLoS Biol* **3**: e255.

Miller, J. H., (1972) *Experiments in molecular genetics*. Cold Spring Harbor Laboratory, Cold Spring Harbor, N.Y.

Mingorance, J., G. Rivas, M. Velez, P. Gomez-Puertas & M. Vicente, (2010) Strong FtsZ is with the force: mechanisms to constrict bacteria. *Trends Microbiol* **18**: 348-356.

Mingorance, J., S. Rueda, P. Gómez-Puertas, A. Valencia & M. Vicente, (2001) *Escherichia coli* FtsZ polymers contain mostly GTP and have a high nucleotide turnover. *Mol. Microbiol.* **41**: 83-91.

Mohammadi, T., G. E. Ploeger, J. Verheul, A. D. Comvalius, A. Martos, C. Alfonso, J. van Marle, G. Rivas & T. den Blaauwen, (2009) The GTPase activity of Escherichia coli FtsZ determines the magnitude of the FtsZ polymer bundling by ZapA in vitro. *Biochemistry* **48**: 11056-11066.

Mosyak, L., Y. Zhang, E. Glasfeld, S. Haney, M. Stahl, J. Seehra & W. S. Somers, (2000) The bacterial cell-division protein ZipA and its interaction with an FtsZ fragment revealed by X-ray crystallography. *Embo J.* **19**: 3179-3191.

Moy, F. J., E. Glasfeld, L. Mosyak & R. Powers, (2000) Solution structure of ZipA, a crucial component of Escherichia coli cell division. *Biochemistry* **39**: 9146-9156.

Mukherjee, A., C. Cao & J. Lutkenhaus, (1998) Inhibition of FtsZ polymerization by SulA, an inhibitor of septation in Escherichia coli. *Proc Natl Acad Sci U S A* **95**: 2885-2890.

Nagai, T., K. Ibata, E. S. Park, M. Kubota, K. Mikoshiba & A. Miyawaki, (2002) A variant of yellow fluorescent protein with fast and efficient maturation for cell-biological applications. *Nat Biotechnol* **20**: 87-90.

Napolitano, R., R. Janel-Bintz, J. Wagner & R. P. Fuchs, (2000) All three SOS-inducible DNA polymerases (Pol II, Pol IV and Pol V) are involved in induced mutagenesis. *EMBO J* **19**: 6259-6265.

Nogales, E., K. H. Downing, L. A. Amos & J. Löwe, (1998) Tubulin and FtsZ form a distinct family of GTPases. *Nat Struct Biol* **5**: 451-458.

Oliva, M. A., S. C. Cordell & J. Löwe, (2004) Structural insights into FtsZ protofilament formation. *Nat Struct Mol Biol* **11**: 1243-1250.

Oliva, M. A., D. Trambaiolo & J. Löwe, (2007) Structural insights into the conformational variability of FtsZ. *J Mol Biol* **373**: 1229-1242.

Osawa, M., D. E. Anderson & H. P. Erickson, (2008) Reconstitution of contractile FtsZ rings in liposomes. *Science* **320**: 792-794.

Paradis-Bleau, C., F. Sanschagrin & R. C. Levesque, (2005) Peptide inhibitors of the essential cell division protein FtsA. *Protein Eng Des Sel* **18**: 85-91.

Park, K. T., W. Wu, K. P. Battaile, S. Lovell, T. Holyoak & J. Lutkenhaus, (2011) The Min oscillator uses MinD-dependent conformational changes in MinE to spatially regulate cytokinesis. *Cell* **146**: 396-407.

Pichoff, S. & J. Lutkenhaus, (2002) Unique and overlapping roles for ZipA and FtsA in septal ring assembly in *Escherichia coli*. *Embo J.* **21**: 685-693.

Pichoff, S. & J. Lutkenhaus, (2005) Tethering the Z ring to the membrane through a conserved membrane targeting sequence in FtsA. *Mol Microbiol* **55**: 1722-1734.

Pichoff, S., B. Shen, B. Sullivan & J. Lutkenhaus, (2012) FtsA mutants impaired for self-interaction bypass ZipA suggesting a model in which FtsA's self-interaction competes with its ability to recruit downstream division proteins. *Mol Microbiol* **83**: 151-167.

Pla, J., A. Dopazo & M. Vicente, (1990) The native form of FtsA, a septal protein of Escherichia coli, is located in the cytoplasmic membrane. *J. Bacteriol.* **172**: 5097-5102.

Plá, J., P. Palacios, M. Sánchez, T. Garrido & M. Vicente, (1993) Stability of components of the *Escherichia coli* Septator. In: Bacterial Growth and Lysis: Metabolism and Structure of the Bacterial Sacculus. M. A. de Pedro, J. V. Höltje & W. Löffelhardt (eds). New York: Plenum Press, pp. 363-368.

Pla, J., M. Sánchez, P. Palacios, M. Vicente & M. Aldea, (1991) Preferential cytoplasmic location of FtsZ, a protein essential for *Escherichia coli* septation. *Mol. Microbiol.* **5**: 1681-1686.

Raskin, D. M. & P. A. de Boer, (1997) The MinE ring: an FtsZ-independent cell structure required for selection of the correct division site in E. coli. *Cell* **91**: 685-694.

Raskin, D. M. & P. A. de Boer, (1999a) MinDE-dependent pole-to-pole oscillation of division inhibitor MinC in Escherichia coli. *J Bacteriol* **181**: 6419-6424.

Raskin, D. M. & P. A. de Boer, (1999b) Rapid pole-to-pole oscillation of a protein required for directing division to the middle of Escherichia coli. *Proc Natl Acad Sci U S A* **96**: 4971-4976.

RayChaudhuri, D., (1999) ZipA is a MAP-Tau homolog and is essential for structural integrity of the cytokinetic FtsZ ring during bacterial cell division. *Embo J.* **18**: 2372-2383.

Rico, A. I., M. García-Ovalle, J. Mingorance & M. Vicente, (2004) Role of two essential domains of Escherichia coli FtsA in localization and progression of the division ring. *Mol Microbiol* **53**: 1359-1371.

Rico, A. I., M. García-Ovalle, P. Palacios, M. Casanova & M. Vicente, (2010) Role of Escherichia coli FtsN protein in the assembly and stability of the cell division ring. *Mol Microbiol* **76**: 760-771.

Rodrigues, C. D. & E. J. Harry, (2012) The Min system and nucleoid occlusion are not required for identifying the division site in Bacillus subtilis but ensure its efficient utilization. *PLoS Genet* **8**: e1002561.

Romberg, L., (2003) Assembly dynamics of the bacterial cell division protein FtsZ: poised at the edge of stability. *Annu.Rev.Microbiol.* **57**: 125-154.

Rothfield, L., A. Taghbalout & Y. L. Shih, (2005) Spatial control of bacterial division-site placement. *Nat Rev Microbiol* **3**: 959-968.

Rowland, S. L., X. Fu, M. A. Sayed, Y. Zhang, W. R. Cook & L. I. Rothfield, (2000) Membrane redistribution of the Escherichia coli MinD protein induced by MinE. *J Bacteriol* **182**: 613-619.

Rueda, S., M. Vicente & J. Mingorance, (2003) Concentration and assembly of the division ring proteins FtsZ, FtsA, and ZipA during the *Escherichia coli* cell cycle. *J. Bacteriol.* **185**: 3344-3351.

Ryter, A., Y. Hirota & F. Jacob, (1968) DNA-membrane complex and nuclear segregation in bacteria. *Cold Spring Harb Symp Quant Biol* **33**: 669-676.

Sambrook, J., E. F. Fritsch & T. Maniatis, (1989) *Molecular cloning: a laboratory manual, 2nd edition*. Cold Spring Habour Laboratory Press, Cold Spring Habour, NY.

Sancar, A., A. M. Hack & W. D. Rupp, (1979) Simple method for identification of plasmid-coded proteins. *J Bacteriol* **137**: 692-693.

Sauer, R. T., D. N. Bolon, B. M. Burton, R. E. Burton, J. M. Flynn, R. A. Grant, G. L. Hersch, S. A. Joshi, J. A. Kenniston, I. Levchenko, S. B. Neher, E. S. Oakes, S. M. Siddiqui, D. A. Wah & T. A. Baker, (2004) Sculpting the proteome with AAA(+) proteases and disassembly machines. *Cell* **119**: 9-18.

Scalenghe, F., E. Turco, J. E. Edstrom, V. Pirrotta & M. Melli, (1981) Microdissection and cloning of DNA from a specific region of Drosophila melanogaster polytene chromosomes. *Chromosoma* **82**: 205-216.

Scheffers, D. J., J. G. de Wit, T. den Blaauwen & A. J. Driessen, (2002) GTP hydrolysis of cell division protein FtsZ: evidence that the active site is formed by the association of monomers. *Biochemistry* **41**: 521-529.

Sedliakova, M., V. Slezarikova, J. Brozmanova, F. Masek & V. Bayerova, (1980) Role of UV-inducible proteins in repair of various wild-type Escherichia coli cells. *Mutat Res* **71**: 15-23.

Shen, B. & J. Lutkenhaus, (2009) The conserved C-terminal tail of FtsZ is required for the septal localization and division inhibitory activity of MinC(C)/MinD. *Mol Microbiol* **72**: 410-424.

Shevchenko, A., M. Wilm, O. Vorm & M. Mann, (1996) Mass spectrometric sequencing of proteins silver-stained polyacrylamide gels. *Anal Chem* **68**: 850-858.

Shiomi, D. & W. Margolin, (2007) The C-terminal domain of MinC inhibits assembly of the Z ring in Escherichia coli. *J Bacteriol* **189**: 236-243.

Shurvinton, C. E. & R. G. Lloyd, (1982) Damage to DNA induces expression of the ruv gene of Escherichia coli. *Mol Gen Genet* **185**: 352-355.

Siegel, E. C., (1983) The Escherichia coli uvrD gene is inducible by DNA damage. *Mol Gen Genet* **191**: 397-400.

Singh, J. K., R. D. Makde, V. Kumar & D. Panda, (2007) A membrane protein, EzrA, regulates assembly dynamics of FtsZ by interacting with the C-terminal tail of FtsZ. *Biochemistry* **46**: 11013-11022.

Singh, J. K., R. D. Makde, V. Kumar & D. Panda, (2008) SepF increases the assembly and bundling of FtsZ polymers and stabilizes FtsZ protofilaments by binding along its length. *J Biol Chem* **283**: 31116-31124.

Skarstad, K. & E. Boye, (1993) Degradation of individual chromosomes in recA mutants of Escherichia coli. *J Bacteriol* **175**: 5505-5509.

Skoog, K. & D. O. Daley, (2012) The Escherichia coli cell division protein ZipA forms homodimers prior to association with FtsZ. *Biochemistry* **51**: 1407-1415.

Small, E., R. Marrington, A. Rodger, D. J. Scott, K. Sloan, D. Roper, T. R. Dafforn & S. G. Addinall, (2007) FtsZ polymer-bundling by the Escherichia coli ZapA orthologue, YgfE, involves a conformational change in bound GTP. *J Mol Biol* **369**: 210-221.

Sossong, T. M., Jr., M. R. Brigham-Burke, P. Hensley & K. H. Pearce, Jr., (1999) Self-activation of guanosine triphosphatase activity by oligomerization of the bacterial cell division protein FtsZ. *Biochemistry* **38**: 14843-14850.

Sourjik, V. & H. C. Berg, (2004) Functional interactions between receptors in bacterial chemotaxis. *Nature* **428**: 437-441.

Stricker, J., P. Maddox, E. D. Salmon & H. P. Erickson, (2002) Rapid assembly dynamics of the *Escherichia coli* FtsZ-ring demonstrated by fluorescence recovery after photobleaching. *Proc. Natl. Acad. Sci. U. S. A.* **99**: 3171-3175.

Suefuji, K., R. Valluzzi & D. RayChaudhuri, (2002) Dynamic assembly of MinD into filament bundles modulated by ATP, phospholipids, and MinE. *Proc Natl Acad Sci U S A* **99**: 16776-16781.

Sun, Q. & W. Margolin, (2004) Effects of perturbing nucleoid structure on nucleoid occlusion-mediated toporegulation of FtsZ ring assembly. *J Bacteriol* **186**: 3951-3959.

Sun, Q., X. C. Yu & W. Margolin, (1998) Assembly of the FtsZ ring at the central division site in the absence of the chromosome. *Mol Microbiol* **29**: 491-503.

Szeto, T. H., S. L. Rowland, C. L. Habrukowich & G. F. King, (2003) The MinD membrane targeting sequence is a transplantable lipid-binding helix. *J Biol Chem* **278**: 40050-40056.

Szeto, T. H., S. L. Rowland, L. I. Rothfield & G. F. King, (2002) Membrane localization of MinD is mediated by a C-terminal motif that is conserved across eubacteria, archaea, and chloroplasts. *Proc Natl Acad Sci U S A* **99**: 15693-15698.

Szwedziak, P., Q. Wang, S. M. Freund & J. Löwe, (2012) FtsA forms actin-like protofilaments. *EMBO J*. **31**: 2249-2260

Tadros, M., J. M. Gonzalez, G. Rivas, M. Vicente & J. Mingorance, (2006) Activation of the Escherichia coli cell division protein FtsZ by a low-affinity interaction with monovalent cations. *FEBS Lett* **580**: 4941-4946.

Tamames, J., M. Gonzalez-Moreno, J. Mingorance, A. Valencia & M. Vicente, (2001) Bringing gene order into bacterial shape. *Trends Genet* **17**: 124-126.

Teather, R. M., J. F. Collins & W. D. Donachie, (1974) Quantal behavior of a diffusible factor which initiates septum formation at potential division sites in Escherichia coli. *J Bacteriol* **118**: 407-413.

Thanedar, S. & W. Margolin, (2004) FtsZ exhibits rapid movement and oscillation waves in helix-like patterns in Escherichia coli. *Curr Biol* **14**: 1167-1173.

Tonthat, N. K., S. T. Arold, B. F. Pickering, M. W. Van Dyke, S. Liang, Y. Lu, T. K. Beuria, W. Margolin & M. A. Schumacher, (2011) Molecular mechanism by which the nucleoid occlusion factor, SlmA, keeps cytokinesis in check. *EMBO J* **30**: 154-164.

Tormo, A. & M. Vicente, (1984) The ftsA gene product participates in formation of the Escherichia coli septum structure. *J Bacteriol* **157**: 779-784.

Towbin, H., T. Staehelin & J. Gordon, (1979) Electrophoretic transfer of proteins from polyacrylamide gels to nitrocellulose sheets: procedure and some applications. *Proc Natl Acad Sci U S A* **76**: 4350-4354.

Trusca, D., S. Scott, C. Thompson & D. Bramhill, (1998) Bacterial SOS checkpoint protein SulA inhibits polymerization of purified FtsZ cell division protein. *J Bacteriol* **180**: 3946-3953.

van den Ent, F. & J. Löwe, (2000) Crystal structure of the cell division protein FtsA from *Thermotoga maritima*. *Embo J* **19**: 5300-5307.

Vicente, M. & J. Errington, (1996) Structure, function and controls in microbial division. *Mol Microbiol* **20**: 1-7.

Vicente, M. & A. I. Rico, (2006) The order of the ring: assembly of Escherichia coli cell division components. *Mol Microbiol* **61**: 5-8.

Vicente, M., A. I. Rico, R. Martínez-Arteaga & J. Mingorance, (2006) Septum enlightenment: assembly of bacterial division proteins. *J Bacteriol* **188**: 19-27.

Wagner, J., P. Gruz, S. R. Kim, M. Yamada, K. Matsui, R. P. Fuchs & T. Nohmi, (1999) The dinB gene encodes a novel E. coli DNA polymerase, DNA pol IV, involved in mutagenesis. *Mol Cell* **4**: 281-286.

Wang, H. & R. C. Gayda, (1992) Quantitative determination of FtsA at different growth rates in *Escherichia coli* using monoclonal antibodies. *Mol Microbiol* **6**: 2517-2524.

Wang, L. & J. Lutkenhaus, (1998) FtsK is an essential cell division protein that is localized to the septum and induced as part of the SOS response. *Mol Microbiol* **29**: 731-740.

Wang, X., J. Huang, A. Mukherjee, C. Cao & J. Lutkenhaus, (1997) Analysis of the interaction of FtsZ with itself, GTP, and FtsA. *J Bacteriol* **179**: 5551-5559.

Ward, J. E., Jr. & J. Lutkenhaus, (1985) Overproduction of FtsZ induces minicell formation in E. coli. *Cell* **42**: 941-949.

Woldringh, C. L., E. Mulder, P. G. Huls & N. Vischer, (1991) Toporegulation of bacterial division according to the nucleoid occlusion model. *Res Microbiol* **142**: 309-320.

Wu, W., K. T. Park, T. Holyoak & J. Lutkenhaus, (2011) Determination of the structure of the MinD-ATP complex reveals the orientation of MinD on the membrane and the relative location of the binding sites for MinE and MinC. *Mol Microbiol* **79**: 1515-1528.

Yim, L., G. Vandenbussche, J. Mingorance, S. Rueda, M. Casanova, J. M. Ruysschaert & M. Vicente, (2000) Role of the carboxy terminus of *Escherichia coli* FtsA in self-interaction and cell division. *J. Bacteriol.* **182**: 6366-6373.

Yu, X. C., A. H. Tran, Q. Sun & W. Margolin, (1998a) Localization of cell division protein FtsK to the Escherichia coli septum and identification of a potential N-terminal targeting domain. *J Bacteriol* **180**: 1296-1304.

Yu, X. C., E. K. Weihe & W. Margolin, (1998b) Role of the C terminus of FtsK in Escherichia coli chromosome segregation. *J Bacteriol* **180**: 6424-6428.

Zhou, H. & J. Lutkenhaus, (2005) MinC mutants deficient in MinD- and DicB-mediated cell division inhibition due to loss of interaction with MinD, DicB, or a septal component. *J Bacteriol* **187**: 2846-2857.

Supplemental figures

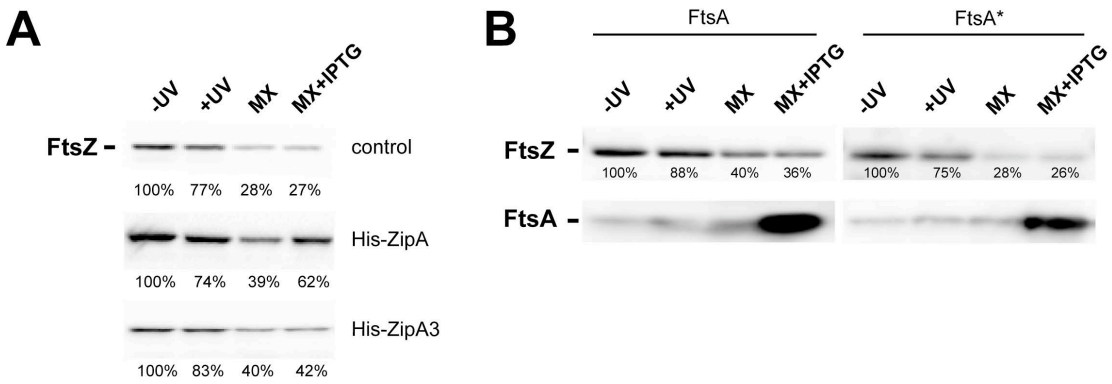

Figure 34. Protection of FtsZ from degradation by overproduction of ZipA in maxicells.

(A) FtsZ protein levels during the maxicells production procedure of *E. coli* CSR603 cells bearing empty plasmid (control) and overproducing His-ZipA (pPZV23) and His-ZipA3 (pPZV24). (B) FtsZ and FtsA/FtsA* protein level during the maxicell production procedure of *E. coli* CSR603 cells overproducing FtsA (pPNV40) or FtsA* (pPZV33). (-UV) non-UV irradiated cells, (+UV) 3 hours after irradiation, (MX) 16 hours after D-cycloserine addition and (MX+IPTG) 16 hours after addition of D-cycloserine and IPTG. Relative amount of FtsZ is indicated below each sample.

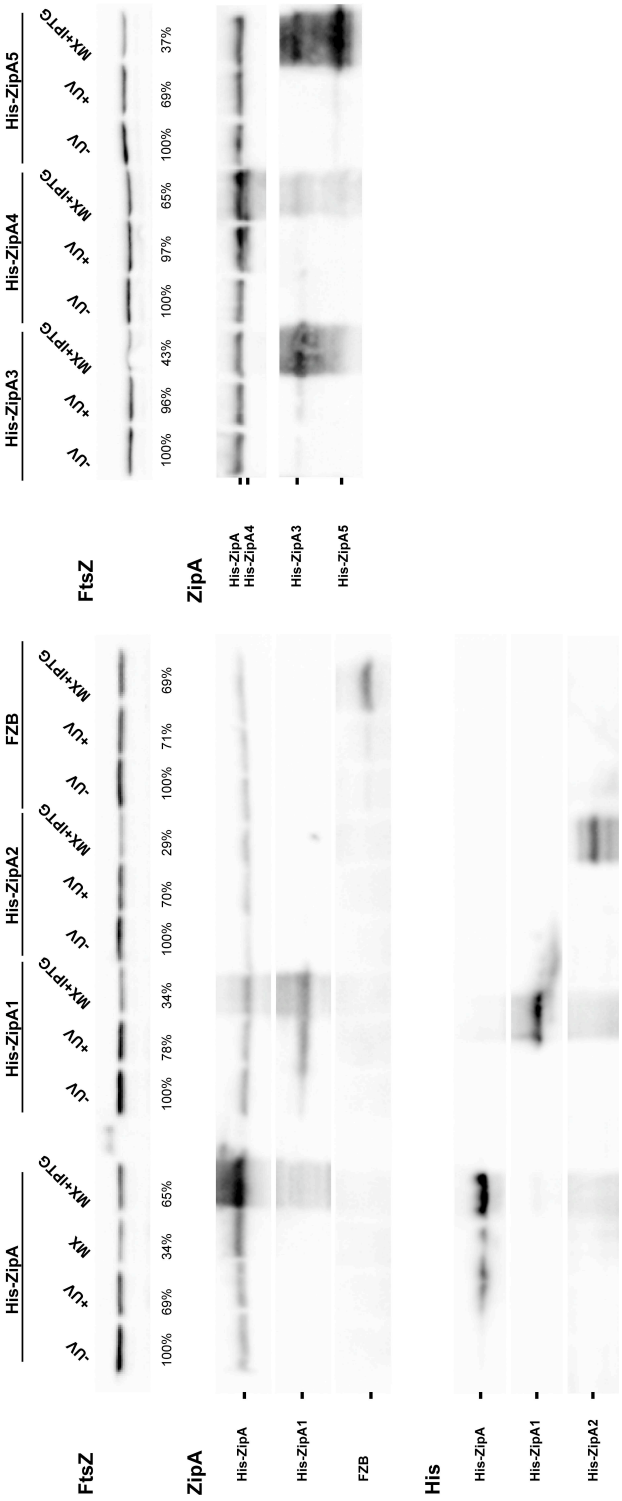

Figure 35. FtsZ-protective properties of different ZipA mutants.

FtsZ and ZipA protein levels during the maxicells production procedure of *E. coli* CSR603 cells overproducing the different ZipA mutants. (-UV) non-UV irradiated cells, (+UV) 3 hours after irradiation, (MX) 16 hours after D-cycloserine addition and (MX+IPTG) 16 hours after addition of D-cycloserine and IPTG. Relative amount of FtsZ is indicated below each sample.

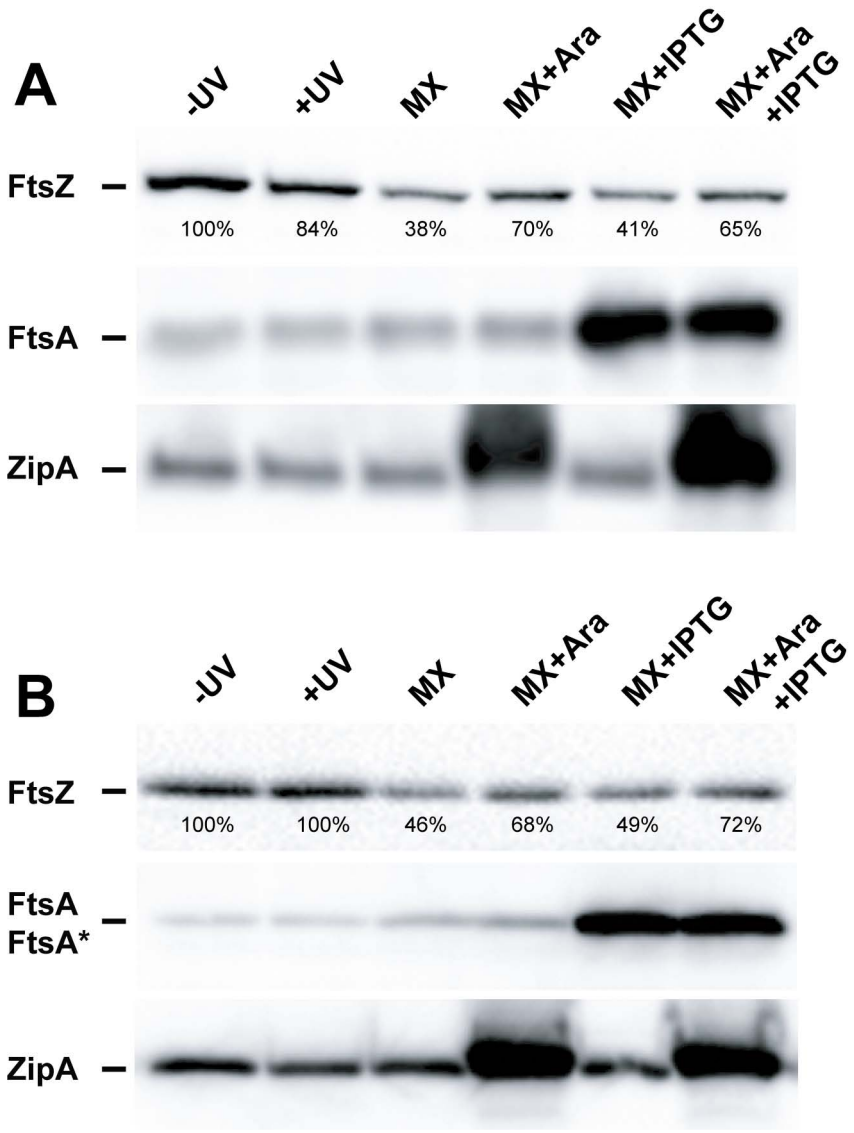

Figure 36. FtsZ-protection under ZipA+FtsA or ZipA+FtsA* overproducing conditions.

FtsZ, FtsA and ZipA protein levels during the maxicell production procedure of *E. coli* CSR603 cells overproducing (A) ZipA (pPZV128) or FtsA (pPNV40) or a combination of ZipA with FtsA; (B) ZipA (pPZV128) or FtsA* (pPZV33) or a combination of ZipA with FtsA*. (-UV) non-UV irradiated cells, (+UV) 3 hours after irradiation, (MX) 16 hours after D-cycloserine addition and (MX+Ara), (MX+IPTG) and (MX+Ara+IPTG) 16 hours after addition of arabinose, IPTG or both, respectively, and D-cycloserine. Relative amount of FtsZ is indicated below each sample.

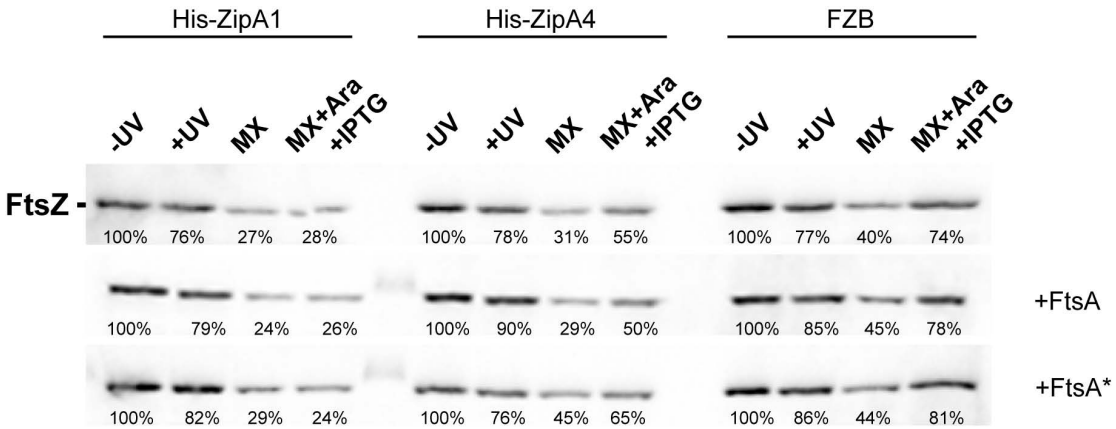

Figure 37. FtsA or FtsA* cannot substitute or interfere with FZB in FtsZ protection.

FtsZ levels on maxicells overproducing His-ZipA1 (pPZV29), His-ZipA4 (pPZV30) and FZB (pPZV38) alone (upper panel), or in combination with FtsA (pPZV131) (middle lane) or FtsA* (pPZV132) (bottom panel). (-UV) non-UV irradiated cells, (+UV) 3 hours after irradiation, (MX) 16 hours after D-cycloserine addition and (MX+Ara+IPTG) 16 hours after addition of arabinose, IPTG and D-cycloserine. Relative amount of FtsZ is indicated below each sample.

Appendix I: Proteome without chromosome

Historically, maxicells have been used as a tool to express plasmid-encoded genes. The absence of the bacterial nucleoid does not impair transcription and translation systems in the cell (Sancar *et al.*, 1979). This ability allows the study of plasmid-encoded genes after bacterial chromosome degradation, transforming a growing cell into a container that maintains metabolic activity, a biovessel. This apendix describes a general comparative proteome analysis of these biovessels compared to the non-UV irradiated CSR603 cells.

Proteomic is frequently used to compare and analyze changes in protein production profiles in response to stresses changing the environmental or physiological condition of a bacterial strain. The obtained data will be important to understand the metabolic state of our tool and will point out its advantages and limitations. For that purpose we used a combination of two-dimensional fluorescence difference gel electrophoresis (2D-DIGE) and conventional sypro-stained 2D gel electrophoresis (2-DE) analysis. 2D-DIGE allows the simultaneous analysis of non UV and UV-irradiated cells within the same 2D gel, whereas conventional 2-DE is necessary to pick protein spots of low concentration to be identified by matrix-assisted laser desorption/ionization time-of-flight (MALDI-TOF) mass spectrometry. Peptide masses obtained by MALDI-TOF were analyzed by peptide mass fingerprinting using Mascot search engine (Matrix Science) coupled to the *E. coli K12* UniProtKB database. Further information about the identified proteins was obtained using EcoCyc ((Keseler *et al.*, 2011)), a bioinformatic database of *E. coli* K12 MG1655.

Comparative Analysis of the CSR603 proteome

The response of the total *E. coli* CSR603 proteome to the low dose UV-irradiation and chromosome degradation was evaluated. Good spot separation and reproducibility allowed to consider all spot changes within a confidence of $P < 0,01$ as significant. A total of 127 proteins showed at least a two-fold change in protein level. Genome sequencing revealed that *E. coli* contains 4290 protein coding genes (Blattner *et al.*, 1997). This is about 3 % of the estimated total *E. coli* protein content. The up and down regulated proteins were classified into one of the following ten categories: cell processes, cytoplasm, DNA related, extra-chromosomal (e.g viral proteins), metabolism, ORF, protein related, regulation, RNA related and transport. These categories were chosen according to the *E. coli* EcoCyc database (Keseler *et al.*, 2011).

1. Cell processes

Gene	Full name / Protein function	pI	Mw	Average Ratio	T-test	Matches	Score	Coverage (%)	Probability	SUB-CLASS
amiC	N-acetylmuramoyl-L-alanine amidase	10,00	45474	-4,58	1,20E-05	12	130	28,06	4,40E-10	Cell stucture (murein cleavage), cytokinesis
era	GTP-binding protein, essential gene	6,73	33846	3,73	4,40E-05	7	84	28,24	4,70E-05	Cell cycle physiology
ftsA	Cell division protein	5,84	5815	2,1	0,00054	4	70	9,52	0,0012	Cell division
minD	Septum site-determining protein	5,25	29710	2,05	1,40E-04	24	402	61,85	7.8E-37	Cell division
minD	Septum site-determining protein	5,25	29710	2,49	0,0016	13	269	41,48	1,60E-23	Cell division
minD	Septum site-determining protein	5,25	29710	5,64	4,30E-06	20	466	49,63	3,10E-43	Cell division
mreB	Rod shape-determining protein	5,17	37100	-3,41	7,40E-06	9	70	35,45	0,0013	Cell division
murA	UDP-N-acetylglucosamine 1-carboxyvinyltransferase	5,74	44656	3,33	3,40E-06	16	150	31,26	4,4E-12	Peptidoglycan synthesis
murA	UDP-N-acetylglucosamine 1-carboxyvinyltransferase	5,74	44656	3,76	4,40E-06	15	138	30,31	7,00E-11	Peptidoglycan synthesis
murI	Glutamate racemase	5,08	30850	2,05	0,00014	6	82	36,49	8,00E-05	Peptidoglycan synthesis
yggX	Probable Fe(2+)-trafficking protein	5,89	10814	2,3	9,30E-05	9	218	54,95	7,00E-19	Mechanical, nutritional, oxidative stress

2. Cytoplasm

Gene	Full name / Protein function	pI	Mw	Average Ratio	T-test	Matches	Score	Coverage (%)	Probability	SUB-CLASS
deaD	Cold-shock DEAD box protein A	8,96	70368	-4,08	0,00063	20	328	34,50	2,00E-29	N/A
deaD	Cold-shock DEAD box protein A	8,96	70368	-6,57	1,70E-06	35	737	44,04	3,10E-69	N/A
deaD	Cold-shock DEAD box protein A	8,96	70368	-4,03	3,30E-05	29	508	41,49	2,50E-46	N/A
deaD	Cold-shock DEAD box protein A	8,96	70368	-9,03	5,30E-06	21	475	29,89	3,90E-44	N/A
gor	Glutathione reductase	5,57	48608	3,24	2,80E-05	11	78	21,33	7E-05	N/A
gor	Glutathione reductase	5,57	48608	3,36	9,60E-06	11	103	27,33	6,20E-07	N/A
sodA	Superoxide dismutase	6,50	22951	2,73	2,40E-05	14	333	49,03	2,20E-30	N/A
sodA	Superoxide dismutase	6,50	22951	2,51	2,90E-05	14	313	51,94	2,20E-28	N/A
ybiT	Uncharacterized ABC transporter ATP-binding protein	4,79	59686	-3,26	1,90E-05	22	339	26,80	5,60E-31	N/A

3. DNA related

Gene	Full name / Protein function	pI	Mw	Average Ratio	T-test	Matches	Score	Coverage (%)	Probability	SUB-CLASS
ligA	DNA ligase	5,24	73426	3,18	1,50E-05	14	119	27,87	5,60E-09	DNA repair

4. Extra-chromosomal

Gene	Full name / Protein function	pI	Mw	Average Ratio	T-test	Matches	Score	Coverage (%)	Probability	SUB-CLASS
ompX	Outer membrane protein X	6,92	18459	2,01	0,0014	13	335	54,39	1,40E-30	Prophage genes and phage related functions
ompX	Outer membrane protein X	6,92	18459	2,92	0,00065	9	134	32,16	1,80E-10	Prophage genes and phage related functions

5. Metabolism

5.1. Embden–Meyerhof–Parnas (EMP) pathway

Gene	Full name / Protein function	pI	Mw	Average Ratio	T-test	Matches	Score	Coverage (%)	Probability	SUB-CLASS
eno	Enolase	5,16	45491	-3,02	4,50E-06	15	179	44,91	5,60E-15	Anaerobic respiration glycolysis
fbp	Fructose-1,6-bisphosphatase class 1	5,59	36678	2,29	0,0028	12	185	36,75	3,90E-15	Central intermediary metabolism
fbaA	Fructose-bisphosphate aldolase class 2	5,45	38990	-3,17	1,20E-06	7	85	35,24	1,30E-05	Carbon compounds
gapA	Glyceraldehyde-3-phosphate dehydrogenase A	6,69	35377	3,68	4,90E-06	21	399	50,45	1,60E-36	Central intermediary metabolism, glycolysis
gpmM (gpmI)	2,3-bisphosphoglycerate-independent phosphoglycerate mutase	5,14	56194	-2,29	0,004	25	467	54,28	2,50E-43	Carbon compounds
gpmM (gpmI)	2,3-bisphosphoglycerate-independent phosphoglycerate mutase	5,14	56194	3,99	4,10E-06	11	105	25,49	3,90E-07	Carbon compounds
tnaA	Tryptophanase	5,81	52607	3,24	2,80E-05	32	877	64,54	8,80E-85	Amino acids
tnaA	Tryptophanase	5,81	52607	3,36	9,60E-06	32	454	48,62	4,90E-42	Amino acids
tnaA	Tryptophanase	5,81	52607	4	5,30E-05	17	94	26,54	5,00E-06	Amino acids

5.2 Hexose monophosphate (HMP) pathway

Gene	Full name / Protein function	pI	Mw	Average Ratio	T-test	Matches	Score	Coverage (%)	Probability	SUB-CLASS
hldD (rfaD)	ADP-L-glycero-D-manno-heptose-6-epimerase	4,80	34893	3,99	2,10E-05	34	866	62,58	1,10E-83	Core region
hldD (rfaD)	ADP-L-glycero-D-manno-heptose-6-epimerase	4,80	34893	2	9,10E-06	12	296	31,29	3,10E-26	Core region
kdsB	3-deoxy-manno-octulosonate cytidylyltransferase	4,98	27465	2,49	0,0016	12	295	41,94	3,90E-26	Core region
prs	Ribose-phosphate pyrophosphokinase	5,06	34064	2,05	1,60E-05	12	196	35,87	3,10E-16	Purine ribonucleotide biosynthesis
prs	Ribose-phosphate pyrophosphokinase	5,06	34064	5,36	2,20E-07	20	302	41,59	7,80E-27	Purine ribonucleotide biosynthesis
prs	Ribose-phosphate pyrophosphokinase	5,06	34064	3,1	1,80E-05	12	131	33,65	9,80E-10	Purine ribonucleotide biosynthesis
talB	Transaldolase B	4,92	35064	2	9,10E-06	8	101	34,38	9,80E-07	Non-oxidative branch, pentose pathway
talB	Transaldolase B	4,92	35064	2,57	2,10E-05	29	645	67,51	3,90E-61	Non-oxidative branch, pentose pathway
tktA	Transketolase 1	5,31	72020	3,18	1,50E-05	22	425	24,28	1,40E-39	Carbon compounds, non-oxidative branch, pentose pathway
tktA	Transketolase 1	5,31	72020	4,33	2,30E-05	15	160	15,69	4,40E-13	Carbon compounds, non-oxidative branch, pentose pathway

5.3. Tricarboxylic acid (TCA) cycle

Gene	Full name / Protein function	pI	Mw	Average Ratio	T-test	Matches	Score	Coverage (%)	Probability	SUB-CLASS
aceE	Pyruvate dehydrogenase E1 component	5,33	99471	-3,15	6,90E-05	12	102	62,67	7,80E-07	Carbon compounds, glyoxylate degradation, anaerobic respiration, pyruvate dehydrogenase
acnB	Aconitate hydratase 2	5,07	93303	-3,15	6,90E-05	26	419	91,00	1,60E-38	TCA cycle
icd	Isocitrate dehydrogenase	4,97	45594	5,31	1,40E-06	14	108	30,05	7,00E-08	TCA cycle
icd	Isocitrate dehydrogenase	4,97	45594	9,57	1,20E-06	20	254	34,86	1,80E-22	TCA cycle
lpdA	Dihydrolipoyl dehydrogenase	5,78	50688	2,67	0,0034	30	791	48,95	9,80E-76	Carbon utilization, carbon compounds, formyl-THF biosynthesis, aerobic respiration, anaerobic respiration, pyruvate dehydrogenase
lpdA	Dihydrolipoyl dehydrogenase	5,78	50688	4,76	2,10E-05	12	85	26,85	4,20E-05	Carbon utilization, carbon compounds, formyl-THF biosynthesis, aerobic respiration, anaerobic respiration, pyruvate dehydrogenase
lpdA	Dihydrolipoyl dehydrogenase	5,78	50688	4,84	9,10E-06	20	303	37,13	6,20E-27	Carbon utilization, carbon compounds, formyl-THF biosynthesis, aerobic respiration, anaerobic respiration, pyruvate dehydrogenase
pflB	Formate acetyltransferase 1	5,60	85167	-3,9	0,0043	34	534	35,53	4,90E-50	Amino acids, threonine catabolism, anaerobic respiration

5.4. Fatty acid lipid biosynthesis

Gene	Full name / Protein function	pI	Mw	Average Ratio	T-test	Matches	Score	Coverage (%)	Probability	SUB-CLASS
fabA	3-hydroxydecanoyl-[acyl-carrier-protein] dehydratase	6,13	18825	2,61	0,00013	20	417	51,74	8,80E-39	Fatty acids and phosphatidic acid
fabA	3-hydroxydecanoyl-[acyl-carrier-protein] dehydratase	6,13	18825	3,08	1,00E-08	21	402	45,93	2,80E-37	Fatty acids and phosphatidic acid
fabA	3-hydroxydecanoyl-[acyl-carrier-protein] dehydratase	6,13	18825	2,74	1,00E-05	14	352	38,95	2,80E-32	Fatty acids and phosphatidic acid
fabI	Enoyl-[acyl-carrier-protein] reductase	5,48	27713	2,05	0,00014	12	94	43,51	4,60E-06	Fatty acids and phosphatidic acid
fabZ	(3R)-hydroxymyristoyl-[acyl-carrier-protein] dehydratase	7,12	16891	2,15	5,10E-06	14	358	52,32	7,00E-33	Fatty acids and phosphatidic acid
fabZ	(3R)-hydroxymyristoyl-[acyl-carrier-protein] dehydratase	7,12	16891	2,45	0,00082	11	273	44,37	2,20E-24	Fatty acids and phosphatidic acid
lipA	Lipoyl synthase	7,78	35916	-2,86	6,50E-07	14	195	38,94	3,90E-16	Lipoate
lipA	Lipoyl synthase	7,78	35916	-2,94	9,10E-07	11	176	32,71	3,10E-14	Lipoate
panC	pantothenate synthetase	5,86	31446	-2,21	1,90E-05	13	208	45,42	2,00E-17	Coenzyme A

5.5. Amino acids

Gene	Full name / Protein function	pI	Mw	Average Ratio	T-test	Matches	Score	Coverage (%)	Probability	SUB-CLASS
argG	Argininosuccinate synthase	5,07	49733	4,52	5,90E-05	10	100	28,41	1,20E-06	Amino acids
aroA	Phosphoshikimate 1-carboxyvinyltransferase	5,23	45932	-3,02	4,50E-06	20	268	30,21	7,00E-24	Chorismate
dapD	2,3,4,5-tetrahydropyridine-2-carboxylate N-succinyltransferase	5,41	29741	3,6	4,60E-05	17	205	37,96	3,90E-17	Lysine
dapF	Diaminopimelate epimerase	5,83	30058	-2,1	6,70E-08	14	159	55,89	1,60E-12	Amino acids
speB	Agmatinase	4,97	33403	2,06	0,001	14	164	42,48	4,90E-13	Polyamine biosynthesis
speE	Spermidine synthase	5,24	32169	2,05	0,00014	13	410	37,85	1,20E-37	Polyamine biosynthesis

5.6. Cofactor-electron carrier

Gene	Full name / Protein function	pI	Mw	Average Ratio	T-test	Matches	Score	Coverage (%)	Probability	SUB-CLASS
ahpF	Alkyl hydroperoxide reductase subunit F	5,34	56008	2,15	3,10E-05	9	129	23,99	1,60E-09	Riboflavin
dld	D-lactate dehydrogenase	6,19	64439	-3,65	3,70E-06	6	84	14,01	5,00E-05	Aerobic respiration electron donors
fre	NAD(P)H-flavin reductase	5,29	26242	2,29	3,00E-05	8	122	27,90	7,80E-09	Electron carriers
gltX	Glutamyl-tRNA synthetase	5,52	53649	3,2	0,00015	10	76	24,84	0,0003	Heme, porphyrine
gltX	Glutamyl-tRNA synthetase	5,52	53649	3,12	0,0002	17	205	33,76	3,90E-17	Heme, porphyrine
gltX	Glutamyl-tRNA synthetase	5,52	53649	2,15	3,10E-05	25	741	49,26	9,80E-71	Heme, porphyrine
grxB	Glutaredoxin-2	7,89	24203	2,82	0,00051	10	255	48,84	1,40E-22	Thioredoxin, glutaredoxin
grxB	Glutaredoxin-2	7,89	24203	2,58	0,00062	18	439	60,00	5,60E-41	Thioredoxin, glutaredoxin
grxB	Glutaredoxin-2	7,89	24203	3,01	0,00094	16	674	47,44	1,80E-64	Thioredoxin, glutaredoxin
mdaB	Modulator of drug activity B; NADPH quinone reductase	5,82	21746	3,3	7,40E-06	13	448	60,62	7,00E-42	Electron donors
mdaB	Modulator of drug activity B; NADPH quinone reductase	5,82	21746	3,22	3,60E-06	19	765	64,25	1,40E-73	Electron donors
mdaB	Modulator of drug activity B; NADPH quinone reductase	5,82	21746	2,41	9,80E-05	15	274	54,40	1,80E-24	Electron donors
mdaB	Modulator of drug activity B; NADPH quinone reductase	5,82	21746	2,73	2,20E-07	21	366	67,36	1,10E-33	Electron donors
ubiE	Ubiquinone/menaquinone biosynthesis methyltransferase	7,90	27907	-2,69	1,30E-06	11	234	41,83	4,90E-20	Menaquinone, ubiquinone
ubiE	Ubiquinone/menaquinone biosynthesis methyltransferase	7,90	27907	-4,16	2,90E-07	24	783	58,17	2,20E-75	Menaquinone, ubiquinone

5.7. Others

Gene	Full name / Protein function	pI	Mw	Average Ratio	T-test	Matches	Score	Coverage (%)	Probability	SUB-CLASS
apt	Adenine phosphoribosyltransferase	5,26	19859	2,1	6,40E-05	15	478	71,58	7,00E-45	Nucleotide and nucleoside conversions
bglX	Beta-D-glucoside glucohydrolase, periplasmic	5,78	83272	-5,78	2,20E-07	29	322	39,87	1,30E-27	Carbon utilization
folE	GTP cyclohydrolase 1	6,90	24683	2,82	0,00051	16	302	55,86	2,80E-27	Folic acid biosynthesis
glpK	Glycerol kinase	5,20	56061	3,23	2,30E-05	28	482	40,44	2,80E-45	Glycerol metabolism
guaB	Inosine-5'-monophosphate dehydrogenase	5,98	51855	3,5	2,20E-07	25	328	40,16	7,00E-30	Nucleotide and nucleoside conversions
moaB	Molybdenum cofactor biosynthesis protein B	5,67	18521	2,74	1,00E-05	8	157	40,00	8,80E-13	Molybdenum cofactors biosynthesis
moaB	Molybdenum cofactor biosynthesis protein B	5,67	18521	-2,51	0,0036	11	295	44,71	3,90E-26	Molybdenum cofactors biosynthesis
pckA	Phosphoenolpyruvate carboxykinase	5,45	59643	4,13	9,00E-06	9	96	22,22	1,20E-06	Gluconeogenesis
pckA	Phosphoenolpyruvate carboxykinase	5,45	59643	-3,7	2,30E-06	21	645	35,93	1,40E-61	Gluconeogenesis
pta	Phosphate acetyltransferase	5,11	76988	-3,09	1,40E-05	14	87	20,31	2,60E-05	Carbon utilization, central intermediary metabolism
pta	Phosphate acetyltransferase	5,11	76988	-4,68	7,70E-05	14	115	21,85	3,90E-08	Carbon utilization, central intermediary metabolism
pyrD	Dihydroorotate dehydrogenase	7,68	36620	-2,86	6,50E-07	7	83	26,19	6,50E-05	Pyrimidine biosynthesis
tdk	Thymidine kinase	5,95	23310	7,08	3,20E-06	16	294	46,34	4,90E-26	Nucleotide and nucleoside conversions
treC	Trehalose-6-phosphate hydrolase	5,43	63665	-3,28	1,90E-06	27	381	34,66	3,50E-35	Carbon utilization
udp	Uridine phosphorylase	5,78	27009	2,1	0,00054	5	94	28,06	4,90E-06	Nucleotide and nucleoside conversions
upp	Uracil phosphoribosyltransferase	5,16	22387	2,1	6,40E-05	12	116	64,42	1,10E-08	Nucleotide and nucleoside conversions

6. ORF´s

Gene	Full name / Protein function	pI	Mw	Average Ratio	T-test	Matches	Score	Coverage (%)	Probability	SUB-CLASS
ycfH	Uncharacterized deoxyribonuclease	5,05	29658	2,06	0,001	10	82	48,30	7.3E-05	
ydgA	Conserved protein, DUF945 family	4,88	54521	-3,14	2,40E-05	15	129	34,46	2,50E-08	Conserved-ORFs
yhgF	Protein yhgF	5,87	84932	-4,99	1,90E-06	20	266	25,61	3,10E-23	Conserved-Hypothetical-ORFs
yncE	Uncharacterized protein yncE precursor	9,61	38456	-3,25	3,80E-06	20	495	24,64	3,90E-46	

7. Protein related

Gene	Full name / Protein function	pI	Mw	Average Ratio	T-test	Matches	Score	Coverage (%)	Probability	SUB-CLASS
asnS	Asparaginyl-tRNA synthetase	5,00	52404	-2,29	0,004	14	140	42,51	1,20E-10	Amino acid activation
dnaK	Chaperone protein	4,64	68937	3,5	2,10E-05	37	583	49,69	2,20E-55	Chaperoning, repair (refolding)
dnaK	Chaperone protein	4,64	68937	-4,4	4,10E-06	16	156	27,90	1,10E-12	Chaperoning, repair (refolding)
fusA	Elongation factor G	5,07	77397	4,13	2,30E-05	38	623	51,14	6,20E-59	Translation
glyQ	Glycyl-tRNA synthetase alpha subunit	4,71	34621	8,08	4,40E-06	12	242	29,04	7,80E-21	Amino acid activation
glyS	Glycyl-tRNA synthetase beta subunit	5,12	76630	4,38	4,30E-06	9	84	16,26	1,80E-05	Amino acid activation
glyS	Glycyl-tRNA synthetase beta subunit	5,12	76630	-3,85	2,30E-05	37	752	42,24	7,80E-72	Amino acid activation
groL	Chaperone Hsp60 protein	4,85	57137	4,96	1,30E-06	15	146	27,92	1,10E-11	Chaperoning, repair (refolding)
groS	10 kDa chaperonin	4,96	10249	6,64	1,90E-06	9	189	46,39	1,60E-15	Chaperoning, repair (refolding)
hisS	Histidyl-tRNA synthetase	5,55	46867	3,24	2,80E-05	12	108	27,59	7,00E-08	Amino acid activation
hslV	ATP-dependent protease	5,94	18948	3,3	7,40E-06	11	242	47,16	2,80E-21	Chaperoning, repair (refolding)
htpG	Chaperone protein	4,91	71244	2,39	1,30E-06	33	682	58,97	7,80E-65	Chaperoning, repair (refolding)
htpG	Chaperone protein	4,91	71244	10,62	2,70E-06	32	541	36,70	3,50E-51	Chaperoning, repair (refolding)
htpG	Chaperone protein	4,91	71244	6,08	2,40E-06	30	594	37,34	1,80E-56	Chaperoning, repair (refolding)
htpG	Chaperone protein	4,91	71244	-6,04	2,40E-06	11	86	18,75	1,10E-05	Chaperoning, repair (refolding)
lysU	Lysyl-tRNA synthetase	4,93	57656	2,39	1,30E-06	11	84	28,71	4,70E-05	Amino acid activation
proS	Prolyl-tRNA synthetase	4,94	63519	2,39	1,30E-06	24	360	56,82	1,20E-32	Amino acid activation
proS	Prolyl-tRNA synthetase	4,94	63519	10,62	2,70E-06	10	97	19,23	9,00E-07	Amino acid activation
proS	Prolyl-tRNA synthetase	4,94	63519	6,08	2,40E-06	14	131	29,55	3,50E-10	Amino acid activation
rplC	50S ribosomal protein L3	10,41	22098	3,01	0,00094	5	142	27,27	2,80E-11	Ribosomal proteins
rplI	50S ribosomal protein L9	6,16	15627	-3,95	1,20E-05	15	506	55,03	1,10E-47	Ribosomal proteins
rplI	50S ribosomal protein L9	6,16	15627	2,92	0,00065	13	233	67,11	2,20E-20	Ribosomal proteins
rplM	50S ribosomal protein L13	10,30	15877	-2,28	0,00016	6	113	18,15	6,20E-08	Ribosomal proteins
rplU	50S ribosomal protein L21	10,30	11426	3	0,00086	6	212	37,86	2,80E-18	Ribosomal proteins
rplX	50S ribosomal protein L24	10,74	11178	3	0,00086	5	110	41,35	4,40E-08	Ribosomal proteins
rpsA	30S ribosomal protein S1	4,69	60986	-2,07	0,0001	43	1020	63,02	1,20E-98	Ribosomal proteins
rpsA	30S ribosomal protein S1	4,69	60986	3,5	2,10E-05	13	188	22,08	7,00E-16	Ribosomal proteins
rpsA	30S ribosomal protein S1	4,69	60986	-4,4	4,10E-06	25	439	40,39	5,60E-41	Ribosomal proteins
rpsA	30S ribosomal protein S1	4,69	60986	4,03	0,00051	29	627	43,99	8,80E-60	Ribosomal proteins
rpsA	30S ribosomal protein S1	4,69	60986	-6,04	2,40E-06	22	274	30,70	1,80E-24	Ribosomal proteins
rpsA	30S ribosomal protein S1	4,69	60986	3,24	2,80E-05	32	733	39,68	6,20E-70	Ribosomal proteins
rpsA	30S ribosomal protein S	4,69	60986	-6,11	1,30E-05	29	664	42,37	4,90E-63	Ribosomal proteins
rpsE	30S ribosomal protein S5	10,58	17460	-2,28	0,00016	7	130	31,14	1,20E-09	Ribosomal proteins
rpsJ	30S ribosomal protein S10	10,13	11597	-3,97	7,20E-05	13	426	49,51	1,10E-39	Ribosomal proteins
rpsK	30S ribosomal protein S11	11,81	13705	-5,2	1,10E-05	6	157	20,93	8,80E-13	Ribosomal proteins
tig	Trigger factor	4,63	48029	2,55	0,0092	13	107	26,16	2,50E-07	Chaperoning, repair (refolding)
tig	Trigger factor	4,63	48029	-3,96	1,40E-06	28	313	43,29	2,20E-28	Chaperoning, repair (refolding) , cell division
tsf	Elongation factor Ts	5,04	30270	2,06	0,001	12	95	45,23	3,60E-06	Translation
tufA	Elongation factor Tu 1	5,15	43123	-4,58	1,20E-05	15	270	38,58	4,40E-24	Translation
tufA	Elongation factor Tu 1	5,15	43123	-3,02	4,50E-06	23	271	62,69	3,50E-24	Translation
tufA	Elongation factor Tu 1	5,15	43123	3,33	0,00013	24	365	58,88	1,40E-33	Translation
tufA	Elongation factor Tu 1	5,15	43123	5,08	2,10E-05	35	824	72,34	1,80E-79	Translation
typA	GTP-binding protein typA/BipA	4,92	65272	-3,07	0,00056	21	276	27,07	3,10E-24	Translation regulation
typA	GTP-binding protein typA/BipA	4,92	65272	-3,76	3,70E-05	40	958	52,28	2,00E-92	Translation regulation

8. Regulation

Gene	Full name / Protein function	pI	Mw	Average Ratio	T-test	Matches	Score	Coverage (%)	Probability	SUB-CLASS
clpP	ATP-dependent Clp protease, proteolytic subunit	5,43	23040	3,22	3,60E-06	7	188	30,43	7,00E-16	Proteases
cspE	Cold shock protein E	8,82	7327	-7,64	3,50E-07	13	619	86,96	5,60E-59	Transcriptional level
cspE	Cold shock protein E	8,82	7327	-5,21	1,90E-07	11	484	73,91	1,80E-45	Transcriptional level
cspE	Cold shock protein E	8,82	7327	-6,21	4,80E-07	7	262	60,87	2,80E-23	Transcriptional level
eco	Ecotin precursor	6,89	18049	2,25	0,00018	15	423	50,00	2,20E-39	Inhibition / activation of enzymes
gcp	Probable tRNA threonylcarbamoyladenosine biosynthesis protein	5,91	36008	2,4	1,50E-05	14	396	43,62	3,10E-36	Proteases
nanR	Transcriptional regulator	6,00	29524	-2,55	3,50E-06	16	262	36,45	7,80E-23	Operon repressor
ompT	Outer membrane protease 7	5,66	35407	-4,3	9,50E-07	28	497	57,10	2,50E-46	Proteases
pepQ	Xaa-Pro dipeptidase	5,55	50013	4,84	9,10E-06	18	265	41,31	3,90E-23	Proteases
pepQ	Xaa-Pro dipeptidase	5,55	50013	4,76	2,10E-05	15	98	31,38	2,00E-06	Proteases
prlC	Oligopeptidase A	4,98	76985	2,39	1,30E-06	12	165	22,50	3,90E-13	Proteases
suhB	Inositol-1-monophosphatase	6,52	29021	-2,1	6,70E-08	9	120	35,11	1,20E-08	Posttranscriptional

9. RNA-related

Gene	Full name / Protein function	pI	Mw	Average Ratio	T-test	Matches	Score	Coverage (%)	Probability	SUB-CLASS
arcA	Aerobic respiration control protein	5,03	27142	2,1	6,40E-05	13	344	39,50	4,90E-31	Transcription related
crp	cAMP receptor protein	8,20	23494	-3,64	1,00E-07	19	598	49,52	7,00E-57	Transcription related
crp	cAMP receptor protein	8,20	23494	-3,37	4,00E-06	15	382	32,38	2,80E-05	Transcription related
cspC	Cold shock-like protein C	7,02	7267	-13,36	3,10E-07	7	376	73,91	1,10E-34	Transcription related
cspC	Cold shock-like protein C	7,02	7267	-2,18	6,60E-05	11	379	100,00	1,60E-34	Transcription related
cspC	Cold shock-like protein C	7,02	7267	-2,06	3,80E-05	8	289	73,91	1,60E-25	Transcription related
greA	Transcription elongation factor	4,52	17498	2,15	0,0029	6	95	40,51	1,40E-06	Transcription related
miaB	(Dimethylallyl)adenosine tRNA methylthiotransferase	5,19	53663	-2,29	0,004	7	85	14,02	4,00E-05	RNA modification
mnmG	tRNA uridine 5-carboxymethylaminomethyl modification enzyme	6,20	695212	-3,65	3,70E-06	6	120	10,02	1,20E-08	RNA modification
nusG	Transcription antitermination protein	6,39	20387	3,3	7,40E-06	9	177	38,67	8.8e-015	Transcription related
pnp	Polyribonucleotide nucleotidyltransferase	4,92	76918	3,03	5,60E-05	21	258	22,36	2,00E-22	RNA degradation
rnhB	RNase H; degrades RNA of DNA-RNA hybrids	7,42	21381	-3,98	0,00018	8	188	45,96	7,00E-16	RNA degradation
rpoA	DNA-directed RNA polymerase subunit alpha	4,78	36357	-3,25	6,90E-06	28	454	55,32	1,80E-42	Transcription related
rraA	Regulator of ribonuclease activity A	4,07	17360	2,61	0,0003	15	280	75,16	4,40E-25	RNA degradation
tgt	Queuine tRNA-ribosyltransferase	5,94	42434	2,1	0,00054	12	183	27,20	6,20E-15	RNA modification

10. Transport

Gene	Full name / Protein function	pI	Mw	Average Ratio	T-test	Matches	Score	Coverage (%)	Probability	SUB-CLASS
atpA	ATP synthase subunit alpha	5,72	55054	-3,25	2,70E-06	43	1160	56,14	4,40E-113	H^+- or Na^+-translocating F-type, V-type and A-type ATPase (F-ATPase) Su
atpA	ATP synthase subunit alpha	5,72	55054	3,2	0,00015	31	757	51,85	2,50E-72	H+- or Na+-translocating F-type, V-type and A-type ATPase (F-ATPase) Su
atpA	ATP synthase subunit alpha	5,72	55054	3,12	0,0002	11	97	26,90	2,60E-06	H+- or Na+-translocating F-type, V-type and A-type ATPase (F-ATPase) Su
atpD	ATP synthase subunit beta	5,72	55054	2,55	0,0092	23	538	48,70	2,00E-50	H+- or Na+-translocating F-type, V-type and A-type ATPase (F-ATPase) Su
atpD	ATP synthase subunit beta	5,72	55054	-3,14	5,40E-06	31	414	59,57	4,90E-38	H+- or Na+-translocating F-type, V-type and A-type ATPase (F-ATPase) Su
btuB	Vitamin B12 transporter	5,08	68232	-3,06	1,40E-05	32	536	84,42	1,10E-50	Beta barrel porins (outer membrane porin (OMP) functional superfamily)
cirA	Colicin I receptor	4,93	73715	-3,71	4,00E-05	23	206	26,55	1,10E-17	Transporters of Unknown Classification
crr	Glucose-specific phosphotransferase enzyme IIA component	4,54	18108	2,15	0,0029	9	182	44,97	2,80E-15	Phosphotransferase Systems (PEP-dependent PTS)
fecA	Fe(3+) dicitrate transport protein	5,50	85134	-4,68	7,70E-05	34	885	40,96	3,90E-85	Beta barrel porins (outer membrane porin (OMP) functional superfamily)
fecA	Fe(3+) dicitrate transport protein	5,50	85134	-3,76	3,70E-05	11	82	19,38	7,60E-05	Beta barrel porins (outer membrane porin (OMP) functional superfamily)
fecB	Iron(III) dicitrate-binding periplasmic protein	9,25	32994	-2,02	1,00E-05	16	335	37,33	3,90E-30	ABC superfamily, periplasmic binding component
fecB	Fe(3+) dicitrate-binding periplasmic protein	9,25	32994	-3,48	7,50E-08	21	634	45,33	1,80E-60	ABC superfamily, periplasmic binding component
fiu	Predicted iron outer membrane transporter	5,55	81960	-3,09	1,40E-05	24	354	35,00	4,90E-32	Beta barrel porins (outer membrane porin (OMP) functional superfamily)
mlaC (yrbC)	Probable phospholipid-binding protein	9,65	23816	2,16	2,70E-05	14	385	39,81	1,40E-35	ABC superfamily, periplasmic binding component
ompA	Outer membrane protein A	5,97	37045	2,05	1,60E-05	22	554	56,87	6,80E-51	Beta barrel porins (outer membrane porin (OMP) functional superfamily)
ompA	Outer membrane protein A	5,97	37045	2,57	2,10E-05	8	80	29,19	0,00012	Beta barrel porins (outer membrane porin (OMP) functional superfamily)
ompA	Outer membrane protein A	5,97	37045	2,05	0,00014	6	84	28,02	4,90E-05	Beta barrel porins (outer membrane porin (OMP) functional superfamily)
ompA	Outer membrane protein A	5,97	37045	2,06	0,001	20	393	51,92	6,20E-36	Beta barrel porins (outer membrane porin (OMP) functional superfamily)
ompA	Outer membrane protein A	5,97	37045	3,57	7,70E-06	6	293	17,05	2,20E-26	Beta barrel porins (outer membrane porin (OMP) functional superfamily)
ompA	Outer membrane protein A	5,97	37045	9,08	1,90E-09	7	178	18,26	7,00E-15	Beta barrel porins (outer membrane porin (OMP) functional superfamily)
ompA	Outer membrane protein A	5,97	37045	3,14	3,50E-06	17	301	34,68	9,80E-27	Beta barrel porins (outer membrane porin (OMP) functional superfamily)
ompC	Outer membrane protein C	4,39	40210	-2,56	3,20E-06	21	739	53,68	5,6E-71	Beta barrel porins (outer membrane porin (OMP) functional superfamily)
ompC	Outer membrane protein C	4,39	40210	3,57	7,70E-06	6	98	21,25	6,80E-07	Beta barrel porins (outer membrane porin (OMP) functional superfamily)
ompF	Outer membrane protein F	4,57	39175	-2,56	3,20E-06	21	533	54,70	2,2E-50	Beta barrel porins (outer membrane porin (OMP) functional superfamily)
ompF	Outer membrane protein F	4,57	39175	-3,41	7,40E-06	22	636	43,37	3,10E-60	Beta barrel porins (outer membrane porin (OMP) functional superfamily)

Gene	Full name / Protein function	pI	Mw	Average Ratio	T-test	Matches	Score	Coverage (%)	Probability	SUB-CLASS
oppA	Periplasmic oligopeptide-binding protein	6,03	60728	-4,06	3,20E-06	16	170	26,15	4,40E-14	ABC superfamily, periplasmic binding component
oppF	Oligopeptide transport ATP-binding protein	7,55	37043	-2,94	9,10E-07	21	318	51,20	2,00E-28	ABC superfamily ATP binding cytoplasmic component
oppF	Oligopeptide transport ATP-binding protein	7,55	37043	-2,86	6,50E-07	15	209	44,01	1,60E-17	ABC superfamily ATP binding cytoplasmic component
potD	Polyamine transporter	5,06	38709	2	9,10E-06	18	342	49,43	7.8E-31	ABC superfamily, periplasmic binding component
pstS	Phosphate-binding protein	8,78	36868	3,73	4,40E-05	27	1040	50,55	4,40E-101	ABC superfamily, periplasmic binding component

Experimental Procedures

The experimental procedures were done by Servicio de Proteómica del Centro Nacional de Biotecnología (CNB-CSIC).

Two-dimensional difference gel electrophoresis (2D-DIGE). For 2D-DIGE, four biological replicates were run on four individual 2D gels together with an internal standard control. The internal standard allows the comparison of the individual gels among each other. The individual methanol-chloroform precipitated samples were quantified and minimally labelled with N-hydroxy-succinimidyl (NHS) ester-derivatives of the cyanine dyes Cy2, Cy3, and Cy5 according manufacturers instructions (GE Life Science). 50 μg of proteins from the non UV-irradiated sample and its corresponding maxicells samples were labelled with 400 pmol of Cy3 or Cy5 or vice versa (non UV-irradiated samples with Cy5 and its corresponding maxicells with Cy3). Cy2 was used to label the same amount of internal standard, resulting from the pooling of the eight individual parts of each protein sample of the four non UV-irradiated and the four maxicells samples. Separation in the first dimension of 2-DE was performed at 0.05 mA per immobilized pH gradient strip (IPG) in the IPGphor IEF System at 20ºC. Protein pellets were rehydrated in rehydration buffer (7 M urea; 2 M thiourea; 4% CHAPS; 20 mM DTT and 1% of carrier ampholites for pH 3-11 or pH 4-7) up to final volume of 100 μl, and applied by cup loading to a 24 cm non-linear IPG strip pH 3-11 (GE Healthcare) or non-linear IPG strip pH 4-7 (GE Healthcare) previously rehydrated with 440 μl of rehydration buffer supplemented with 1.2% DeStreak (GE Life Science). Isoelectric focusing of the rehydrated protein samples was then performed following a 5 step voltage increase starting with 300 V/h for 3 hours followed by a linear voltage gradient up to 1000 V/h in 6 hours, then increased up to 8000 V/h in 3 hours and finally maintained until 64000 V/h. For the second dimension, strips were equilibrated in the dark with SDS equilibration buffer (75 mM Tris pH 8.8; 6 M urea; 30% (v/v) glycerol; 2% (w/v) SDS and bromophenol blue) containing 1% (w/v) DTT for 15 min and thereafter in SDS equilibration buffer containing 4% (w/v) iodoacetamide for 15 additional minutes. Proteins were separated on home-casted 15% and 12.5% Tris-glycine gels using an Ettan Dalt Six device (GE Healthcare) at 20 ºC until the bromophenol blue migrated off the bottom of the gel. Preparative 2D protein gels were loaded with non-labelled material of one condition and after sypro (Molecular Probes, Inc.) staining gels were matched automatically with 2D DIGE gels and spots were picked by spot-picking robot.

Image acquisition and biology variation analysis. Labelled proteins were visualized using a Typhoon 9400 Imager. Cy2, Cy3 and Cy5 images were scanned using 488 nm excitation and

520BP40 emission filter, 532 nm excitation and 580BP30 emission filter and 633 nm excitation and 670BP30 emission filter respectively. All gels were scanned at 100 dpi resolution and relative protein quantification across non UV-irradiated and maxicells samples was performed using DeCyder Differential In-gel Analysis (DIA) software (GE healthcare). For comparison 2-D DIGE image pairs are intrinsically linked to their in-gel standard used for matching between individual gels followed by statistical analysis of protein abundance change between samples using the DeCyder DIA and DeCyder Biological Variation Analysis (BVA) software module, setting Student's t-test to $P< 0.01$. After imaging for CyDye components and DeCyder analysis, the gels were fixed in 10% methanol, 7% acetic acid for 30 minutes and then incubated overnight in the dark with Sypro Ruby (Molecular Probes). Sypro Ruby images scanned on the same imager and for spot-pickings, the Sypro stained image was compared to the CyDye images by the DeCyder software that coordinates automatically spot-picking by the spot-picking robot.

In-gel digestion and MALDI-TOF/TOF protein identification. Proteins of interest were excised automatically from 2D-GE and 2D-DIGE gels that were either silver (Shevchenko *et al.*, 1996) or sypro stained (Molecular Probes, Inc.), deposited in 96-well plates and processed automatically in a Proteineer DP (Bruker Daltonics, Bremen, Germany). For protein digestion gel, discs were washed with 50 mM ammonium bicarbonate and treated with sinapinic acid before reduction with 10 mM DTT in 25 mM ammonium bicarbonate and alkylation with 55 mM iodoacetamide in 50 mM ammonium bicarbonate. Next, gel pieces were rinsed first with 50 mM ammonium bicarbonate and then with sinapinic acid and dried under a nitrogen stream. Dimethylated trypsin from porcine pancreas (Proteomics Grade, Sigma-Aldrich, CA, USA) at a final concentration of 16 ng/µl dissolved in 25% sinapinic acid and 50 mM ammonium bicarbonate solution was added for protein digestion at 37ºC for 6 hours. The reaction was stopped by the addition 0.5% trifluoroacetic acid (TFA) and dried by speed-vacuum centrifugation. Dried peptides were resuspended in 4 ml of MALDI solution (30% acetonitrile; 15% isopropanol and 0.5% TFA) and 0.8 ml aliquot of each peptide mixture was deposited onto a 386-well OptiTOFTM MALDI Plate (Applied Biosystems, Framingham, MA, USA) and dried at room temperature. A 0.8 µl aliquot of matrix solution (3 mg/mL α-Cyano-4-hydroxycinnamic acid dissolved in MALDI solution) was then deposited onto dried digest and allowed to dry at room temperature. For Matrix-Assisted Laser Desorption Ionization-Time of Flight /Time of Flight (MALDI TOF/TOF) analysis, samples were automatically acquired in an ABi 4800 MALDI TOF/TOF mass spectrometer (Applied Biosystems, Framingham, MA, USA) operating in positive ion reflector mode with an ion acceleration voltage of 25 kV to mass spectra (MS) acquisition and 2 kV to tandem mass spectrometry (MS/MS). Peptide mass fingerprinting (PMF) and MS/MS

fragment ion spectra were smoothed and corrected to zero baseline using routines embedded in ABi 4000 Series Explorer Software v3.6 where each PMF spectrum was internally calibrated with the mass signals of trypsin autolysis ions to reach a typical mass measurement accuracy of < 25 ppm. Known trypsin and keratin mass signals, as well as potential sodium and potassium adducts (+21 Da and +39 Da) were removed from the peak list.

Database searches. For protein identification, the obtained PMF and MS/MS data were batch processed and searched against the *Escherichia coli* K-12 UniProtKB database (UniProtKB[ref-83333]: UKBsp_p562_201106 2011 with 4411 sequences and 1384155 amino acid residues) using the software MASCOT v2.2.04 (www.matrixscience.com; Matrix Science, London, UK). In all protein identifications, only candidates with significant Mowse scores ($p < 0.05$) were considered.

Appendix II: Publications

- Pazos, M., Natale, P. and Vicente, M. (2012). "A specific role for the ZipA protein in cell division: stabilization of the FtsZ protein". *J. Biol. Chem.* (In press).

- Pazos, M., Casanova, M., Natale, P. and Vicente, M. "Selection of FtsZ placement in nucleoid-free bacterial cells". (In preparation).

- Pazos, M., Natale, P., Margolin, W. and Vicente, M. "Bimolecular Fluorescence Complementation to study protein-protein interactions of the early stages of the divisome assembly". (In preparation).